

Tropospheric Particle Formation in Forests: Global Modeling of Secondary Organic  
Aerosol Production from Reaction of  $\text{NO}_3$  Radical with Speciated Monoterpenes

---

A Thesis

Presented to

The Division of Mathematics and Natural Sciences

Reed College

---

In Partial Fulfillment

of the Requirements for the Degree

Bachelor of Arts

---

Makoto Kelp

May 2016

Approved for the Division

(Chemistry)

---

Juliane L. Fry

# Table of Contents

<b>Introduction.....</b>	<b>1</b>
1.1: Atmospheric Composition and Climate Change .....	1
1.2: Aerosols .....	4
1.3: Secondary Organic Aerosol .....	5
1.3.1: Volatile Organic Compounds .....	6
1.3.2: Oxidants .....	9
1.3.3: Chamber Experiments and Yields .....	11
1.4: Traditional Absorptive Partitioning Models .....	13
1.4.1: Odum 2-Product Model for SVOC Partitioning.....	15
1.4.2: Volatility Basis Set Model for SVOC Partitioning.....	15
1.5: A Paradox: Anthropogenic Emissions Enhance Biogenic SOA? .....	18
1.6: Model-to-Measurement Discrepancies in SOA Loading .....	19
1.7: Chemical Transport Models and GEOS-Chem .....	20
1.7.1: Nitrate Parameterizations in GEOS-Chem .....	23
<b>Methods.....</b>	<b>27</b>
2.1: Model Overview .....	27
2.2: Model Description .....	29
2.3: Model Suggestions.....	29
2.4: Downloading GEOS-Chem Run Directories .....	30
2.5: Separating Out $\alpha$ -Pinene from the Lumped Bicyclic Monoterpenes.....	32
2.6: Compiling and Running GEOS-Chem .....	50
2.7: Adding Tracers and Making New Restart Files .....	54
<b>Results and Discussion.....</b>	<b>59</b>
3.1: Unlumping Control Analysis.....	59
3.2: Global and Regional Simulation Results of a Reduced $\alpha$ -Pinene-NO <sub>3</sub> Pathway...	63
3.3: Global Yearly Budgets .....	79

<b>Future Work.....</b>	<b>81</b>
<b>Conclusions.....</b>	<b>83</b>
<b>Appendix A.....</b>	<b>85</b>
<b>Bibliography .....</b>	<b>89</b>

## List of Tables

Table 1.1: Reported SOA yields from chamber experiments .....	12
Table 2.1: Location of files that need to be edited in the GEOS-Chem Code.v10-01 in order to unlump $\alpha$ -pinene from MTPA .....	33
Table 2.2: What tracer species to add to the tracerinfo.dat for a new SOA simulation....	55
Table 3.1: Global Yearly SOA Budgets for GEOS-Chem simulations .....	79

# List of Figures

Figure 1.1: IPCC summary of radiative forcing contributions .....	3
Figure 1.2: Geographic distribution of organic and inorganic aerosol .....	5
Figure 1.3: Regional distribution of monoterpenes in the United States .....	8
Figure 1.4: Alabama field campaign data of NO <sub>3</sub> -terpene measurements.....	11
Figure 1.5: VBS parameter fitting procedure .....	16
Figure 1.6: Multi-study comparison of modeled vs. observed ambient organic aerosol concentrations .....	20
Figure 1.7: Elements of a mathematical atmospheric chemical transport model .....	22
Figure 1.8: GEOS-Chem SOA mechanistic pathway .....	24
Figure 1.9: Enhancement in surface-level SOA in August 2000 from terpenes from the nitrate oxidation pathway.....	25
Figure 1.10: GEOS-Chem model-to-measurement analysis for the Eastern USA .....	26
Figure 2.1: Updated GEOS-Chem monoterpene SOA mechanistic pathway.....	28
Figure 2.2: CopyRunDirs.input file to create a geos5_4x5_soa .....	31
Figure 2.3: tracerid_mod.F line 220 .....	33
Figure 2.4: input_mod.F line 2039 .....	34
Figure 2.5: gamap_mod.F line 1360 .....	34
Figure 2.6: gamap_mod.F lines 4540 and 4575.....	35
Figure 2.7: drydep_mod.F line 5064.....	36
Figure 2.8: wetscav_mod.F lines 1851 to 1896. ....	37
Figure 2.9: wetscav_mod.F lines 3774 to 3807. ....	38
Figure 2.10: wetscav_mod.F line 4807 .....	39
Figure 2.11: wetscav_mod.F lines line 8215 .....	39

Figure 2.12: diag3.F line 823 .....	40
Figure 2.13: diag3.F line 864 under (2) BETA-PINENE .....	41
Figure 2.14: diag3.F line 1124, created an OC-APIN diagnostic .....	42
Figure 2.15: carbon_mod.F line 218.....	43
Figure 2.16: carbon_mod.F line 2422.....	43
Figure 2.17: carbon_mod.F line 3835, VBS yields for APIN SOA .....	44
Figure 2.18: carbon_mod.F starting from line 4202, chem_nvoc subroutine.....	45
Figure 2.19: carbon_mod.F line 4494, end of chem_nvoc subroutine .....	46
Figure 2.20: carbon_mod.F line 8284.....	46
Figure 2.21: carbon_mod.F line 8616.....	46
Figure 2.22: carbon_mod.F line 9062, init_carbon subroutine.....	47
Figure 2.23: carbon_mod.F line 9249.....	47
Figure 2.24: hcox_megan_mod.F line 379 .....	48
Figure 2.25: hcox_megan_mod.F line 1104, HCOX_MEGAN_Run subroutine.....	48
Figure 2.26: hcox_megan_mod.F line 1213 .....	49
Figure 2.27: hcox_megan_mod.F line 1428 .....	49
Figure 2.28: hcox_megan_mod.F line 4117 .....	50
Figure 2.29: input.geos, simulation menu.....	51
Figure 2.30: input.geos output, GAMAP, and diagnostic menus .....	52
Figure 2.31: compile.sh, manual GEOS-Chem compiler .....	53
Figure 2.32: run.geos.cluster, Colorado State University example .....	54
Figure 2.33: Creating new restart files in IDL .....	56
Figure 2.34: IDL command to create a new partial restart file .....	56
Figure 2.35: Merged new and old restart files in IDL .....	57

Figure 3.1: Global absolute and percent difference plots total terpene SOA mass loading (TSOA) from monoterpenes in August.....	60
Figure 3.2: Absolute difference analysis for all C* volatility bins in August .....	62
Figure 3.3: Regional distribution of $\alpha$ -pinene during July in the USA relative to total monoterpene emissions in the GEOS-Chem model.....	64
Figure 3.4: Global distribution of percent terpene emissions that are $\alpha$ -pinene during July in the GEOS-Chem model .....	65
Figure 3.5: Global absolute and percent difference plots for total SOA from monoterpenes in August for the unlumped control and APIN-NO <sub>3</sub> SOA yield equal zero simulations .....	67
Figure 3.6: Global absolute and percent difference plots for total SOA from monoterpenes in January for the unlump control and APIN-NO <sub>3</sub> SOA yield equal zero simulations .....	68
Figure 3.7: Global absolute differences for total SOA from monoterpenes in July for the unlump control and APIN-NO <sub>3</sub> SOA yield equal zero simulations.....	69
Figure 3.8: Absolute differences for total SOA from monoterpenes in August in the USA for the unlump control and APIN-NO <sub>3</sub> SOA yield zeroed simulations .....	70
Figure 3.9: Global absolute differences for total SOA from monoterpenes in January for the unlump control and APIN-NO <sub>3</sub> SOA yield equal zero simulations.....	70
Figure 3.10: Absolute differences for total SOA from monoterpenes in January in the USA for the unlump control and APIN-NO <sub>3</sub> SOA yield equal zero simulations ....	71
Figure 3.11: $\alpha$ -pinene emissions in August in the GEOS model (v.10) .....	72
Figure 3.12: Monthly total OA, SOA from terpenes, and monitored PM <sub>2.5</sub> data from Reed College Warehouse in Portland, OR time series.....	74
Figure 3.13: 4x5° spatial grid containing Portland, OR.....	74
Figure 3.14: Monthly total OA and SOA from terpenes in Congo Forest time series .....	76
Figure 3.15: Differences in monthly SOA from monoterpenes in the Congo Forest between the unlump control simulation and the nitrate yield set to zero run .....	76

Figure 3.16: Monthly total OA and SOA from terpenes in Northern Boreal Forest in Russia time series.....	78
Figure 3.17: Differences in monthly SOA from terpenes in a Northern Boreal Forest between the unlump control simulation and the nitrate yield set to zero run .....	78
Figure A.1: Coding a difference plot .....	85
Figure A.2: Code template used to create maps for Figure 3.11-3.14.....	86
Figure A.3: Code template used to create time series plots for Figure 3.16-3.23 .....	87
Figure A.4: Code template used to calculate yearly global budget of $\alpha$ -pinene.....	88

## Abstract

Historically, global modeling of secondary organic aerosol (SOA) formation from monoterpenes has been based on an oversimplified lumped mechanism, which parameterizes all monoterpene-NO<sub>3</sub> reactions as  $\beta$ -pinene. The resulting global spatial patterns and annual budgets of organic aerosol gave poor matches with observations. This simplified scheme is inconsistent with recent chamber studies revealing  $\alpha$ -pinene reaction with NO<sub>3</sub> radical oxidant to have a much lower SOA yield than compared to the other bicyclic monoterpenes. To assess how a more realistic, lower  $\alpha$ -pinene-NO<sub>3</sub> SOA-producing pathway affects global organic aerosol concentrations, the global 3-D chemical transport model GEOS-Chem was updated with a new volatility basis set (VBS) based aerosol parameterization where  $\alpha$ -pinene was unlumped from the lumped parameterized terpenes tracer and speciated with unique chemistry. As a result of the new parameterization, there were predicted model differences of up to 3.5  $\mu\text{g}/\text{m}^3$  less SOA in the summer months in high organic aerosol producing source regions. Integrated over the globe, the reduction led to an annual decrease of 2 Tg organic aerosol between the control and novel VBS mechanism, a 10% change from previous model terpene organic aerosol budgets. This study demonstrates that lumped terpene mechanisms may cause substantial errors in predicting SOA spatial patterns, with consequences for global budgets of highly climate relevant aerosol mass loading. Wherever computationally possible, such models should include more detailed, speciated chemical mechanisms.

# Introduction

## 1.1: Atmospheric Composition and Climate Change

The atmosphere is a complex and dynamic, yet sensitive environmental system. Its discrete layers have distinct composition and chemistry. In a way, the atmosphere itself resembles a robust ecosystem that possesses properties of self-sustainability and internal linkages among chemical species. There exists a natural balance between the atmosphere and the Earth's biosphere. However, recent studies have revealed that the contribution of anthropogenic emissions has counterweighed this balance and thus disturbed greatly the natural equilibrium that existed between the atmosphere and the terrestrial biosphere, ushering in an era of the Anthropocene (Crutzen and Stoermer, 2000). As a result, these human emissions have led to dramatic change in atmospheric chemistry, composition, and climate on a global scale.

Perhaps the most prominent examples of environmental change caused by humans are those of the ozone hole and global warming. Ozone ( $O_3$ ) at surface level is considered an environmental air pollutant and health hazard, as it is a main ingredient in photochemical smog. It is a secondary pollutant derived from reactions involving reactive nitrogen species ( $NO_x$ ) emitted from vehicular exhaust with primary emissions in the presence of sunlight. Although surface level  $O_3$  is considered harmful (and predominately human-made), the ozone layer 20-30 km above the Earth is helpful and natural as it helps shield the surface by absorbing damaging ultraviolet radiation. However, the anthropogenically emitted compound chlorofluorocarbon (CFC), a popular refrigerant used until the mid-1990s, has had a deleterious effect on the ozone layer as it has tended to aggregate in the stratosphere and deplete ozone (Rowland and Molina, 1994).

In addition, rapid climate change and global warming is caused by human emissions of greenhouse gases (GHGs), most notably carbon dioxide ( $CO_2$ ).  $CO_2$  is the main byproduct of the combustion of fossil fuels. It and other GHGs such as methane ( $CH_4$ ) absorb infrared (IR) radiation (thermal radiation possessing longer wavelengths than visible light), which represent the major emitted wavelengths from Earth's surface.

These greenhouse gases can reemit some of this radiation back towards the surface of the planet, which warms the atmosphere. To be sure, greenhouse gases are necessary for the stable temperatures that sustain human life; however, the large source of modern CO<sub>2</sub> that humans are contributing to the Earth through industrial processes and fossil fuel combustion have greatly upset the natural equilibrium of sources and sinks that existed long before humans.

A convenient summary of important climate forcing anthropogenic emissions can be found in Figure 1.1 from the Intergovernmental Panel on Climate Change Fifth Assessment Report, which compares 2011 global average radiative forcing estimates (IPCC, 2013). Radiative forcing is the ability of an atmospheric species to affect the energy balance to contribute to climate change. These forcings are measured in watts per square meter (W/m<sup>2</sup>) and reflect the perturbation of the Earth's natural radiative balance in relation to the pre-industrialization baseline year of 1750. A positive forcing value, such as from CO<sub>2</sub> and other greenhouse gases, causes a global warming effect. However, a class of compounds known as aerosols actually causes a global cooling effect. The reasons for aerosols' radiative cooling are poorly understood and represent a large measure of uncertainty in global anthropogenic radiative forcings. Further research into aerosol mechanisms is required to provide better-constrained global estimates and ultimately a greater understanding of the composition of the atmosphere and its responses to human activities.

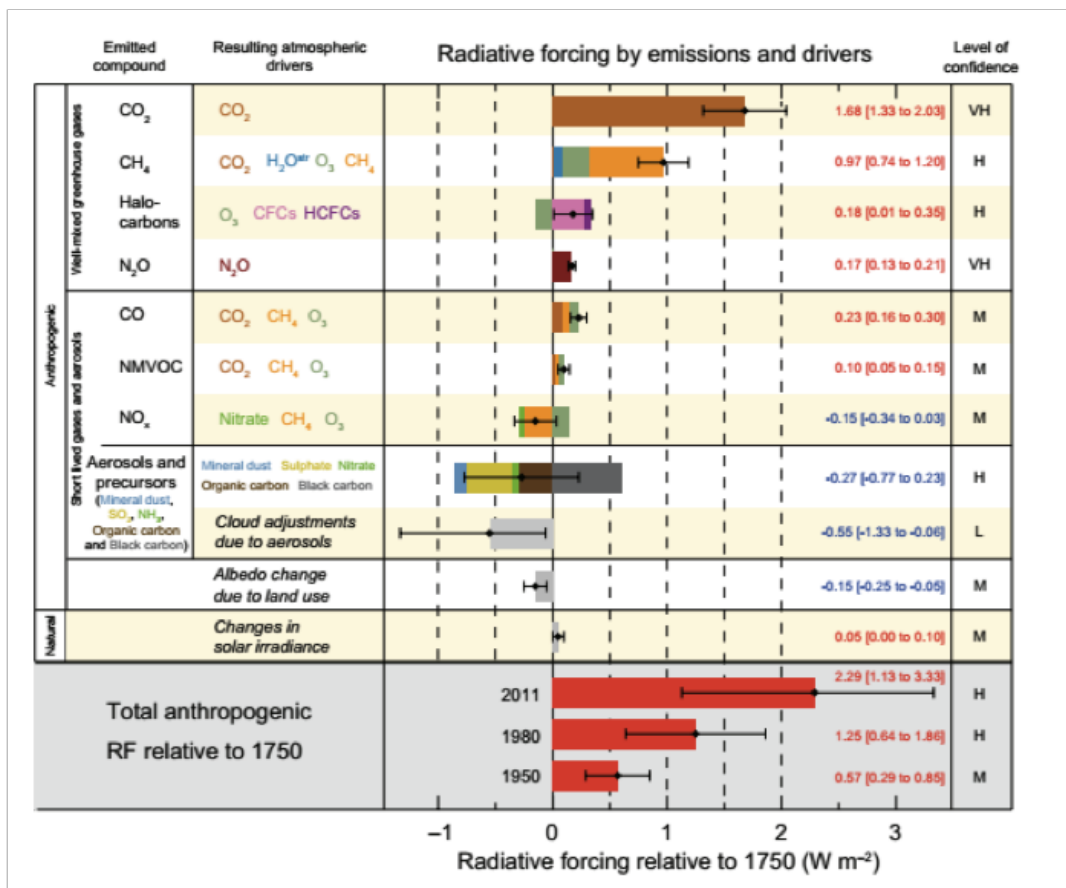


Figure 1.1: IPCC summary of radiative forcing contributions

Global average radiative forcing estimates (in W/m<sup>2</sup>) of compounds from anthropogenic sources in 2011 relative to the year 1750 based on concentration change (IPCC, 2013). Uncertainties are calculated using an intercomparison of coupled models that calculate the radiative forcings by specific compounds. The deviation between different model outputs account for the error bars for a given atmospheric species. The primary factor of uncertainty in the total anthropogenic forcing is the low agreement on the time evolution of the total aerosol effective radiative forcing and the role of cloud responses. Substantial uncertainties remain in long term trends of global properties of aerosols due to difficulties in measurement and lack of observations of high spatial and temporal variability, and the relatively short observational records that exist. In addition, total anthropogenic radiative forcing is derived by summing asymmetric uncertainty estimates from component terms, and thus cannot be obtained by simple addition.

## 1.2: Aerosols

An aerosol is a suspension of solid or liquid particles in a gas. Aerosols can come from a variety of sources including dust, smog, clouds, mist, and smoke. These sources can be from both biogenic and anthropogenic origins.

In addition, aerosols can be classified as either primary or secondary (Seinfeld and Pandis, 2006). Primary aerosols are particles introduced directly into the atmosphere. For example, sea spray, vehicular exhaust and even emissions from meat cooking all produce primary aerosols (Huang et al., 2010). Secondary aerosols are formed through the gas-to-particle conversions of primary emissions such as from primary  $\text{NO}_x$  emissions.

Furthermore, aerosols and gases exhibit a range of volatilities. Volatility is a compound's tendency to vaporize given its vapor pressure and unique thermodynamic properties. At a given temperature, a substance with a higher vapor pressure vaporizes more readily than a substance with a lower vapor pressure. Thus, if a source is known to produce nonvolatile products, then these emissions are thought to permanently exist in the particle phase. However, if a source emits intermediate-volatility species (semivolatiles), these products can partition between both the gas and aerosol phases and redistribute themselves depending on temperature and gas-phase dilutions.

The classes of aerosols existing in a given region are highly variable depending on their emitting source and their immediate chemical environment. Semivolatile gases that can partition to the particle phase may undergo a vast number of transformations that can affect their volatility, such as oxidation, which typically lower volatility (Liang et al., 2007). For example, high vapor pressure compounds are highly volatile and thus exist exclusively in the gas phase at atmospheric temperatures. These gas-phase species can react with oxidants in the air to form more highly substituted compounds, a process known as oligomerization, which lowers the compounds vapor pressure and volatility. These oxidized compounds can further undergo reactions with more oxidants and/or gas-phase molecules to create lower volatility compounds that can eventually condense into the aerosol (condensed) phase (Seinfeld and Pandis, 2006). Conversely, these larger, oxidized aerosols can fragment and revolatilize smaller particles back into the gas phase.

In addition to primary and secondary aerosols, there are different compositions of aerosols defined as either organic or inorganic. Organic aerosol, specifically secondary organic aerosol (SOA), is the focus of this thesis. The most common aerosol species include organic molecules (hydrocarbons,  $C_xH_y$ , containing O, N, and/or S heteroatoms), sulfates ( $SO_4^{2-}$ ), nitrates ( $NO_3^-$ ), ammonium ( $NH_4^+$ ), and chloride ions ( $Cl^-$ ) (Zhang et al., 2007). Figure 1.2 shows that organics are major components of aerosol everywhere, whether urban or rural. Although inorganic aerosols are also shown to constitute a substantial fraction of aerosol mass in many locations, they are outside the main scope of this analysis.

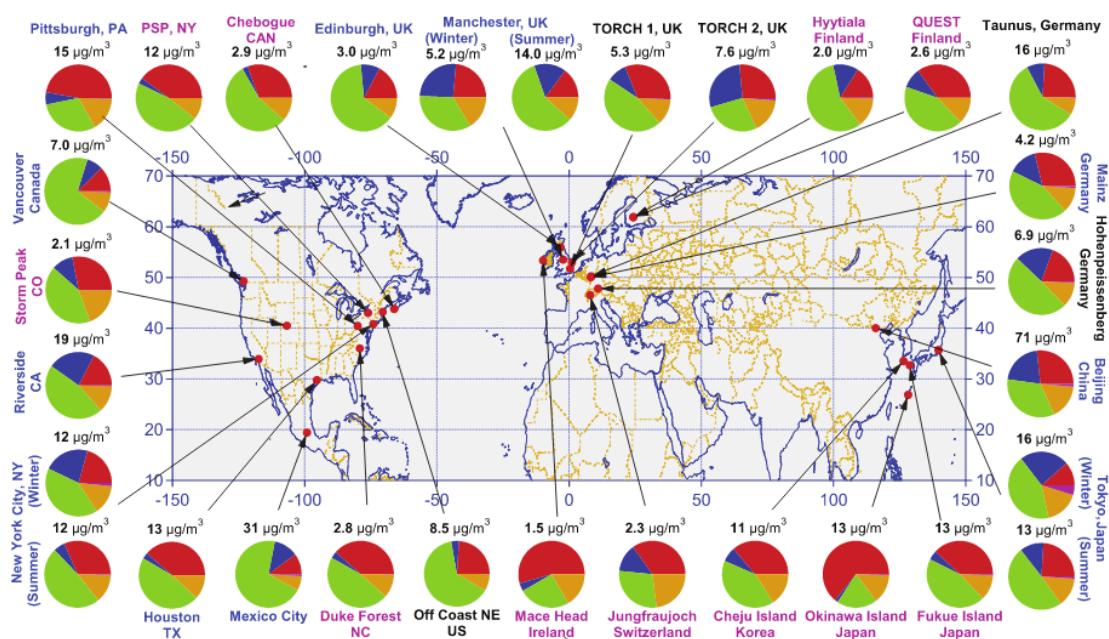


Figure 1.2: Geographic distribution of organic and inorganic aerosol

Organic and inorganic aerosol fractions measured at various sampling locations. Colors for the study labels indicate the type of sampling location: urban areas (blue), <100 miles downwind of major cities (black), and rural/remote areas >100 miles downwind (pink). Pie charts show the average mass concentration and chemical composition: organics (green), sulfate (red), nitrate (blue), ammonium (orange), and chloride (purple) (Zhang et al., 2007).

### 1.3: Secondary Organic Aerosol

There are a multitude of reaction pathways that lead to the creation of SOA. SOA

is a subset of aerosols formed by the mass transfer to the condensed phase of low volatility products specifically derived from an organic parent gas. It is estimated that 70% of global organic aerosols are SOA (Zhang et al., 2007). As mentioned above, secondary species can partition between the gas and particle phase depending on temperature, dilution, and the amount of surface area of existing aerosol. This process can be described by equilibrium partitioning models that will be discussed in Section 1.4. Once there exists SOA, these compounds can undergo reactions to convert into different chemical compounds.

There is an abundance of evidence that SOA contributes to global cooling (Volkamer et al., 2006) and causes deleterious effects on human health (Baltensperger et al., 2008). These radiative forcings and health effects of aerosols give these compounds real world significance, so it is essential to understand the chemical processes that govern their formation. This analysis focuses on mechanisms of SOA formation in an attempt to better understand how, why, and where SOA exists.

The sections that follow provide a more detailed treatment of each component of understanding the production of SOA: parent precursor volatile organic compounds (VOC), oxidants, and yields.

### **1.3.1: Volatile Organic Compounds**

The term volatile organic compound is used to denote the entire set of gas-phase atmospheric organics excluding CO and CO<sub>2</sub> (Seinfeld and Pandis, 2006). VOCs are emitted from both human-made and natural sources. Many scents and odors that humans smell are VOCs. In terms of aerosol formation, VOCs act as parent precursor gases that initiate atmospheric oxidative cycles that lead to the formation of secondary aerosol.

In terms of the types of VOC sources, anthropogenic species include aromatic hydrocarbons and high molecular weight alkanes and alkenes produced by industrial processes. In addition, biogenic species that have the potential to form aerosols include isoprene (C<sub>5</sub>H<sub>8</sub>), monoterpenes (C<sub>10</sub>H<sub>16</sub>), and sesquiterpenes (C<sub>15</sub>H<sub>24</sub>) emitted from

vegetation. These emitted VOCs eventually react with oxidants in the atmosphere to create secondary products that partition between the gas and aerosol phases.

On a global scale, VOCs of biogenic origin contribute significantly more to SOA formation than those from anthropogenic sources (Hoyle et al., 2011). Perhaps this claim sounds paradoxical, as emissions from the biosphere are considered natural, while anthropogenic emissions are considered harmful pollutants. Yet, the biosphere produces more climate- and health-harming SOA than do humans (Hoyle et al., 2011). However, this fact is not unusual if we compare the emissions of VOCs from the terrestrial biosphere to those from humans. That is, the biosphere contributes 1007 Tg/yr of VOCs to the atmosphere (Guenther et al., 2012) while anthropogenic sources contribute only ~130 Tg/yr of VOCs (Lemarque et al., 2010). This discrepancy is not unbelievable if we consider that urban areas occupy only 2-3% of the Earth's surface (WRI 1998).

Although the global source of VOC is mainly biogenic, the conversion of biogenic VOCs to SOA often utilizes an anthropogenic input in the form of an oxidant (Hoyle et al., 2011). This mechanism suggests that anthropogenic pollution further enhances SOA formation. In addition, it must be reiterated that SOA can be produced by both an anthropogenic and a biogenic source. For the purposes of this thesis, the biogenic source will be the main focus.

The most dominant class of BVOCs in SOA formation is thought to be the monoterpenes (Sakulyanontvittaya et al., 2008). Monoterpenes are a class of aerosol precursors that are emitted predominantly by conifers and are thought to defend against herbivory (Griffin et al., 1999b). Due to their diverse chemical structures, which include endo- and exocyclic double bonds, monoterpenes have high reactivity and are readily oxidizable. These gas-phase compounds include  $\alpha$ -pinene,  $\beta$ -pinene,  $\Delta$ -carene, and limonene, among others. Furthermore, because monoterpenes are generally emitted from conifers there is a certain regional variability associated with their BVOC emissions and concomitant SOA formation. For example, SOA formation from monoterpenes is predicted to account for 60-75% of total SOA over the northwestern and northeastern United States; however, conifers are not abundant in the American southwest so very little SOA from monoterpenes is formed there (Liao et al., 2007). Instead 60-75% of SOA in the southwestern United States is formed by another terpene, isoprene, which is

emitted from deciduous trees. Because of its smaller size ( $C_5H_8$ ), isoprene has generally lower SOA percent yields, but its high abundance globally somewhat offsets its relatively lower yield. In Figure 1.3, notice the high percentage of  $\alpha$ -pinene and  $\beta$ -pinene in the Pacific Northwest due to a high concentration of conifers. Conversely, the Northeast, Midwest, and Appalachian regions have more deciduous-broadleaf forests and their monoterpene composition is much more varied.

Moreover, another example of regional variability involves the monoterpene sabinene. Although sabinene exists in trace amounts in the United States and has very small global production relative to the other terpene species, it is a dominant source of SOA in rural Europe as several native trees produce sabinene in abundance (Carrasco et al., 2006).

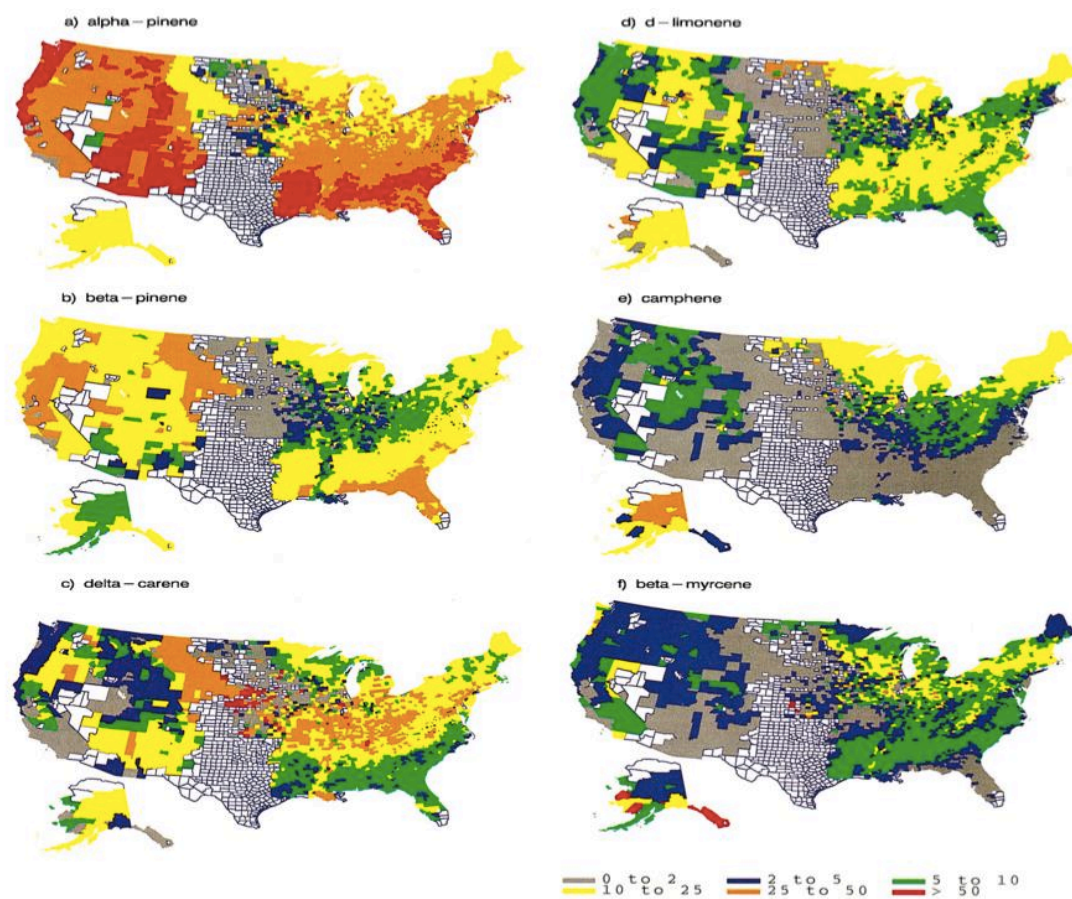


Figure 1.3: Regional distribution of monoterpenes in the United States

Maps showing the percentage of estimated total monoterpene emission ( $\alpha$ -pinene,  $\beta$ -pinene,  $\Delta$ -carene, limonene, camphene, and myrcene) during summertime conditions (Geron et al., 2000).

To be sure, BVOC emissions from vegetation are the dominant parent precursors to SOA formation. However, these emissions from the biosphere are regionally diverse. Because SOA yields also vary substantially for different BVOC (see Section 1.3.3 below), in order to understand spatially variable SOA concentrations, we must track these speciated BVOCs.

### 1.3.2: Oxidants

VOCs are oxidized in the atmosphere dominantly by the hydroxyl radical (OH) during daylight hours and by nitrate radicals (NO<sub>3</sub>) during the night. Ozone (O<sub>3</sub>) oxidation also occurs throughout the day and night, but is not the focus of this thesis. OH radicals are an abundant oxidant in the atmosphere during the day, because they are photochemically produced from the decomposition of hydroperoxides (ROOH) or by the reaction of excited atomic oxygen with water in the atmosphere. NO<sub>3</sub> is predominantly a nighttime oxidant because it is rapidly photolyzed to NO<sub>2</sub> + O by visible light. Radical species such as OH and NO<sub>3</sub> are highly reactive as they have an unpaired valence electron. These unpaired electrons, called free radicals, have a high affinity to pair with other unpaired electron and thus are highly chemically reactive with other molecules.

A general mechanism for VOC + OH chemistry involves a hydrogen removal from a VOC forming water and an alkyl radical (R). For the sake of convention, because radicals are ubiquitous in the atmosphere, atmospheric chemists typically do not include notation for them in chemical equations. Thus, an “OH” is actually a “•OH” and similarly for other compounds.



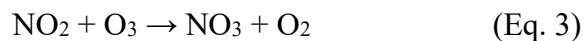
This alkyl radical will typically react rapidly with oxygen forming a peroxy radical, or rather, an oxidized VOC.



Generally, the OH radical has received the most attention for its role in SOA formation

due to its rapid reactivity (Griffin et al., 1999a). However, OH is only created during the day, as it needs the dissociative energy from the sun to be chemically produced.

At night, NO<sub>3</sub> is the dominant oxidant and is produced from anthropogenic NO<sub>x</sub> emissions in the form of NO<sub>2</sub> reacting with O<sub>3</sub>.



In previous studies of atmospheric oxidation, many thought that NO<sub>3</sub> was insignificant to SOA formation as it was believed that most emitted biogenic hydrocarbons reacted with OH primarily during the day and that only ~9% reacted at night with NO<sub>3</sub> (Chung and Seinfeld, 2002). In addition, NO<sub>3</sub> is known to photolyze rapidly under visible radiation and thus was considered unavailable during daylight hours for reactions (Geyer et al., 2002). In short, NO<sub>3</sub> was seen as an inconsequential oxidant vis-à-vis the OH radical.

However, recent studies have begun to find that NO<sub>3</sub> oxidation is more prevalent than formerly believed. For example, a recent field campaign in the southeastern United States revealed that BVOC reactions with NO<sub>3</sub> actually compete with photolysis during the day (Figure 1.4). According to this study, approximately half the daytime losses of NO<sub>3</sub> are due to reactions with BVOCs, meaning that oxidation by NO<sub>3</sub> is actually more available during the day than previously thought. In addition, the next section reveals through chamber experiments that NO<sub>3</sub>-VOC chemistry yields much more SOA than previously predicted. These new findings in NO<sub>3</sub> chemistry dramatically change our temporal and spatial understanding of the role that atmospheric oxidants play in SOA formation.

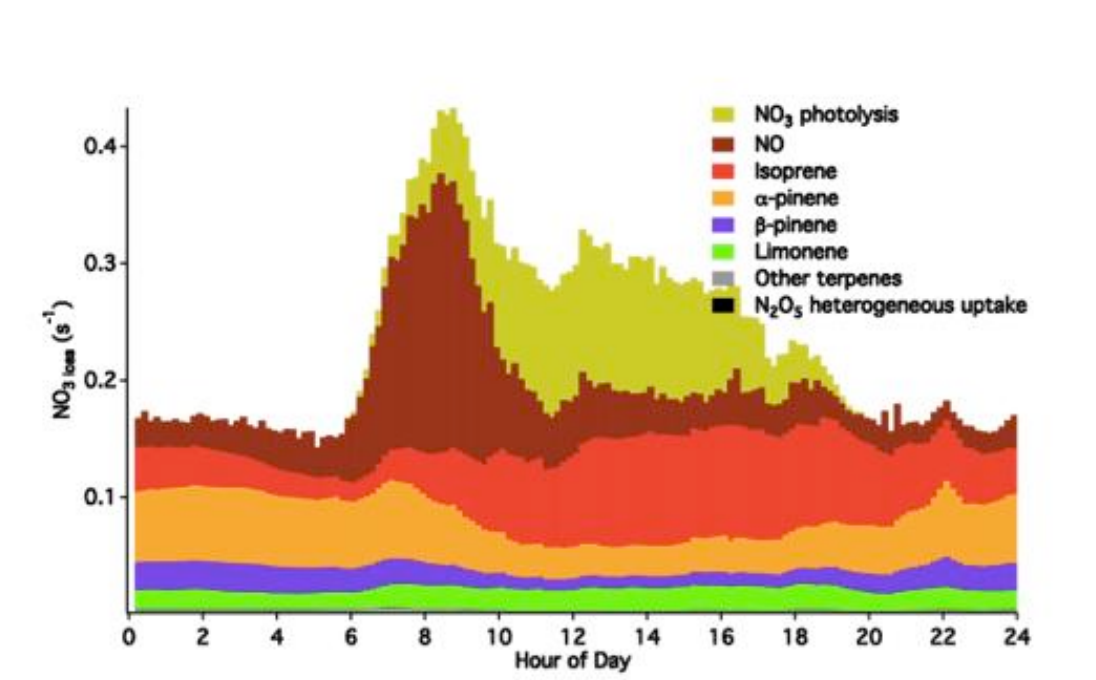


Figure 1.4: Alabama field campaign data of  $\text{NO}_3$ -terpene measurements  
Average diurnal profile of  $\text{NO}_3/\text{N}_2\text{O}_5$  losses from 1 June–15 July 2013 in central Alabama (Ayres et al., 2015). Notice that  $\text{NO}_3$  reactions to terpenes compete with photolysis during the daytime, because of the high reactivity in this forest ecosystem in hot weather when BVOC emissions are high.

### 1.3.3: Chamber Experiments and Yields

Experiments conducted in an environmental aerosol chamber are studies that attempt to recreate the composition of the atmosphere *in vitro* in order to study specific mechanisms, such as SOA formation from terpenes. Typically composed of a large Teflon bag and various inlets for reagents and dilution flows, atmospheric chambers provide empirical data of fractional aerosol yield ( $Y$ ) given total organic aerosol mass formed ( $C_{OA}$ ) and amount of hydrocarbon VOC consumed ( $\Delta HC$ ).

$$Y = \frac{C_{OA}}{\Delta HC} \quad (\text{Eq. 4})$$

Most chamber studies of atmospheric oxidation of monoterpenes have focused on OH- and  $\text{O}_3$ -initiated oxidation, while only a few have studied the role of  $\text{NO}_3$ .

Previously, monoterpenes were believed to yield little aerosol when oxidized by NO<sub>3</sub>.

Table 1.1 displays aerosol yields from various NO<sub>3</sub>-initiated oxidation chamber studies.

Table 1.1: Reported SOA yields from chamber experiments

Yields from a variety of NO<sub>3</sub>-initiated SOA formation experiments with  $\alpha$ -pinene,  $\beta$ -pinene,  $\Delta$ -carene, limonene, and sabinene. Because SOA yields depend on existing aerosol volume, these yields may depend on the amount of reacted hydrocarbon ( $\Delta$ H<sub>C</sub>).

Reaction	$\Delta$ H <sub>C</sub> ( $\mu$ g/m <sup>3</sup> )	Literature SOA Yield	Reference
$\beta$ -pinene + NO <sub>3</sub>		10%	Hallquist et al., 1999
$\beta$ -pinene + NO <sub>3</sub>	32.4	32.2%	Griffin et al., 1999a
$\beta$ -pinene + NO <sub>3</sub>	41	46%	Fry et al., 2009
$\beta$ -pinene + NO <sub>3</sub>	34.8	52.7%	Nah et al., 2015
$\alpha$ -pinene + NO <sub>3</sub>		0.2%	Hallquist et al. 1999
$\alpha$ -pinene + NO <sub>3</sub>		4.3%	Spittler et al., 2006
$\alpha$ -pinene + NO <sub>3</sub>	10	0 %	Fry et al., 2014
$\alpha$ -pinene + NO <sub>3</sub>	2.5	3.6%	Nah et al., 2015
$\Delta$ -carene + NO <sub>3</sub>		15%	Hallquist et al., 1999
$\Delta$ -carene + NO <sub>3</sub>	24.4	12.5%	Griffin et al., 1999a
$\Delta$ -carene + NO <sub>3</sub>	10	21%	Fry et al., 2014
Limonene + NO <sub>3</sub>		17%	Hallquist et al., 1999
Limonene + NO <sub>3</sub>		40.4%	Spittler et al., 2006
Limonene + NO <sub>3</sub>	10	30%	Fry et al., 2011
Sabinene + NO <sub>3</sub>	24.3	13.8%	Griffin et al., 1999a
Sabinene + NO <sub>3</sub>	10	25-45%	Fry et al., 2014

However, more recent studies have found substantially higher yields for some monoterpenes (e.g. limonene) than others (e.g.  $\alpha$ -pinene), with large variability depending on VOC precursor and organic aerosol loading (Table 1.1). In several cases, experiments in different chambers found widely different SOA yields even for the same

precursor and loading, suggesting that there are also other experimental parameters controlling SOA yield that are not yet fully understood.

In past model simulations,  $\beta$ -pinene aerosol yields have been used as surrogate values for all the bicyclic monoterpene species ( $\alpha$ -pinene,  $\beta$ -pinene,  $\Delta$ -carene, and sabinene) due to their comparable structures (Pye et al., 2010). However, recent chamber studies reveal that little to no aerosol forms from the  $\text{NO}_3$ -initiated oxidation of  $\alpha$ -pinene (Fry et al., 2014). Although the reason behind the lack of SOA formation from  $\text{NO}_3$ - $\alpha$ -pinene oxidation is still unknown, the variability in SOA formation from different precursors must be taken into account.

To be sure, many recent chamber experiments have contradicted the traditional surrogacy and aerosol mass yields of monoterpene- $\text{NO}_3$  oxidation. However, these new studies better correlate with the latest field measurements (Figure 1.4) and have significantly changed the understanding of the relative importance of  $\text{NO}_3$  oxidation to SOA formation. In order to achieve an even greater understanding of all these novel discoveries on a global scale, these yields must be implemented *in silico* using a chemical transport model.

## 1.4: Traditional Absorptive Partitioning Models

In order to understand how SOA chemistry functions in a chemical transport model, an overview of absorptive partitioning models to describe SOA formation is needed. As mentioned, SOA formation involves the reaction of a parent organic gas with an oxidant that leads to a secondary organic compound. Oftentimes SOA is not initially produced from a VOC-oxidant reaction but rather from a lower volatility gas-phase compound stemming from a multigenerational chemical product. These compounds are considered semivolatile organic compounds (SVOCs) as they have a “medium” volatility that can either partition into the aerosol or gas phase depending on certain physicochemical properties. A parameter that describes this partitioning of a species between the gas and aerosol phase is the equilibrium partitioning coefficient defined as:

$$K_p = \frac{C_{aerosol}}{M_0 C_{gas}} \quad (\text{Eq. 5})$$

where  $K_p$  is a temperature-dependent partitioning coefficient ( $\mu\text{g}/\text{m}^3$ ),  $M_0$  is total ambient aerosol mass concentration ( $\mu\text{g}/\text{m}^3$ ), and  $C_{aerosol}$  and  $C_{gas}$  are the concentrations of the condensed and gas-phase species partitioned between the two phases ( $\mu\text{g}/\text{m}^3$ ), respectively (Seinfeld and Pandis, 2006). Essentially, Eq. 5 is a ratio that describes the behavior of a compound's tendency to be in either the gas or aerosol phase. A larger  $K_p$  implies more of the organic compound in the aerosol phase. The theory of the absorptive partitioning model is that when there is more pre-existing aerosol mass, a greater proportion of new semi-volatiles will partition to the aerosol phase.

In terms of gas/aerosol partitioning parameterizations, secondary aerosol formation relies heavily on organic particles. A field study by Liang et al. (1997) calculated  $K_p$  values for n-alkanes sorbing to ambient aerosol during summertime smog events in Pasadena, California. They found that the partitioning of SVOCs to aerosol was primarily governed by absorption into the organic fraction of aerosol. Consequently, even for an inorganic aerosol, once an organic layer is formed, gas-aerosol partitioning is dominated by absorption to that organic layer.

In order to understand SOA formation in terms of aerosol-partitioning behavior, absorptive partitioning models derive equilibrium partitioning coefficients from aerosol chamber yields to characterize partitioning tendencies of SVOCs from particular precursors. Originally, SOA formation from the oxidation of parent VOCs in partitioning models implemented fixed aerosol product yields from reacted nonvolatile organic compounds (Pandis et al., 1991). However, with an increasing number of chamber studies and a greater understanding of SOA mechanisms, current partitioning models employ free parameter product yields and volatilities from a range of reacted semi-volatile parent hydrocarbon systems to better describe SOA yields at differing existing aerosol concentrations (Donahue et al., 2006). The yields of aerosol from a given VOC-oxidant pair can be parameterized using two common absorptive partitioning models: Odum 2-product model and Volatility Basis Set (VBS).

### 1.4.1: Odum 2-Product Model for SVOC Partitioning

The Odum 2-product model uses measured aerosol mass fractions from chamber studies to generate parameters related to partitioning of SVOCs. Odum et al. (1996) represented SOA yield ( $Y$ ) as the mass of aerosol formed per mass of VOC reacted as:

$$Y = M_0 \sum_{i=1}^n \frac{\alpha_i K_{pi}}{1 + M_0 K_{pi}} \quad (\text{Eq. 6})$$

where  $M_0$  is the amount of absorbing material,  $K_{pi}$  is the equilibrium partitioning coefficient, and  $\alpha_i$  is the mass-based stoichiometric coefficient for the SVOC indicating the mass of SVOC produced per mass of parent VOC reacted. Note that, as a result of the increase in molecular weight upon reaction, the aerosol yield can exceed 1.0. In principle, the number of product SVOCs that can be lumped together with various yields and partitioning coefficients can be as large as desired, but in the application of the Odum 2-product model only two SVOC surrogates are lumped. Thus, empirical data from chamber studies use Eq. 6 to regress the data to fit four parameters ( $\alpha_1$ ,  $\alpha_2$ ,  $K_{p,1}$ , and  $K_{p,2}$ ) for a two-product model.

The Odum 2-product partitioning model is computationally efficient because it requires only two surrogate species per parent VOC. However, lumping multiple VOC systems together requires more data manipulation.

### 1.4.2: Volatility Basis Set Model for SVOC Partitioning

In relation to the Odum 2-product model, the alternative volatility basis set (VBS) formalism employs more SVOC surrogates; usually four per parent VOC-oxidant system (Pathak et al., 2007). However, combining multiple systems using a basis set of surrogate compounds characterized by fixed partitioning coefficients instead of applying species-specific, variable partitioning coefficients is more straightforward (Stainer et al., 2007). For the VBS model, partitioning coefficients can be described interchangeably as effective saturation concentrations ( $C^*$ ). Essentially, a “basis set” of  $C^*$  values (separated by an order of magnitude) is chosen and fit data is derived by fitting the branching ratio between the products found in each volatility bin produced by a given reaction. As a

result, multiple reactions can be mapped onto the same fixed “basis set” of  $C^*$ 's, instead of fitting only two  $K_p$ 's for each reaction, such as in the Odum-2 product model. Thus, for more complex models with many precursors, the final computation will actually be less intensive.

The parameterization for a VBS involves determining values of  $C^*$  and  $\alpha$  so that modeled SOA yields match experimental chamber data. This fitting is done by a nonlinear least squares regression. The regression is straightforward, but there are several challenges related to this parameterization as seen in Figure 1.5 such as selecting the number of basis set saturation concentration bins to use and deciding whether to fix the  $C^*$  values or attempt to optimize them in the regression.

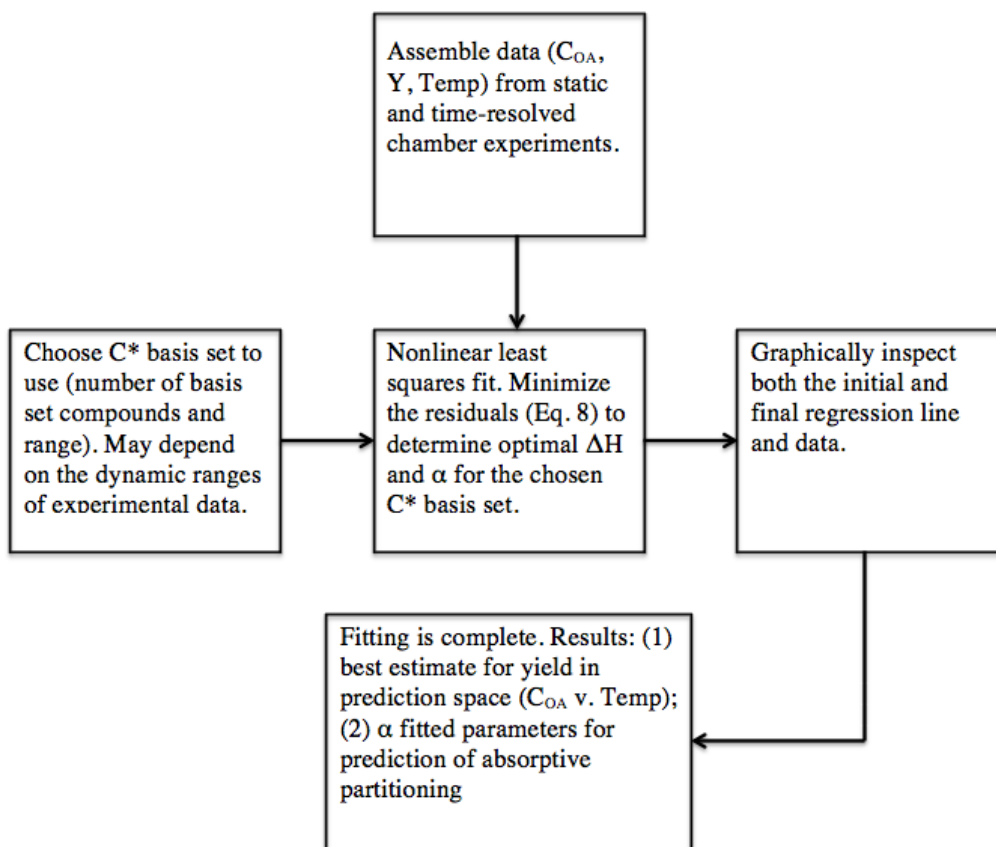


Figure 1.5: VBS parameter fitting procedure

Flow chart of VBS parameter fitting algorithm, adapted from Stainer et al. (2007).

According to Stainer et al. (2007) using fixed  $C^*$  values are advantageous. A fixed basis set of  $C^*$ s reduces the natural covariance between  $\alpha$  and  $C^*$  values through the reduction in the number of surrogate species necessary in a chemical transport model, because the products of different precursors can be lumped into the same volatility bin. As a result, a common basis set includes a subset of:

$$C_i^* = \{0.01, 0.1, 1, 10, 100, 1000, 10000, 100000\} (\mu\text{g}/\text{m}^3) \quad (\text{Eq. 7})$$

where  $C_i^*$  is the basis set of effective saturation concentrations. Most commonly, a set of four  $C^*$  values separated by an order of magnitude each and spanning typical atmospheric aerosol loading are used; for example, for the global model used in this thesis, the volatility bins used are 0.1, 1, 10, 100.

Once a basis set is chosen, a nonlinear least squares regression can be performed to minimize the measurement-to-model residuals:

$$\sum_{i=1}^n [\xi - \hat{\xi}(\alpha_i, \Delta H, C_i^*(T_{ref}), T_{ref}, C_{OA}, T)]^2 \quad (\text{Eq. 8})$$

where  $\xi$  is the measured SOA yield (empirical data) and  $\hat{\xi}$  is the modeled yield calculated using Eq. 9, which minimizes the difference between the observed yield and the yield predicted using the VBS parameters. The modeled aerosol mass fractions yields are calculated using a fixed reference temperature ( $T_{ref}$ ) and empirically derived variables  $C_{OA}$  and  $T$  (temperature). The variable parameters are  $\alpha_i$  and  $\Delta H$  (enthalpy of evaporation). Fixed saturation concentrations  $C_i^*$  are used from the basis set.

$$\frac{C_{OA}}{\Delta ROG} = \zeta = \sum \frac{\alpha_i}{1 + \left(\frac{C_i^*}{C_{OA}}\right)} \quad (\text{Eq. 9})$$

Many VBS calculations assume an organic aerosol density of 1 g/cm<sup>3</sup> to convert the typically measured aerosol volume density to an aerosol mass loading ( $C_{OA}$ ). However, there is uncertainty about the density of organic aerosol. Although the density is assumed to be unity, in order to unify across different laboratory datasets, there have been laboratory and field studies that have measured the organic fraction of aerosol to have a density of ~1.2 g/cm<sup>3</sup> (Turpin and Lim, 2001). As a result, if a density other than unity is assumed, then a density correction must be applied to Eq. 9:

$$\frac{C_{OA}}{\Delta ROG} = \zeta = \sum \rho \frac{\alpha_i}{1 + \left(\frac{C_i^*}{C_{OA}}\right)} \quad (\text{Eq. 10})$$

where  $\rho$  is the specified organic aerosol density. Similar updated density calculations can be performed to solve for  $C_{OA}$  and  $\zeta$ .

Although VBS calculations are more involved than the Odum 2-product model, there is much greater computational efficiency when lumping multiple VOC-oxidant systems that have greater than two SVOCs per parent hydrocarbon. In addition, using a 4-product VBS scheme can allow the parameterization to fit over a larger range of mass loadings since  $C^*$  can be spanned over a broader range.

## **1.5: A Paradox: Anthropogenic Emissions Enhance Biogenic SOA?**

Most of the prior discussion of SOA formation has been about the precursor BVOC emissions from nature. However, there is a paradox concerning SOA measurements in that SOA plumes in both urban (50%) and remote areas (80-100%) have been correlated with anthropogenic sources (Schichtel et al., 2008). That is, biogenic species can form SOA without any anthropogenic VOCs; however, biogenic SOA can be enhanced by anthropogenic activity when the latter enhances oxidation and thus lowers the volatility of more of the BVOC emissions.

Although nature is the major source of VOCs, anthropogenic enhancement of these emissions is quite significant. According to Hoyle et al. (2011), anthropogenic VOC and particulate matter (PM) contribute directly to the total organic aerosol (OA) burden both in and downwind of urban areas. Anthropogenic emissions from fossil fuel combustion, meat cooking, and biomass burning are direct sources of anthropogenic SVOCs and POAs. These anthropogenic PM surfaces provide thermodynamically and kinetically favorable scenarios for biogenic compounds to condense. For example, in terms of equilibrium gas/aerosol partitioning, an increase in aerosol leads to a shift in partitioning from the gas to the condensed phase, therefore increased anthropogenic

emissions of organic PM and SVOCs may contribute to an overall shift of biogenic emissions from the gas to the aerosol phase.

Certainly, SOA formation cannot be constrained solely to the biosphere. The atmosphere is a dynamic chemical system that interconnects all regions of the planet, from the urban to the remote. As a result, every source of emission must be taken into account as they all have the ability to contribute to air pollution.

## **1.6: Model-to-Measurement Discrepancies in SOA Loading**

Although SOA comprises the largest portion of total organic aerosol globally, estimates of total organic aerosol flux vary dramatically among different predictions. When compared to aerosol measured in field campaigns, global chemical transport models tend to under-predict aerosol concentrations up to two orders of magnitude (Heald et al., 2011). Figure 1.6 presents the model-to-measurement discrepancy of organic aerosol for seventeen field campaigns spanning five continents. Certainly, the model underestimates aerosol concentrations in both urban and remote areas. Because this underprediction occurs across the board, missing source pathways or overestimated sinks are suspected in global atmospheric chemistry models. Substantial laboratory chamber experiment research efforts have been made to identify these missing sources and refining understanding of sink mechanisms.

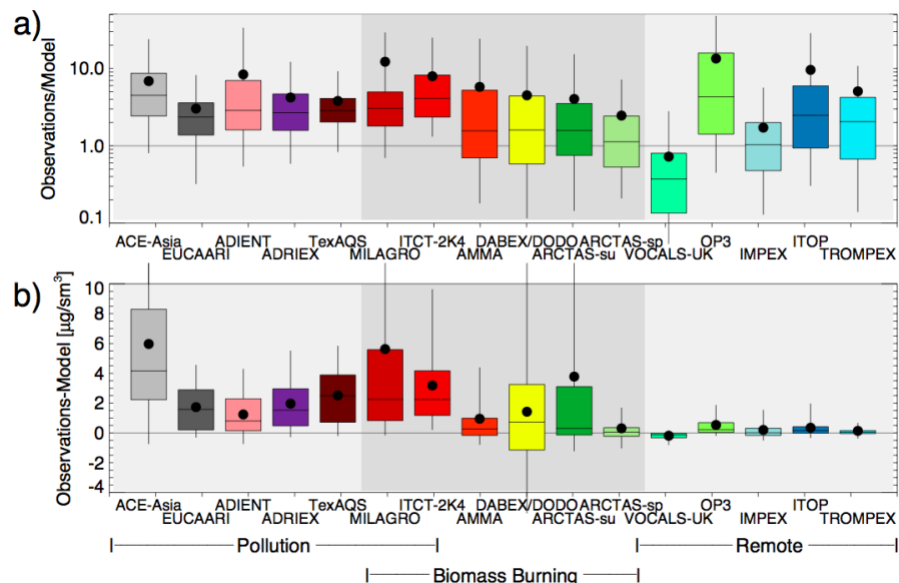


Figure 1.6: Multi-study comparison of modeled vs. observed ambient organic aerosol concentrations

Distribution of (a) ratio and (b) difference in observed and simulated (GEOS-Chem) OA concentrations for 17 field campaigns. Means of the gridded comparisons are shown as a solid dot, median as a horizontal line. The boxes denote 25th and 75th percentile, whiskers denote 5th and 95th percentile (Heald et al., 2011).

## 1.7: Chemical Transport Models and GEOS-Chem

Global three-dimensional models of tropospheric chemistry are becoming standard tools for improving knowledge of chemical budgets and processes in the atmosphere. They can be used to produce chemical air quality forecasts and provide *a priori* estimates for satellite retrieval to examine climate-chemistry interactions (Bey et al., 2001). They also may be used to guide international environmental policy makers such as the Intergovernmental Panel on Climate Change (IPCC, 2013).

Perhaps the most characteristic aspect of chemical transport models vis-à-vis other atmospheric and meteorological models are the state-of-the-science oxidative chemistry reaction mechanisms. Many meteorological models such as general circulation models focus on simulating overall atmospheric dynamics such as weather patterns, while chemical transport models focus on the stocks and flows of chemical species through

sophisticated O<sub>3</sub>-NO<sub>x</sub>-VOC chemistry. This O<sub>3</sub>-NO<sub>x</sub>-VOC chemistry is central to the model and is used to determine radical and oxidant processes affecting tropospheric composition. In addition, a number of independently developed models have been reported in the literature over the past few years (e.g., Collins et al., 1997: 3-D Lagrangian model with UK Meteorology Office global model; Brasseur et al., 1998: MOZART ozone chemical transport model; Lawrence et al., 1999: MATCH-MPIC atmospheric photochemistry and transport model; Levy et al., 1999: Geophysical Fluid Dynamics Laboratory global chemical transport model). They share similar theoretical foundations but differ in many ways including resolution, the driving meteorological fields, and the approaches for simulating emissions, chemical processes, and deposition.

There are many problems with chemical transport models such as the large number of chemical species involved (>100), the sometimes nonlinearity of the chemical kinetics, and the numerical stiffness of the system. It is not unusual for these models to be composed of a series of modules, each of which has its own specific meteorological and/or chemical inputs that calculate the stocks and flows of species, and are in turn processed among other modules. Indeed, there are a lot of “moving parts” in chemical transport models that create plenty of room for errors. Refer to Figure 1.7 for an example of the many elements found in a chemical transport model.

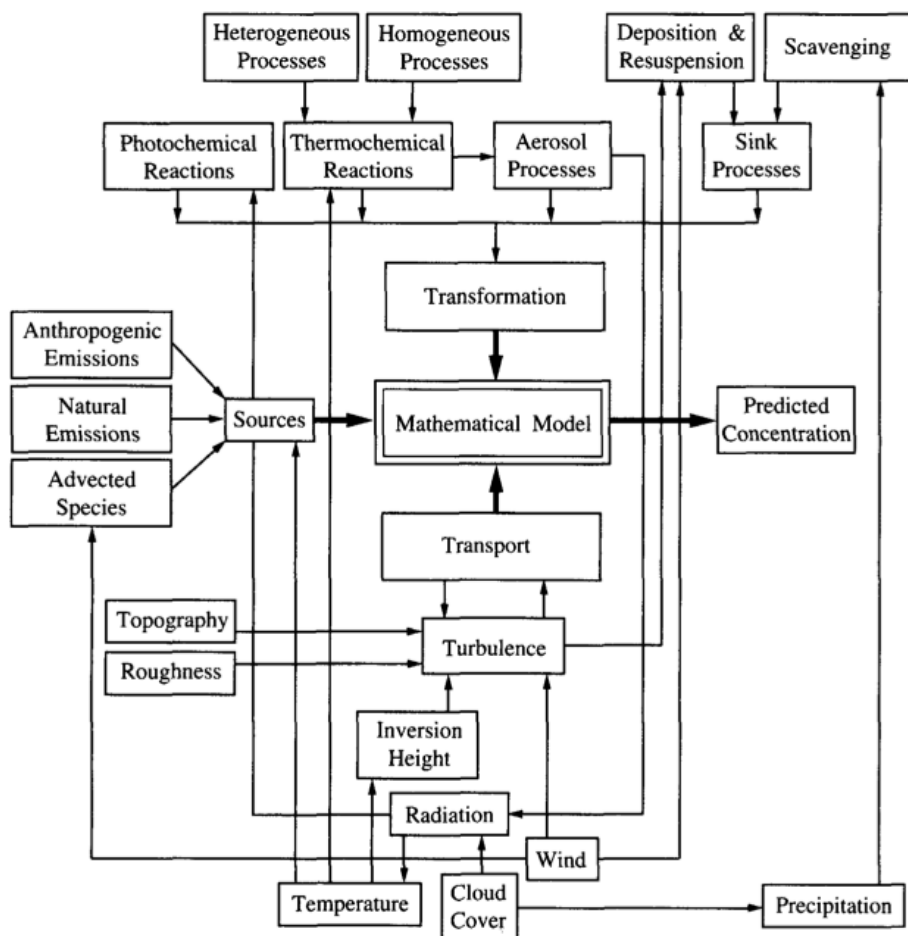


Figure 1.7: Elements of a mathematical atmospheric chemical transport model

Chemical transport models contain complicated interrelationships between chemistry, meteorology, and computer science (Seinfeld and Pandis, 2006).

We desire highly accurate model-to-measurement comparison simulations not only to predict how much of a chemical species exists at a certain time and place, but also to understand fundamentally why and how the atmosphere behaves as observed. The more accurate the output of a model simulation is to observations, the closer we are to more fully understanding atmospheric phenomena that affects our climate and human health.

For the purposes of this thesis, the chemical transport model GEOS-Chem will be used. GEOS-Chem is a global three-dimensional chemical transport model for atmospheric composition driven by meteorological input from the Goddard Earth Observing System (GEOS) of the NASA Global Modeling and Assimilation Office. It is

employed by research groups around the world to study a wide range of atmospheric problems. The model is managed by the GEOS-Chem Support Team, based at Harvard University and Dalhousie University, with support from the US NASA Earth Science Division and the Canadian National and Engineering Research Council (GEOS). More about GEOS-Chem's model framework will be discussed in the Methods section.

Overall, chemical transport models can be used to answer a multitude of research questions. They can be used to interpret atmospheric observations and provide source-receptor relationships to understand how concentrations at a specific location exist. Chemical transport models allow for the calculation of global and regional budgets of atmospheric species, which may allow for future projections of an array of scenarios. In addition, they may provide a model comparison for retrieval of satellite observations of atmospheric composition. To be sure, there is an inexhaustible number of ways a chemical transport model can be used for research, limited only by human ingenuity.

### **1.7.1: Nitrate Parameterizations in GEOS-Chem**

Much of the premise of this thesis was inspired by Dr. Havala Pye's paper on the importance of reactive nitrogen ( $\text{NO}_x$  and  $\text{NO}_3$ ) on the global modeling of organic aerosol (Pye et al., 2010). Her SOA scheme in the GEOS-Chem model is depicted in Figure 1.8. For the purposes of this thesis, the biogenic emissions pathway is highlighted. Biogenic emissions from a separate model called the Model of Emissions of Gases and Aerosols from Nature (MEGAN2.1) have been inputted into the SOA module, which are then lumped into more specific tracers such as the bicyclic monoterpenes ( $\alpha$ -pinene,  $\beta$ -pinene,  $\Delta$ -carene, sabinene), sesquiterpenes, and isoprene. Once lumped into these tracers, these VOC species undergo reactions with specific oxidants ( $\text{OH}$ ,  $\text{O}_3$ , and  $\text{NO}_3$ ) and are then sequestered into four SOG (secondary organic gas) volatility bins according to specified VBS saturation concentrations, which in this case are 0.1, 1, 10, 100  $\mu\text{g}/\text{m}^3$ . Depending on the partitioning coefficients of the species and the calculated  $\alpha$  values fitted from the VBS calculations, SOG species may partition into SOA in the model.

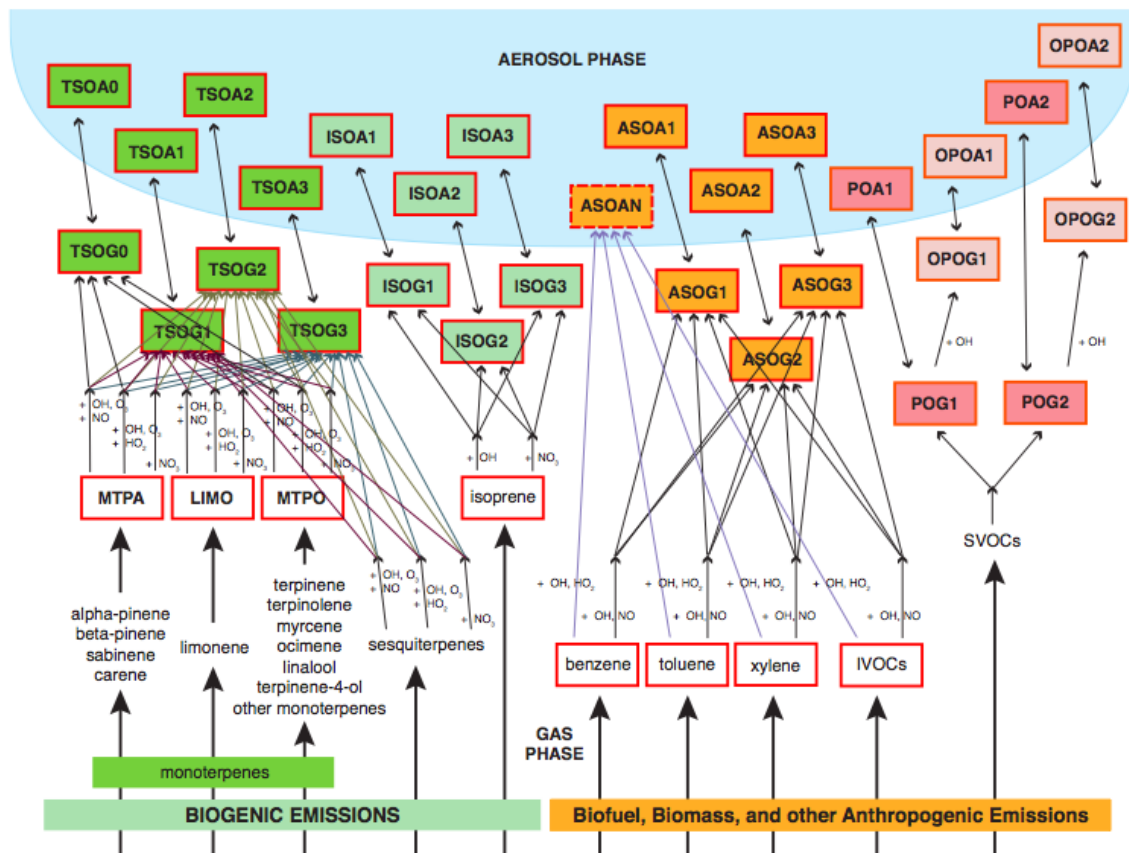


Figure 1.8: GEOS-Chem SOA mechanistic pathway

Schematic of SOA module in GEOS-Chem. Species appearing in boxes are tracers. A bidirectional arrow across the aerosol/gas interface indicates a semivolatile species. ASOAN is nonvolatile. SOA/G0-3 species have saturation concentrations of 0.1, 1, 10, 100  $\mu\text{g}/\text{m}^3$ . For a traditional simulation, POA are treated as nonvolatile. (Pye et al., 2010).

GEOS-Chem version 10-01i parameterizes all terpene (monoterpene and sesquiterpene) derived SOA from the  $\text{NO}_3$  oxidation pathway based on  $\beta$ -pinene experiments by Griffin et al. (1999a) found in Table 1.1. A density of 1.3  $\text{g}/\text{cm}^3$  was used. In the context of the model, VBS  $\alpha_i$  values are used to specify yields from different oxidant-VOC systems. These parameterized yields are obtained by treating all monoterpenes, including  $\alpha$ -pinene, as if they were  $\beta$ -pinene reacting with  $\text{NO}_3$ . However,  $\alpha$ -pinene is thought to produce little to no SOA (Fry et al. 2014), so this lumping scheme is seemingly inaccurate. In addition, Figure 1.9 reveals that SOA is in fact enhanced by

NO<sub>3</sub> reactions to terpenes in the GEOS-Chem model, meaning that nitrate is a significant oxidant in the model.

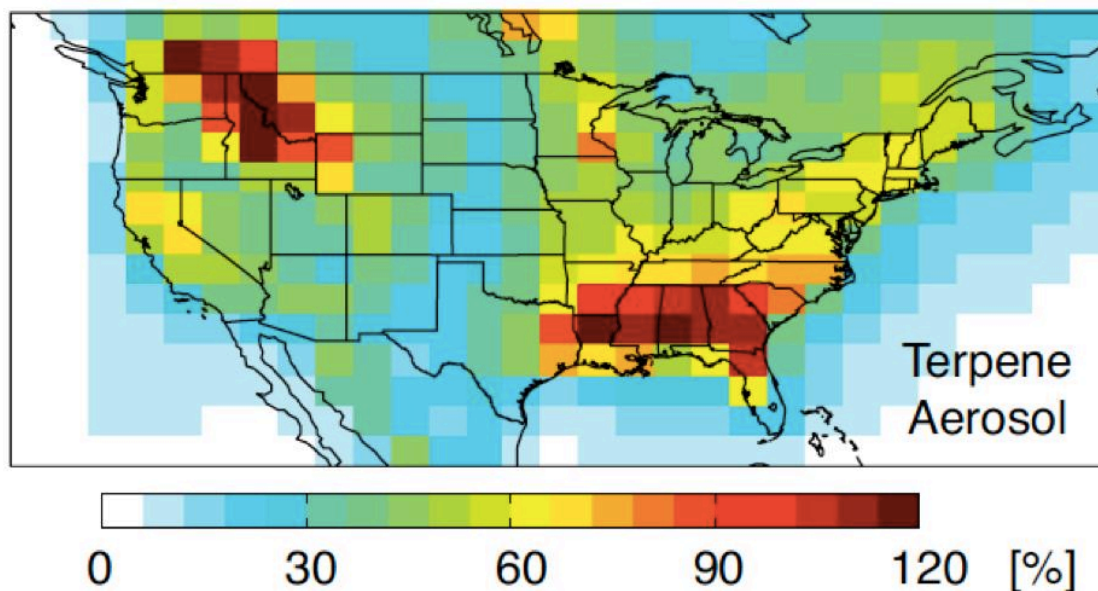


Figure 1.9: Enhancement in surface-level SOA in August 2000 from terpenes from the nitrate oxidation pathway

The change is relative to a simulation with yields set to zero for nitrate oxidation. (Pye et al., 2010).

This thesis will attempt to understand what happens as a result of unlumping  $\alpha$ -pinene from this NO<sub>3</sub> parameterization and speciating it with its own yields. On the Earth,  $\alpha$ -pinene is a dominant BVOC, contributing up to a third of all monoterpene emissions based on the region (Geron et al., 2000). However, based on  $\alpha$ -pinene emissions, the species is also a spatially variable fraction of BVOC. To reiterate, in our current models,  $\alpha$ -pinene-NO<sub>3</sub> chemistry is parameterized with  $\beta$ -pinene-NO<sub>3</sub> SOA yields. However, recent chamber studies (Table 1.1) indicate that  $\alpha$ -pinene-NO<sub>3</sub> reactions actually produce a yield closer to zero for SOA formation. Given that NO<sub>3</sub> has been shown to increase SOA formation (Figure 1.9) and that the  $\alpha$ -pinene-NO<sub>3</sub> pathway is not as effective as producing SOA as previously thought, the scientific question examined by this thesis is how will implementing a  $\alpha$ -pinene-NO<sub>3</sub> SOA yield of zero affect regional and global distribution of SOA.

Perhaps implementing this updated scheme might help improve the predictive skill of the spatial distribution of SOA loading. Ultimately, any model output should be compared to field and satellite data to test the accuracy of model simulations. An example of a potential model-to-measurement analysis is found in Figure 1.10. To be sure, there will be a change in total global SOA produced, as  $\alpha$ -pinene will not contribute any aerosol to the budget. However, there may also be a stark change in the regional distribution of SOA if aerosol production from  $\alpha$ -pinene is essentially “turned off”. This study shall explore the effects of this mechanistic pathway change and its implications for chemical transport models and tropospheric SOA as they are now understood.

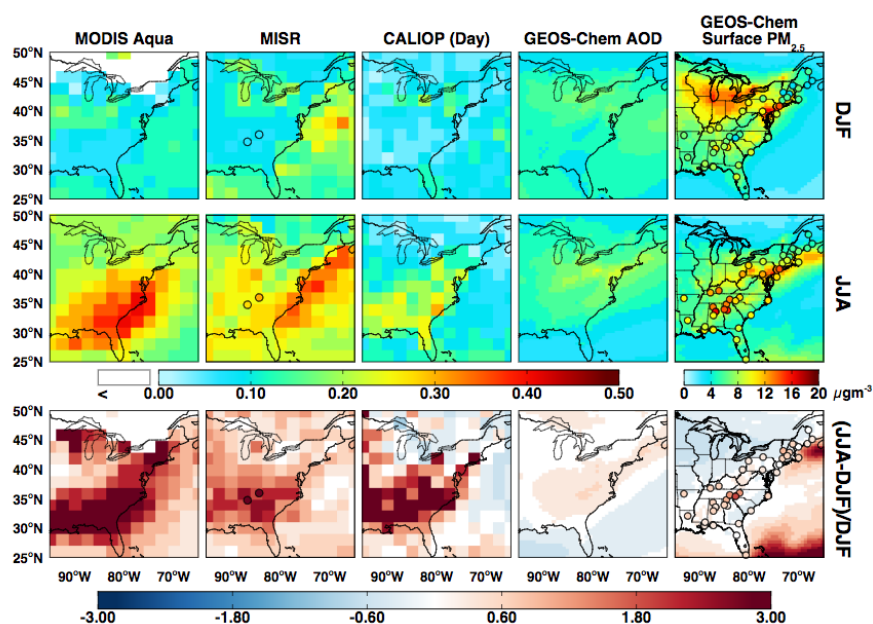


Figure 1.10: GEOS-Chem model-to-measurement analysis for the Eastern USA. Seasonally averaged total column AOD for winter (DJF, top row) and summer (JJA, middle row) for December 2006–August 2009 as observed by MODIS (column 1), MISR (column 2), and CALIOP (daytime, column 3) gridded to  $2^{\circ} \times 2.5^{\circ}$  and compared to simulated AOD from GEOS-Chem (column 4). Concentrations of surface  $PM_{2.5}$  simulated by GEOS-Chem are overlaid with concentrations measured at IMPROVE and SEARCH network sites (circles) in column 5. Bottom row shows the relative enhancement of summer over winter for observed and simulated AOD and surface concentrations. Average AOD observed at the University of Alabama, Huntsville, and Walker Branch AERONET sites for 2008–2009 is overlaid (circles) on the MISR maps. (Ford et al., 2013).

# Methods

## 2.1: Model Overview

In terms of the scientific question at hand, this thesis utilizes the chemical transport model GEOS-Chem to analyze the effects of eliminating the SOA producing pathway of the  $\alpha$ -pinene-NO<sub>3</sub> reaction. To accomplish such a change, the SOA model framework in GEOS-Chem associated with monoterpene SOA chemistry was changed from the network found in Figure 1.8 to that in Figure 2.1. In Figure 2.1, a new  $\alpha$ -pinene parent hydrocarbon was added (APIN) by unlumping that species from the lumped bicyclic monoterpenes tracer (MTPA) found in the old model framework. The OH and O<sub>3</sub> SOA chemistry was kept the same in terms of the gas-to-aerosol partitioning, but the NO<sub>3</sub> +  $\alpha$ -pinene pathway (signified by a red arrow in Figure 2.1) was set to zero SOA yield according to chamber studies discussed in the introduction. This change in the parameterization will keep all products of  $\alpha$ -pinene-NO<sub>3</sub> reactions in the gas phase as SOG.

Similar to many chemical transport models, GEOS-Chem employs a network of modules that handle different aspects of chemistry and meteorology. Referring to Figure 1.7, a module can be visualized as a box that takes inputs from other modules, handles a specific function such as the turbulence or deposition of a species, and returns output values for the same parameters at the end of the model time step.

In this chapter, the operation of the GEOS-Chem model is described, including details on how to download and run GEOS-Chem and to unlump  $\alpha$ -pinene from the lumped bicyclic monoterpene species.

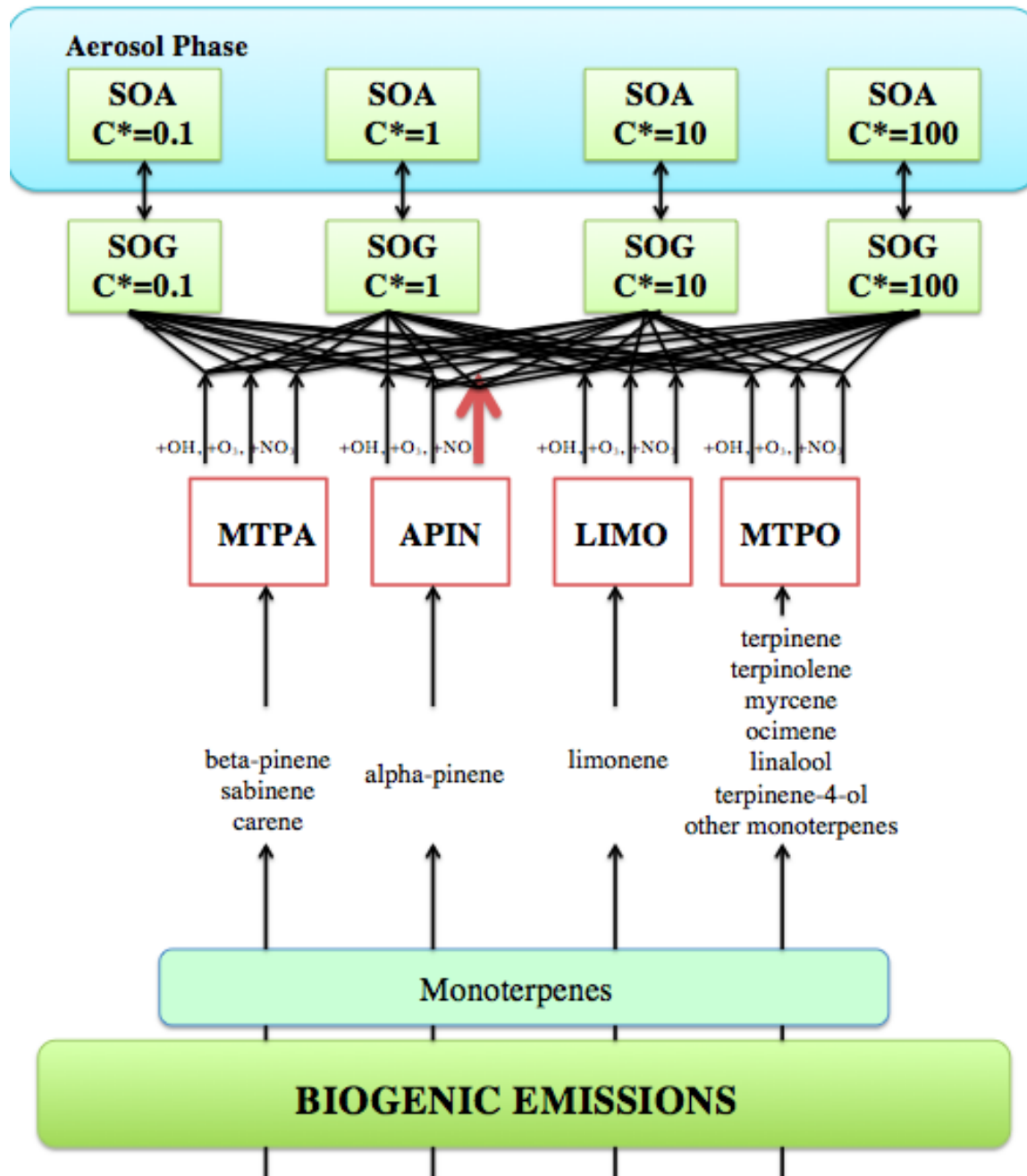


Figure 2.1: Updated GEOS-Chem monoterpene SOA mechanistic pathway

A new  $\alpha$ -pinene parent hydrocarbon tracer (APIN) was added by un lumping  $\alpha$ -pinene from the lumped bicyclic monoterpenes (MTPA). The red arrow for  $\alpha$ -pinene- $NO_3$  chemistry highlights the scientific question of this thesis in that how does eliminating this SOA producing pathway affect global and regional distributions of SOA. A bidirectional arrow across the aerosol/gas interface indicates a semivolatile species.

## 2.2: Model Description

For this study, the GEOS-Chem simulations were run through a supercomputer cluster at Colorado State University in collaboration with Professors Emily Fischer and Jeff Pierce in the Department of Atmospheric Science. All data and code manipulations were done on a MacBook Air with a 1.6GHz dual-core Intel Core i5 processor. A Unix-based system is needed to run GEOS-Chem. This study employed GEOS-Chem v.10-01i. Code in GEOS-Chem is written in Fortran-90 (GEOS-Chem v10-01 Online User's Guide Appendix 7) and the IDL and GAMAP packages are used to create maps (GAMAP). IDL, or interactive data language, is a programming tool used for data analysis. GAMAP is a self-contained and consistent software package developed by the GEOS-Chem support team at Harvard University for reading and visualizing output from chemical tracer models and consists of a suite of routines written in IDL. The principle output file format from GEOS-Chem simulations and the subsequent input files for IDL and GAMAP are binary punch files. These files contain all atmospheric tracer data of interest from the model simulations that will be used to create maps and calculate global yearly budgets.

For additional help, there is an extensive GEOS-Chem wiki page available online (GEOS-Chem Wiki).

## 2.3: Model Suggestions

In order to improve the readability and appearance of the GEOS-Chem source code, a good habit is to comment out one's name and the date after editing the hard code. This way the next time the code may need editing, one can simply search his/her name to find the section of code he/she edited.

In terms of restart files (Section 2.6), note that it is typical to run a yearly model simulation of 'spin-up'; this model run is used to reduce the effects of initialization of the 'dummy' data found in the out-of-the-box restart files. That is, if a model simulation for the year 2006 is run, then the model must be 'spun-up' for the year beforehand in order to reduce any of the effects of these generic restart values. For the purposes of this thesis, all

model runs were ‘spun up’ in the year 2005 and the simulation values used for analysis were from the year 2006. In addition, yearlong simulations are needed in order to cover all the seasons (winter, spring, summer, fall), which is an important part of the temporal analysis.

## 2.4: Downloading GEOS-Chem Run Directories

In order to download new GEOS-Chem run directories, a Unix operating system, the bash Unix shell (pre-installed on Unix systems), the Perl programming language (pre-installed on Unix systems), and the GNU make utility (pre-installed on Unix systems) are needed. In addition, the Unix system requires GEOS-Chem v.9-02o or newer. All new run directories are created using the GEOS-Chem Unit Tester, which is a package of scripts and Makefiles that compile and run GEOS-Chem with a set of debugging flags. An individual GEOS-Chem Unit Test will create a customized run directory for computational simulations for a given combination of meteorological field types, horizontal grids, and different simulation types (GEOS-Chem v10-01 Online User's Guide Appendix 1).

For this study, a  $4 \times 5^\circ$  horizontal grid resolution (pixel-size is roughly the area of Colorado), GEOS5 meteorology (archived meteorology data from NASA's system of models integrated using the Earth System Modeling Framework [GEOS-5]), and an SOA-specific simulation type (GEOS-Chem v10-01 Online User's Guide Appendix 1) were used to investigate how a reduced  $\alpha$ -pinene- $\text{NO}_3$  aerosol producing pathway affects global and regional SOA concentrations.

The Unit Tester provides a streamlined method of creating customized run directories. To download the Unit Tester, the GEOS-Chem Unit Tester package was cloned by typing the following command in the Unix terminal:

```
git clone -b v10-01-Release git://git.as.harvard.edu/bmy/GEOS-Chem-UnitTest UT
```

This created a copy of the GEOS-Chem Unit Tester version 10-01 package in a directory named ‘UT’. Once the Unit Tester was downloaded, the ‘perl’ directory was employed to download a customized run directory.

In this directory there is a perl file named `gcCopyRunDirs.input` that was used to generate new copies of GEOS-Chem run directories. The `gcCopyRunDirs.input` script specifies options for the customized run directory of interest. Figure 2.2 reveals how to edit the file to create a new `geos5_4x5_soa` run directory. Note that there are many different simulation types, such as those that only deal with methane (CH<sub>4</sub>) or carbon dioxide (CO<sub>2</sub>), but for this thesis the SOA simulation type is desired.

```

# !INPUTS:
#
VERSION      : v10-01i
DESCRIPTION  : Initial UT Test Run
COPY_PATH    : /home/{USER}/geoschemv10-1/thesis_soa
DATA_ROOT    : /shared-scratch/GEOS-Chem/ExtData
HEMCO_ROOT   : {DATAROOT}/HEMCO
RUN_ROOT     : /home/{USER}/geoschemv10-1/UT/runs
RUN_DIR      : {RUNROOT}/{RUNDIR}
PERL_DIR     : /home/{USER}/geoschemv10-1/UT/perl
COPY_CMD     : cp -rfl

#
# !RUNS:
# Specify the runs directories that you want to copy below.
# Here we provide a few examples, but you may copy additional entries from
# UnitTest.input and modify the dates as needed. You can deactivate copying
# run certain directories by commenting them out with "#".
#
#-----|-----|-----|-----|-----|-----|-----|
# MET     | GRID   | NEST  | SIMULATION | START DATE | END DATE | EXTRA? |
#-----|-----|-----|-----|-----|-----|-----|
# geos5   | 4x5    | -     | soa        | 2005010100 | 2007010100 | -       |
# geosfp  | 4x5    | -     | soa        | 2013070100 | 2013070101 | -       |
# geosfp  | 4x5    | -     | soa_svpoa  | 2013070100 | 2013070101 | -       |
# geosfp  | 4x5    | -     | UCX        | 2013070100 | 2013070101 | UCX=y   |
# geosfp  | 4x5    | -     | RRTMG      | 2013070100 | 2013070101 | RRTMG=y |
# geosfp  | 4x5    | -     | RnPbBe     | 2013070100 | 2013070101 | -       |
# geosfp  | 4x5    | -     | Hg          | 2013070100 | 2013070101 | -       |
# geosfp  | 4x5    | -     | POPs       | 2013070100 | 2013070101 | -       |
# geosfp  | 4x5    | -     | CH4        | 2013070100 | 2013070101 | -       |
# geosfp  | 4x5    | -     | tagO3      | 2013070100 | 2013070101 | -       |
# geosfp  | 4x5    | -     | tagCO      | 2013070100 | 2013070101 | -       |

```

Figure 2.2: CopyRunDirs.input file to create a `geos5_4x5_soa`

The ‘INPUTS’ section needed to be edited so that the file directories containing the correct information are in their proper paths. For example, the `DATA_ROOT` input requires the file path for the root GEOS-Chem data directory. The ‘RUNS’ section required the desired custom run directory type. This file specifies for a `geos5_4x5_soa` run directory. The start and end date refer to the date range that will be used to initialize the `input.geos` file that is read during a GEOS-Chem simulation (these can be changed later at any point).

In the same ‘perl’ directory, the Makefile script was opened and the source code location was edited to contain the proper path where the Code.v10-01 was located. Once the

CopyRunDirs.input and the Makefile scripts were edited, the new run directory was downloaded by typing the command:

```
gcCopyRunDirs
```

in the 'perl' directory. This command created a new run directory in the location that was specified by the COPY\_PATH in the gcCopyRunDirs.input script. Once the new run directory was created, the next step was to start editing the 'hard code' of the chemical transport model.

## 2.5: Separating Out $\alpha$ -Pinene from the Lumped Bicyclic Monoterpenes

If the reader is interested in running GEOS-Chem 'out-of-the-box' then the following section is not needed. This section describes how to unlump  $\alpha$ -pinene from the lumped bicyclic monoterpenes and speciate it with its own VBS SOA yields as discussed in the introductory sections.

In order to unlump APIN, we must know in which directories and scripts it is contained. To iteratively search for the presence of APIN, this study searched for the lumped monoterpene species MTPA. To accomplish this, focus was switched to the Code.v10-01 directory of the GEOS-Chem model and following command was entered:

```
grep -r 'MTPA'
```

this iteratively searched for the MTPA diagnostic in every directory/module of the GEOS Code. There were many locations in which the diagnostic was found, but there were only two scripts that required significant coding changes. Table 2.1 lists those files that needed to be edited and their respective functions in the model.

Table 2.1: Location of files that need to be edited in the GEOS-Chem Code.v10-01 in order to unlump  $\alpha$ -pinene from MTPA

All scripts are in the GeosCore directory except for the hcox\_megan\_mod.F, which is found in the HEMCO/Extensions directory.

Script	Function
tracerid_mod.F	Links tracer species with a diagnostic identification number
input_mod.F	Reads GEOS-Chem input files at the start of a simulation and passes information to other modules
gamap_mod.F	Creates GAMAP "tracerinfo.dat" and "diaginfo.dat" files
drydep_mod.F	Dry deposition schemes
wetscav_mod.F	Wet scavenging of tracer in cloud updrafts, rainout, and washout
diag3.F	Prints out diagnostics to the binary punch format file
carbon_mod.F	Carbonaceous aerosol and SOA simulations
hcox_megan_mod.F	Controls the MEGAN inventory of biogenic emissions

Operationally, wherever there was an MTPA diagnostic manipulation, a duplicate APIN diagnostic was created in order to separate  $\alpha$ -pinene from the lumped MTPA species. To note, the files under ‘GeosAPM’ (aerosol microphysics package) do not need to be edited, because this module is not used in SOA simulations in geos v.10-01.

In the tracerid\_mod.F in the GeosCore directory, a variable ‘IDTAPIN’ was added on line 220, see Figure 2.3 for reference.

```
! SOAupdate: new mtp gas phase precursors (hotp 5/20/10, mkelp 09/15)
INTEGER          :: IDTMTPA, IDTLIMO, IDTMTPO, IDTAPIN
```

Figure 2.3: tracerid\_mod.F line 220

Added the variable IDTAPIN, ‘IDT’ is a tracer identification element.

On line 750, the following code was added:

```
CASE ('APIN' )
  IDTAPIN = N
```

This code adds a unique APIN gas phase precursor tracer number. Next, on line 4050, the following was added:

```
IDTAPIN = 0
```

this command will set the module's variables to zero during initialization of the model. These are all the changes needed for the tracerid\_mod.F script.

The next script is the input\_mod.F in the GeosCore. Similar to the previous module, on line 1719 the following variable was added:

```
IDTAPIN
```

this change allows the model to recognize APIN during the aerosol menu subroutine. Then on line 2039, the same variable IDTAPIN was added, but with the inclusion of an addition sign to fit into the SOA error check as shown in Figure 2.4.

```
!-----
! Error check 2dy ORG AEROSOLS
!-----
! SOAupdate: update for new mtp (hotp 5/24/10, mkelp 10/15)
I = IDTMTPA + IDTLIMO + IDTMTP0 + IDTAPIN +
& IDTBENZ + IDTTOLU + IDTXYLE +
& IDTTSOA1 + IDTTSOA2 + IDTTSOA3 +
& IDTISOA1 + IDTISOA2 + IDTISOA3 +
& IDTASOA1 + IDTASOA2 + IDTASOA3 + IDTASOAN +
& IDTSOAG + IDTSOAM
```

Figure 2.4: input\_mod.F line 2039

Added the new variable IDTAPIN in the same series with the other SOA precursor parent hydrocarbons.

The next script that was edited was the gamap\_mod.F file in GeosCore. On line 1360 the following code was added:

```
N          = N + 1
CATEGORY (N) = 'OC-APIN'
DESCRIPT (N) = 'Biogenic APIN emission'
OFFSET (N)  = SPACING * 33
```

Figure 2.5: gamap\_mod.F line 1360

Created a new emissions inventory specific to OC-APIN

this code will separate the organic carbon (OC) species in OC-MTPA into OC-MTPA and OC-APIN. This subroutine initializes the category, description, and offsets variables, that are used to define the "diaginfo.dat" file for the visualization tool GAMAP. See Figure 2.6 for reference in editing lines 4540 and 4575.

```

! Number of tracers
IF ( Input_Opt%SOA ) THEN
! hotp updated for SOA (7/31/08) mkelp (10/15)
NTRAC(07) = 16
ELSE
NTRAC(07) = 2
ENDIF

! Loop over tracers
DO T = 1, NTRAC(07)

! Define the default quantities
UNIT (T,07) = 'kg'
MOLC (T,07) = 1
MWT (T,07) = 12e-3
SCALE(T,07) = 1e0

! Get name, long-name, tracer number
SELECT CASE( T )
CASE( 1 )
NAME (T,07) = 'BLKC'
FNAME(T,07) = 'Black (Elemental) Carbon'
INDEX(T,07) = IDTBCPI + ( SPACING * 33 )
UNIT (T,07) = 'kgC' ! SOAupdate (hotp 7/29/10)
CASE( 2 )
NAME (T,07) = 'ORGC'
FNAME(T,07) = 'Organic Carbon'
UNIT (T,07) = 'kgC' ! SOAupdate (hotp 7/29/10)
! SOAupdate: semivolpoa: replace OCPI with POA (hotp 2/17/09)
IF ( IDTOCPI > 0 )
& INDEX(T,07) = IDTOCPI + ( SPACING * 33 )
IF ( IDTPOA1 > 0 )
& INDEX(T,07) = IDTPOA1 + ( SPACING * 33 )
CASE( 3 ) ! SOAupdate (hotp 7/29/10, mkelp 10/15)
NAME (T,07) = 'MTPA'
FNAME(T,07) = 'lumped ALPH'
INDEX(T,07) = IDTMTPA + ( SPACING * 33 )
MWT (T,07) = 136e-3
CASE( 16 ) ! SOAupdate (NEW CASE #)
NAME (T,07) = 'APIN'
FNAME(T,07) = 'APIN'
INDEX(T,07) = IDTAPIN + ( SPACING * 33 )
MWT (T,07) = 136e-3

```

Figure 2.6: gamap\_mod.F lines 4540 and 4575.

This section of code dealt with adding APIN to the carbonaceous aerosol diagnostic (ND07). Code inside black boxes indicates where the code was either changed or added. Line 4540 was changed from  $NTRAC(07)=15$  to  $NTRAC(07)=16$  (first black box) so that the added APIN variable can be used. Line 4575 found at the bottom of the figure (second black box) implements the APIN diagnostic.

The script drydep\_mod.F only has one section that needed editing. The following code was added on line 5064:

```

ELSE IF ( N == IDTAPIN ) THEN
  NUMDEP          = NUMDEP + 1
  NTRAIIND(NUMDEP) = IDTAPIN
  NDVZIND(NUMDEP) = NUMDEP
  DEPNAME(NUMDEP) = 'APIN'
  HSTAR(NUMDEP)   = 0.049e+0_f8
  FO(NUMDEP)      = 0e+0_f8
  XMW(NUMDEP)     = 136.23e-3_f8
  AIROSOL(NUMDEP) = .FALSE.

```

Figure 2.7: drydep\_mod.F line 5064

Created a dry deposition variable for APIN.

For the code in Figure 2.7, the same scheme for MTPA was adapted for APIN. The HSTAR(NUMDEP) command specifies the Henry's Law constant (0.049) for the VOC. APIN should have the same Henry's Law constant as MTPA because they are both C<sub>10</sub>H<sub>16</sub> hydrocarbons.

The next module edited was the wetscav\_mod.F in the GeosCore. See Figure 2.8 for the code that is used to compute the fraction of soluble tracer lost by scavenging in convective cloud updrafts. This code is the exact same code used for the scavenging of MTPA. The code was adapted to create unique wet scavenging of the added APIN tracer.

```

!-----
! APIN (liquid phase only) mkelp 10/15 (MTPA surrogate #s)
!-----
! new mtp (hotp 5/24/10), SOAupdate
ELSE IF ( N == IDTAPIN ) THEN
  ! No scavenging at the surface
  F(:, :, 1) = 0e+0_fp

  ! Start scavenging at level 2
  DO L = 2, LLPAR
  DO J = 1, JJPAR
  DO I = 1, IIPAR
    ! Compute liquid to gas ratio for MTPA, using
    ! the appropriate parameters for Henry's law
    ! (Eqs. 7, 8, and Table 1, Jacob et al, 2000)
    ! Use H-law of 0.049 for all pinene (Sander, 1999)
    ! updated for new mtp (hotp 5/24/10), SOAupdate
    CALL COMPUTE_L2G( 0.049e+0_fp, 0.e+0_fp,
& T(I,J,L), CLDLIQ(I,J,L), L2G )

    ! Fraction of MTPA in liquid phase
    ! (Eq. 4, 5, 6, Jacob et al, 2000)
    C_TOT = 1e+0_fp + L2G
    F_L = L2G / C_TOT

    ! Compute the rate constant K. Assume retention factor
    ! for liquid MTPA is 0.0 for T <= 248 K and 0.02 for
    ! 248 K < T < 268 K. (Eq. 1, Jacob et al, 2000)
    IF ( T(I,J,L) >= 268e+0_fp ) THEN
      K = KC * F_L

& ELSE IF ( T(I,J,L) > 248e+0_fp .and. T(I,J,L) < 268e+0_fp )
      THEN
      K = KC * ( 2e-2_fp * F_L )

    ELSE
      K = 0e+0_fp

    ENENDIF
    ! F is the fraction of MTPA scavenged out of the updraft
    ! (Eq. 2, Jacob et al, 2000)
    F(I,J,L) = GET_F( State_Met, I, J, L, K )
  ENDDO
  ENDDO
  ENDDO
  ISOL = GET_ISOL( N, N_TRACERS )

```

Figure 2.8: wetscav\_mod.F lines 1851 to 1896.

Wet scavenging of APIN, the same Henry's Laws constant (0.049) was used for all terpenes in this module.

On line 3011, IDTAPIN was added to the identification list to be used in the subroutine that calculates the fraction of soluble tracer lost to rainout events in precipitation. On line 3774, the code found in Figure 2.9 was added to calculate the rainout fraction.

```

!-----
! APIN (liquid phase only)  (mkelp 10/15)
!-----
! new mtp (hotp 5/24/10), SOAupdate
ELSE IF ( N == IDTAPIN ) THEN

    ! Compute liquid to gas ratio for MTPA, using
    ! the appropriate parameters for Henry's law
    ! (Eqs. 7, 8, and Table 1, Jacob et al, 2000)
    ! use H-law of 0.049 (hotp 5/24/10), SOAupdate
    CALL COMPUTE_L2G(0.049e+0_fp, 0.e+0_fp, TK, CLDLIQ(I,J,L), L2G)

    ! Fraction of MTPA in liquid phase
    ! (Eqs. 4, 5, Jacob et al, 2000)
    C_TOT = 1e+0_fp + L2G
    F_L   = L2G / C_TOT

    ! Compute the rate constant K. Assume that the retention factor
    ! for liquid MTPA is 0.02 for 248 K < T < 268 K, and
    ! 1.0 for T > 268 K. (Eq. 1, Jacob et al, 2000)
    IF ( TK >= 268e+0_fp ) THEN
        K = K_RAIN * F_L

    ELSE IF ( TK > 248e+0_fp .and. TK < 268e+0_fp ) THEN
        K = K_RAIN * ( 2e-2_fp * F_L )

    ELSE
        K = 0e+0_fp

    ENDIF

    ! Compute RAINFRAC, the fraction of rained-out MTPA
    ! (Eq. 10, Jacob et al, 2000)
    RAINFRAC = GET_RAINFRAC( K, F, DT )

```

Figure 2.9: wetscav\_mod.F lines 3774 to 3807.

Calculating the fraction of soluble tracer lost to rainout events in precipitation. Again, the same Henry's Law constant (0.049) was used.

On line 4381, IDTAPIN was added to the identification list to calculate the fraction of soluble tracer lost to washout events in precipitation. The following code was added on line 4807 to calculate the washout fraction:

```

!-----
! APIN (liquid & gas) mkelp 10/15
!-----
! new mtp (hotp 5/24/10), SOAupdate
ELSE IF ( N == IDTAPIN ) THEN
  KIN      = .FALSE.
  CALL WASHFRAC_LIQ_GAS( 0.049e+0_fp, 0.e+0_fp, PP, DT, F,
&                      DZ,      TK,  WASHFRAC, KIN )

```

Figure 2.10: wetscav\_mod.F line 4807 .

Code used to calculate the washout fraction of APIN.

Finally, on line 7960 IDTAPIN was added to the identification list to set up the index array of soluble tracers used in the routines that were coded above. Then, on line 8215 the following code was added to create a wet deposition array for APIN:

```

ELSE IF ( N == IDTAPIN ) THEN
  NSOL      = NSOL + 1
  IDWETD(NSOL) = IDTAPIN

```

Figure 2.11: wetscav\_mod.F lines line 8215

Created an array for the wet deposition of APIN.

Once these changes in the above modules were edited, the next step was to edit the diag3.F and carbon\_mod.F scripts in the GeosCore, in which the coding is considerably more involved. The diag3.F file is used to print out diagnostics to the binary punch (.bpch) format file. Most of the coding that was needed in this script was separating the organic carbon contribution of APIN from MTPA. To unlump the organic-carbon diagnostic, the code highlighted in Figure 2.12 was removed. This code can be found on line 823 under the SOA diagnostics. By removing this line of code, the contribution of APIN to the emission of organic carbon under the MTPA diagnostic in the model was effectively removed.

```

! MTPA
!-----
IF ( IDTMTPA > 0 ) THEN
  CATEGORY = 'OC-MTPA'
  NN       = IDTMTPA

  ! (1) ALPHA-PINENE
  DiagnName = 'BIOGENIC_APIN'
  DiagnCnt  => NULL()

  ! Get diagnostics from HEMCO
  CALL Diagn_Get( am_I_Root, .FALSE., DiagnCnt,
&                FLAG, RC,  cName=TRIM(DiagnName),
&                AutoFill=1,
&                COL=HcoDiagnIDManual )
  IF ( RC /= HCO_SUCCESS ) THEN
    MSG = 'Cannot find diagnostics ' // TRIM(DiagnName)
    CALL ERROR_STOP ( MSG, LOC )
  ENDIF

  ! Save into ARRAY and convert units from kg/m2/s to kg
  IF ( FLAG == HCO_SUCCESS ) THEN
&    ARRAY(:, :, 1) = DiagnCnt%Arr2D%Val(:, :)
    * FACTOR * HcoState%Grid%AREA_M2%Val(:, :)
  ELSE
    ARRAY(:, :, 1) = 0.0
    MSG = 'No diagnostics returned: ' // TRIM(DiagnName)
    MSG = TRIM(MSG) // ' - will write zeros!'
    CALL HCO_WARNING ( MSG, RC, THISLOC=LOC )
  ENDIF

  ! (2) BETA-PINENE
  DiagnName = 'BIOGENIC_BPIN'
  DiagnCnt  => NULL()

  ! Get diagnostics from HEMCO
  CALL Diagn_Get( am_I_Root, .FALSE., DiagnCnt,
&                FLAG, RC,  cName=TRIM(DiagnName),
&                AutoFill=1,
&                COL=HcoDiagnIDManual )
  IF ( RC /= HCO_SUCCESS ) THEN
    MSG = 'Cannot find diagnostics ' // TRIM(DiagnName)
    CALL ERROR_STOP ( MSG, LOC )
  ENDIF

```

Figure 2.12: diag3.F line 823

Deleted the highlighted code to remove the contribution of APIN to the emission of organic carbon from MTPA.

However, because the MTPA SOA code was modified for organic carbon by taking out APIN, a minor adjustment to the code in the “(2) BETA\_PINENE” routine below the section of code that was deleted was necessary. On line 864 of the code before the APIN contribution was deleted, the code in Figure 2.13 needed to replace the existing code under the same section.

```

! Save into ARRAY and convert units from kg/m2/s to kg
IF ( FLAG == HCO_SUCCESS ) THEN
  ARRAY(:, :, 1) = ( DiagnCnt%Arr2D%Val(:, :) * FACTOR
&                * HcoState%Grid%AREA_M2%Val(:, :) )
ELSE
  ARRAY(:, :, 1) = 0.0
  MSG = 'No diagnostics returned: ' // TRIM(DiagnName)
  MSG = TRIM(MSG) // ' - will write zeros!'
  CALL HCO_WARNING ( MSG, RC, THISLOC=LOC )
ENDIF

```

Figure 2.13: diag3.F line 864 under (2) BETA-PINENE

Replaced the code found under the (2) BETA-PINENE section with this code to make the data withdraw for loop start with Beta-Pinene instead of Alpha-Pinene.

The code in Figure 2.13 effectively starts the for loop for the data withdraw and emission of organic carbon for the MTPA lumped diagnostic at  $\beta$ -pinene instead of the removed  $\alpha$ -pinene. If these few lines of code are not replaced, then the model will crash.

In addition to taking out the APIN emissions from MTPA, a new organic carbon APIN diagnostic called OC-APIN was created for emissions specific to APIN. To create this new emissions inventory, another chunk of code, similar to the OC-MTPA emissions found in Figure 2.14, was added. These lines of code were inserted after the sesquiterpene organic carbon emissions on line 1124.

```

!-----
!APIN Unlump mkelp 11/15
!-----

      IF ( IDTAPIN > 0 ) THEN
        CATEGORY = 'OC-APIN'
        NN       = IDTAPIN

        ! (1) ALPHA-PINENE
        DiagnName = 'BIOGENIC_APIN'
        DiagnCnt  => NULL()

        ! Get diagnostics from HEMCO
        CALL Diagn_Get( am_I_Root, .FALSE., DiagnCnt,
&                     FLAG, RC, cName=TRIM(DiagnName),
&                     AutoFill=1,
&                     COL=HcoDiagnIDManual )
        IF ( RC /= HCO_SUCCESS ) THEN
          MSG = 'Cannot find diagnostics ' // TRIM(DiagnName)
          CALL ERROR_STOP ( MSG, LOC )
        ENDIF

        ! Save into ARRAY and convert units from kg/m2/s to kg
        IF ( FLAG == HCO_SUCCESS ) THEN
&         ARRAY(:, :, 1) = DiagnCnt%Arr2D%Val(:, :)
          * FACTOR * HcoState%Grid%AREA_M2%Val(:, :)
        ELSE
          ARRAY(:, :, 1) = 0.0
          MSG = 'No diagnostics returned: ' // TRIM(DiagnName)
          MSG = TRIM(MSG) // ' - will write zeros!'
          CALL HCO_WARNING ( MSG, RC, THISLOC=LOC )
        ENDIF

        ! Write combined BIOGENIC APIN to disk
&         CALL BPCH2( IU_BPCH, MODELNAME, LONRES, LATRES,
&                   HALFPOLAR, CENTER180, CATEGORY, NN,
&                   UNIT, DIAGb, DIAGe, RESERVED,
&                   IIPAR, JJPAP, 1, IFIRST,
&                   JFIRST, LFIRST, ARRAY(:, :, 1) )
      ENDIF

```

Figure 2.14: diag3.F line 1124, created an OC-APIN diagnostic

The following code was inserted to create an OC-APIN diagnostic for the emission of organic carbon from APIN parent hydrocarbon.

After editing the diag3.F module, the carbon\_mod.F script is the final file to edit in the GeosCore. This module handles most of the SOA chemistry of interest in GEOS-Chem. The first modification made in the carbon\_mod.F was to change the number of parent hydrocarbon species for SOA chemistry from 11 to 12 as the diagnostic APIN tracer was added. See Figure 2.15 for the coding changes performed.

```

! SOAupdate:(hotp 5/20/10) new mtp
! one parent HC removed (only 3 instead of 4 monoterps)
! all monoterp and sesquiterp SOA lumped together
! NOX: now used to indicate high NOx (1),
!       low NOx(2), and +NO3 (3) so MNOX is 3
! PROD: indicates # of volatilities/products
INTEGER, PARAMETER  :: MHC      = 12 ! max # HCs
INTEGER, PARAMETER  :: MSV      = 5  ! max # lumped semivols
INTEGER, PARAMETER  :: MPROD    = 4  ! max # volatility products
INTEGER, PARAMETER  :: MNOX     = 3  ! max # NOx levels/oxidants

REAL(fp), PARAMETER :: SMALLNUM = 1e-20_fp

! Indicate number of parent HC based on simulation tracers
! (hotp 8/24/09)
!INTEGER, SAVE      :: MAXSIMHC
! Now loop over number of semivolatiles (hotp 5/13/10)
INTEGER, SAVE      :: MAXSIMSV

! Identify parent hydrocarbon by numbers (hotp 5/12/10)(mkelp 12/15)
INTEGER, PARAMETER  :: PARENTMTPA = 1 ! bicyclic monoterpenes
INTEGER, PARAMETER  :: PARENTAPIN = 2 ! alpha-pinene
INTEGER, PARAMETER  :: PARENTLIMO = 3 ! limonene
INTEGER, PARAMETER  :: PARENTMTPO = 4 ! other monoterpenes
INTEGER, PARAMETER  :: PARENTSESQ = 5 ! sesquiterpenes
INTEGER, PARAMETER  :: PARENTISOP = 6 ! isoprene
INTEGER, PARAMETER  :: PARENTBENZ = 7 ! aromatic benzene
INTEGER, PARAMETER  :: PARENTTOLU = 8 ! aromatic toluene
INTEGER, PARAMETER  :: PARENTXYLE = 9 ! aromatic xylene
INTEGER, PARAMETER  :: PARENTPOA  = 10 ! SVOCs (primary SVOCs)
INTEGER, PARAMETER  :: PARENTPOA  = 11 ! oxidized SVOCs (secondary SVOCs)
INTEGER, PARAMETER  :: PARENTNAP  = 12 ! IVOC surrogate (naphthalene)

```

Figure 2.15: carbon\_mod.F line 218

Increased the number of parent hydrocarbon species from 11 to 12 and added a PARENTAPIN parameter to the hydrocarbon list. Make sure that PARENTAPIN = 2, all other species were adjusted accordingly. If PARENTAPIN  $\neq$  2, then the SOA chemistry coding loops become much more complex.

Next, the variable DRYAPIN was added to the integer list on line 261; this addition will include the dry deposition of APIN that was edited in the drydep module. On line 2165, IDTAPIN was added to the tracer identification list.

On line 2422, the following code was added:

```
print*, 'APIN ', PARENTAPIN, IDSV(PARENTAPIN)
```

Figure 2.16: carbon\_mod.F line 2422

Diagnostic debugging of the PARENTAPIN variable.

this line of code will be used for diagnostic debugging if there are errors with the APIN unlumping.

The next few sections are crucial for the SOA chemistry of the carbon\_mod.F script. On line 3835 the following chunk of code found in Figure 2.17 was added for the VBS SOA yields according to chamber studies.

```

!-----
! APIN      mkelp 09/15, no3=0 2/16
!-----

NOX = NHIGHNOX
ALPHA(NOX, 1, PARENT APIN) = 0.0095e+0_fp
ALPHA(NOX, 2, PARENT APIN) = 0.0900e+0_fp
ALPHA(NOX, 3, PARENT APIN) = 0.0150e+0_fp
ALPHA(NOX, 4, PARENT APIN) = 0.0400e+0_fp
NOX = NLOWNOX
ALPHA(NOX, 1, PARENT APIN) = 0.019e+0_fp
ALPHA(NOX, 2, PARENT APIN) = 0.180e+0_fp
ALPHA(NOX, 3, PARENT APIN) = 0.030e+0_fp
ALPHA(NOX, 4, PARENT APIN) = 0.080e+0_fp
NOX = NNO3RXN

ALPHA(NOX, 1, PARENT APIN) = 0.0000e+0_fp
ALPHA(NOX, 2, PARENT APIN) = 0.3207e+0_fp
ALPHA(NOX, 3, PARENT APIN) = 1.0830e+0_fp

```

Figure 2.17: carbon\_mod.F line 3835, VBS yields for APIN SOA  
SOA from APIN according to VBS yields.

On line 4103, IDTAPIN was added as a tracer identification tag in the chem\_nvoc subroutine. In addition to this change, there were multiple alterations to the chem\_nvoc subroutine. This subroutine computes the oxidation of specified parent hydrocarbons by O<sub>3</sub>, OH, and NO<sub>3</sub>. See Figures 2.18 and 2.19 for the changes made in the subroutine code.

```

! update for new mtp lumping (hotp 5/22/10)(mkelp 11/15)
NMVOC(1) = STT(I,J,L,IDTMTPA)
NMVOC(2) = STT(I,J,L,IDTAPIN)
NMVOC(3) = STT(I,J,L,IDLIMO)
NMVOC(4) = STT(I,J,L,IDTMTP0)
!NMVOC(5) = ORVC_SESQ(I,J,L)

! Initialize DELHC so that the values from the previous
! time step are not carried over.
DELHC(:) = 0.e+0_fp

=====
! Change in NVOC concentration due to photooxidation [kg]
=====

! semivolpoa2: update for POA (hotp 2/27/09)
! add POA emissions to GMO here (not to STT in EMITHIGH)

! Only loop over parent hydrocarbons defined for a given simulation
! Max should be 11 for semivolatile POA/IVOC (PARENTNAP =11)
! Max should be 8 for nonvolatile POA/ traditional simulation
IF ( IDTPOA1 > 0 ) THEN ! mkelp (11/15)
  MAXLOOP = PARENTNAP !was 11 (now 12)  MAXLOOP = PARENTNAP
ELSE
  MAXLOOP = PARENTXYLE ! 9  MAXLOOP = PARENTXYLE
ENDIF

DO JHC = 1, MAXLOOP

  ! Initialize again for safety (hotp 5/22/10)
  DELHC = 0e+0_fp

  ! Get JSV (hotp 5/14/10)
  JSV = IDSV(JHC)

  ! update for new mtp (hotp 5/22/10)(mkelp 11/15)
  IF ( JHC == PARENTMTPA .or. JHC == PARENTLIMO .or.
    & JHC == PARENTMTPO .or. JHC == PARENTAPIN ) THEN

```

Figure 2.18: carbon\_mod.F starting from line 4202, chem\_nvoc subroutine  
 Added the line NMVOC(2) = STT(I,J,L,IDTAPIN) under the “update for new mtp lumping” comment (first black box). The ordering of the parent hydrocarbons must be changed in order for APIN to be the second species listed. In addition, JHC == PARENTAPIN on line 4239 was added (second black box). Note: for this study, sesquiterpene SOA chemistry was turned off, as there were multiple array out-of-bounds errors that caused the terpene SOA chemistry to crash. This error may be the result of a problem in the more complex data processing scheme used by the sesquiterpenes.

```

=====
! Store Hydrocarbon remaining after oxidation rxn back into STT
=====
! update for new mtp lumping (hotp 5/22/10)(mkelp 11/15)
STT(I,J,L,IDTMTPA) = MAX( NMVOC(1), 1.e-32_fp )
STT(I,J,L,IDTAPIN) = MAX( NMVOC(2), 1.e-32_fp )
STT(I,J,L,IDLIMO) = MAX( NMVOC(3), 1.e-32_fp )
STT(I,J,L,IDTMTPO) = MAX( NMVOC(4), 1.e-32_fp )
!ORVC_SESQ(I,J,L) = MAX( NMVOC(5), 1.e-32_fp )
! Nothing to do for isoprene or aromatics here,
! as their oxidation is treated online.

! Free pointer
NULLIFY( STT )

END SUBROUTINE CHEM_NVOC

```

Figure 2.19: carbon\_mod.F line 4494, end of chem\_nvoc subroutine

Similar to Figure 2.18, the `STT(I,J,L,IDTAPIN) = MAX( NMVOC(2), 1.e-32_fp )` line was added to the code. This change will store APIN into an array for further oxidation.

Furthermore, on line 8284 the following line of code was added:

```
+ DELTASOGSAVE(I, J, L, NOX, PARENTAPIN) *ALPHA( NOX, IPR, PARENTAPIN)
```

Figure 2.20: carbon\_mod.F line 8284

Includes APIN in the calculation of the SOA and SOG mass balance of monoterpene species

On line 8616 in the check\_mb subroutine, under the “Print diagnostic information to screen” comment and the `print*, 'Global cumulative amount reacted in gas phase [Tg]'` command, added the lines:

```

JHC = 2
print*, 'APIN High NOx Rxn : ', DELTAHCSAVE(1, JHC)
print*, 'APIN Low NOx Rxn : ', DELTAHCSAVE(2, JHC)
print*, 'APIN NO3 Rxn : ', DELTAHCSAVE(3, JHC)

```

Figure 2.21: carbon\_mod.F line 8616

Prints out the APIN SOA species via the oxidant system

For the above section, the JHC numbers for the other parent hydrocarbons must be changed so that APIN will be the second species printed.

On line 9073 in the init\_carbon subroutine the following variable was added:

```
IDSV(PARENTAPIN) = 1 .
```

This line of code is crucial for the module to read over all the arrays involving the PARENTAPIN parameter. If this line of code is forgotten, then the model will not compute any APIN-NO<sub>3</sub> SOA chemistry. See Figure 2.22 for reference.

```

=====
! INIT_CARBON begins here!
=====

! Assume success
RC = GIGC_SUCCESS

! Some parent hydrocarbons are lumped together into 1 or more
! semivolatiles. Map the parent HC to lumped semivolatiles here
! (hotp 5/13/10)
! mono + sesq
IDSV(PARENTMTPA) = 1
IDSV(PARENTAPIN) = 1
IDSV(PARENTLIMO) = 1
IDSV(PARENTMTPO) = 1
!IDSV(PARENTSESQ) = 1

! isoprene
IDSV(PARENTISOP) = 2
! Lumped arom/IVOC
IDSV(PARENTBENZ) = 3
IDSV(PARENTTOLU) = 3
IDSV(PARENTXYLE) = 3
IDSV(PARENTNAP ) = 3
! More individuals
IDSV(PARENTPOA ) = 4
IDSV(PARENTOPOA) = 5

```

Figure 2.22: carbon\_mod.F line 9062, init\_carbon subroutine

Added `IDSV(PARENTMTPA) = 1`. This command will make the SOA chemistry loop through APIN.

On line 9266 under the “Find drydep species in DEPSAV” comment in the `init_carbon` subroutine, the flag `DRYAPIN = 0` was added. Finally, on line 9349 under the “Locate drydep indices for each carbon or SOA aerosol in the list of dry depositing species” comment in the `init_carbon` subroutine, the following lines of code was added:

```

CASE ( 'APIN' )
  DRYAPIN = N

```

Figure 2.23: carbon\_mod.F line 9249

Allows the `carbon_mod.F` to use the dry deposition of APIN in its calculations.

These coding changes conclude the edits needed in the GeosCore directory for the speciated un lumping of APIN from the MTPA lumped diagnostic.

There is one last script to edit in the `Code.v10-01/HEMCO/Extensions` directory. This module primarily handles the biogenic emissions in GEOS-Chem. The script of interest is the `hcox_megan_mod.F` file. On line 205, the integer variable `IDTAPIN` was

added for the splitting out of APIN from MTPA. On line 379 under the emissions array commented title, the following code was added:

```
REAL(hp), TARGET      :: FLUXAPIX (HcoState%NX,HcoState%NY)
```

Figure 2.24: hcox\_megan\_mod.F line 379

Created an APIX (because APIN is in use as a biogenic emissions) SOA parent hydrocarbon emissions array.

Be sure that the flux term is 'FLUXAPIX', we will not use 'FLUXAPIN' because there already exists a dynamic emissions array associated with biogenic APIN. This study codes for the parent hydrocarbon APIN used in SOA chemistry (this might not be a problem if kept the same since typically biogenic emissions should be similar to the SOA parent hydrocarbon precursor).

On line 1108 under the MEGAN MTPA commented title in the HCOX\_MEGAN\_Run subroutine, the emissions contribution of APIN (EMIS\_APIIN) was deleted and a new emissions calculation for our lumped-out APIN term was created; see Figure 2.25.

```
!-----
! MEGAN MTPA
!-----
! MTPA=b-pinene,sabinene,carene (hotp 5/20/10)
IF ( IDTMTPA > 0 ) THEN
&   FLUXMTPA(I,J) = ( EMIS_BPIN +
&                   EMIS_SABI + EMIS_CARE ) * FC1
&   ENDFIF

! Lumped OUT APIN (Mkelp 10/15)
! IF ( IDTMTPA > 0 ) THEN
&   FLUXMTPA(I,J) = ( EMIS_APIIN + EMIS_BPIN +
&                   EMIS_SABI + EMIS_CARE ) * FC1
&   ENDFIF

!-----
! MEGAN APIN mkelp 10/15
!-----
! [kg C/m2/s]
IF ( IDTAPIN > 0 ) THEN
  FLUXAPIX(I,J) = EMIS_APIIN * FC1
ENDFIF
```

Figure 2.25: hcox\_megan\_mod.F line 1104, HCOX\_MEGAN\_Run subroutine

Took out emissions contribution of APIN (Emis\_APIIN) from the MTPA lumped monoterpenes and created a new emissions array for APIN. Do not forget to use the FLUXAPIX variable instead of a FLUXAPIN. FC1 corresponds to a conversion factor for OC/BC.

On line 1213, the following code was added to create a similar emissions array for APIN for if one decides to turn the MEGAN Monoterpenes (MEGAN\_MONO) switch off in the HEMCO\_Config.rc input file (Section 2.6):

```

IF ( IDTAPIN > 0 ) THEN
  FLUXAPIX(I,J) = DIURORVC * FC4 * 0.35_hp
ENDIF

```

Figure 2.26: hcox\_megan\_mod.F line 1213

APIN emissions array for when MEGAN\_MONO switch is turned off so that biogenic emissions are calculated using flux terms only.

This format of code was in older versions of GEOS-Chem (before HEMCO directory) where monoterpene emissions were calculated according to fluxes, but HEMCO has instituted a more reliable emissions based variable. FC4 is a conversion factor for OC/BC specific to the bicyclic monoterpenes and the 0.35\_hp value is a listed standard emissions flux yield for APIN given in older GEOS-Chem versions.

On line 1428 under the commented title “PASS TO HEMCO STATE AND UPDATE DIAGNOSTICS” the code found in Figure 2.27 was added to include the flux term (FLUXAPIX) to the emissions array.

```

! -----
! APIN (mkelp 10/15)
IF ( ( ExtNrSoa > 0 ) .AND. ( IDTAPIN > 0 ) ) THEN

  ! Add flux to emission array
  CALL HCO_EmisAdd( am_I_Root, HcoState, FLUXAPIX, IDTAPIN,
&                RC, ExtNr=ExtNr )
  IF ( RC /= HCO_SUCCESS ) THEN
    CALL HCO_ERROR( 'HCO_EmisAdd error: FLUXAPIX', RC )
    RETURN
  ENDIF

ENDIF

```

Figure 2.27: hcox\_megan\_mod.F line 1428

Linked the flux and emission array variables.

On line 4090 under the “Check for SOA option, this option is only valid together w/ monoterpene,” commented title in the HCOX\_Megan\_Init subroutine, the following variable added was added:

```
IDTAPIN = -1.
```

This addition will tell the model to perform SOA chemistry with the new APIN parent hydrocarbon. Furthermore, on line 4117 the following code found in Figure 2.28 was added to attach a HEMCO identification tag to the new APIN species.

```

! Get HEMCO species IDs of ALPH/LIMO/ALCO (mkelp 10/15)
CALL HCO_GetExtHcoID( HcoState, ExtNrSoa, HcoIDs,
&                    SpcNames, nSpc,      RC      )
IF ( RC /= HCO_SUCCESS ) RETURN

DO I = 1, nSpc
  SELECT CASE ( TRIM(SpcNames(I)) )
    CASE( 'MTPA' )
      IDTMTPA = HcoIDs(I)
      WRITE(MSG,*) '      b-pinene      = ',
&                TRIM(SpcNames(I)),IDTMTPA
    CASE( 'APIN' )
      IDTAPIN = HcoIDs(I)
      WRITE(MSG,*) '      a-pinene      = ',
&                TRIM(SpcNames(I)),IDTAPIN
    CASE( 'MTPO' )
      IDTMTPO = HcoIDs(I)
      WRITE(MSG,*) '      Other monoterp.= ',
&                TRIM(SpcNames(I)),IDTMTPO
    CASE( 'LIMO' )
      IDTLIMO = HcoIDs(I)
      WRITE(MSG,*) '      Limonene      = ',
&                TRIM(SpcNames(I)),IDTLIMO
    CASE( 'SESQ' )
      IDTSESQ = HcoIDs(I)
      WRITE(MSG,*) '      Sesquiterpenes = ',
&                TRIM(SpcNames(I)),IDTSESQ

```

Figure 2.28: hcox\_megan\_mod.F line 4117

Added the code that is highlighted. This code created a unique HEMCO identification tag for our new APIN SOA species.

Having accomplished all of the above coding and compiling so that there are no return errors, this study was prepared to run the new unlumped SOA simulation.

## 2.6: Compiling and Running GEOS-Chem

With new run directories constructed and the hard code edited, the model can now be compiled and run. The first script that must be edited in the run directory of interest is the input.geos file. When this file is opened, many options are available to customize the simulation. See Figure 2.29 for the simulation menu of the input.geos script.

```

GEOS-CHEM UNIT TEST SIMULATION: geos5_4x5_soa
-----+-----
%%% SIMULATION MENU %%% :
Start YYYYMMDD, HHMMSS : 20060101 000000
End   YYYYMMDD, HHMMSS : 20070101 000000
Run directory           : ./
Input restart file      : restart.Feb15spin_control_secondcheck.200601010000
Make new restart file?  : T
Output restart file(s) : restart.Feb16sim_control_secondcheck.YYYYYMMDDhhmm
Root data directory     : /shared-scratch/GEOS-Chem/ExtData
=> GCAP   subdir       : AGRID/YYYY/MM/
=> GEOS-4  subdir       : GEOS_4_v4/YYYY/MM/
=> GEOS-5  subdir       : GEOS_5/YYYY/MM/
=> GEOS-FP subdir       : GEOS_FP/YYYY/MM/
=> MERRA   subdir       : MERRA/YYYY/MM/
Dir w/ 1x1 emissions etc: /shared-scratch/GEOS-Chem/ExtData/GEOS_NATIVE/
Temporary directory     : ./
Unzip met fields?       : F
Wait for met fields?    : F
Use variable tropopause?: T
Global offsets IO, JO   : 0 0
-----+-----

```

Figure 2.29: input.geos, simulation menu

Simulation menu for a GEOS-Chem run. The start and end date, the input and output restart files were customized for the purposes of this thesis.

The start and end dates refer to the period of time the simulation takes place. According to Figure 2.29, this simulation was set to run from January 1 2006 to January 1 2007. The input restart file is an initial file (first month of a simulation) that is used to populate the species of all atmospheric tracers of interest. When a model simulation is first run, an ‘out-of-the-box’ restart file from the Unit Tester is provided. For example, for a `geos5_4x5_soa` simulation, the given restart file to use would be the ‘initial\_trac\_rst.geos5\_4x5\_soa’ file (other restart files for different simulation types will have the same convention of naming).

In addition to input restart files, model simulations produce output restart files that become potential input restart files to use for later simulations. That is, if a simulation for the year 2005 is run using an out-of-the-box input file and a newly outputted restart file called ‘restart.soa.simulation.YYYYYMMDDhhmm’ is specified, there will be new restart files created for every interval of time specified (to be discussed later in this section). This means that if a monthly output for the output restart files is specified, then 12 restart files in a yearly simulation will be created. If the year 2005 is run as a ‘spin up’, then the outputted restart file from this simulation can be used as a new input restart file for a new simulation for the year 2006 using the file ‘restart.soa.simulation.200601010000’.



After editing the `input.geos` file, the `HEMCO_Config.rc` file was edited to turn on SOA chemistry via the MEGAN module. In this file, the `MEGAN_Mono` and the `MEGAN_SOA` switches were turned on. These switches allowed the MEGAN module to implement biogenic emissions of monoterpenes and SOA chemistry. It must also be noted that for this work the switch `ParaNOx` (used mainly for ship emissions) was turned off, as there were multiple bounds errors associated with the HEMCO module. All other switches were kept at ‘out-of-the-box’ settings.

Once the `input.geos` and `HEMCO_Config.rc` files were edited, the model was ready to run. The code must be compiled to make sure there are no errors in the model. Perhaps the easiest method of compiling the code is to manually create a compiler to compile the code instead of typing out the command every time to run a simulation. Figure 2.31 contains the compiler code.

```
#!/bin/sh
make mpbuild -j4 MET=geos5 GRID=4x5 CHEM=SOA GC_BIN=$NC4ROOT/bin
GC_INCLUDE=$NC4ROOT/include NCL='-lnetcdf -lnetcdf' DEBUG=no BOUNDS=no TRACEBACK=no
```

Figure 2.31: `compile.sh`, manual GEOS-Chem compiler

Created a new script in the run directory and named it ‘`compile.sh`’. In order to compile the model (having edited the hard code), the command ‘`make realclean`’ was used in the run directory to remove any files left over from previous unit test runs. Then, the command ‘`compile.sh`’ was typed to activate the compiler. If there is an error that is not obvious in the hard code or run directory interface, then the `DEBUG`, `BOUNDS`, and `TRACEBACK` options in the compiler can be turned on to attempt to identify the error.

The GEOS model in this work was run through a supercomputer cluster at Colorado State University, where a `run.geos.cluster` script was used to run the model on a network separate from a personal computer. That script is found in Figure 2.32 and may be used if one has access to a supercomputer cluster.

---

```
#!/bin/bash

### Job name
#PBS -N kelp_soa_apin_unlump_20160203

## Number of nodes and processors per node.
## This job will run on 8 nodes with 8 cores per node
#PBS -l nodes=1:ppn=16

### Specify queue if necessary
##PBS -q batch

### Join standard output and standard error in one file
#PBS -j oe
#source $HOME/.bashrc
module load intel/14.0.1 hdf5/1.8.11-intel14.0.1 netcdf/4.3.0-intel14.0.1

##### set the run number#####
run=1

# ./usr/local/Modules/3.2.10/init/bash

export OMP_NUM_THREADS=16
export KMP_STACKSIZE=500000000

#ulimit -t unlimited          # cputime
#ulimit -f unlimited          # filesize
#ulimit -l unlimited          # memorylocked
#ulimit -c unlimited          # coredumpsize
#ulimit -m unlimited          # memoryuse
ulimit -s unlimited          # stacksize

# run the model
cd /home/mkelp/geoschemv10-1/thesis_soa/Feb/geos5_4x5_soa

# rm -f log.geos.$run
# ln -s input.geos.$run input.geos

echo STARTING AT `date`

./geos.mp 2>&1 | tee log.geos.$run

echo ENDING RUN AT `date`
```

Figure 2.32: run.geos.cluster, Colorado State University example

Script used to run a GEOS-Chem simulation at Colorado State University. Potentially may be edited for use on a different cluster.

## 2.7: Adding Tracers and Making New Restart Files

In order to add new tracers to simulations, such as the APIN term, the IDL and GAMAP programs are required. To create a new restart file, the model must be run without any added tracers or changes to the code; it does not matter what period of time the simulation covers (can simulate a single day). Once the model is run, changes can be

made to the hard code. The first step taken was to add the new tracer in the input.geos file under the tracer menu:

Tracer #94    94    APIN 136.23

After this addition, the appropriate GEOS-Chem tracer section of the tracerinfo.dat file was modified to include additional tracers found in Table 2.2.

Table 2.2: What tracer species to add to the tracerinfo.dat for a new SOA simulation

Added the following tracer species to the tracerinfo.dat file in the new SOA run directory. Do not use tabs to fill out the columns when adding new tracers to tracerinfo.dat. Use spaces instead. Note that there will be no tracerinfo.dat file if the model is not first run in the directory.

Name	Full Tracer Name	Molecular Weight (kg/mol)		Tracer Number	Scale Factor to Convert to Unit	Unit
APIN	APIN tracer	1.362E-01	1	94	1.000E+09	ppbv
APIN	APIN tracer	1.362E-01	1	1094	1.000E+00	molec/cm2/s
APIN	APIN tracer	1.362E-01	1	2094	1.000E+00	molec/cm2
APIN	APIN tracer	1.362E-01	1	3094	1.000E+00	kg/s
APIN	APIN tracer	1.362E-01	1	4094	1.000E+00	kg
APIN	APIN	1.360E-01	1	33094	1.000E+00	kg
APINdf	APIN drydep flux	1.362E-01	1	36094	1.000E+00	molec/cm2/s
APINdv	APIN drydep velocity	1.362E-01	1	37094	1.000E+00	cm/s

Special attention was paid so that the tracer number (94) was the same in both files for the APIN variable.

Once the input.geos and tracerinfo.dat files have been updated with the added tracer information, a new restart file is needed to incorporate this additional tracer. IDL was opened and the following list of commands found in Figure 2.33 was used.

a) Load the new tracerinfo.dat in IDL.

```
IDL> ctm_tracerinfo, file= 'tracerinfo.dat', /force      ; Uses input from updated tracerinfo.dat
IDL> ctm_cleanup                                       ; Clears memory
IDL> gamap, file='restart.YYYMMDDhh'                  ; Loads selected restart file & lists tracers
>> q                                                 ; Quits GAMAP
IDL> ctm_cleanup
```

2. Edit and run make\_restart.pro.

a) View the contents of make\_restart.pro.

```
cd ~/IDL/gamap2/file_io
more make_restart.pro
```

Figure 2.33: Creating new restart files in IDL

Followed the commands to load the edited tracerinfo.dat file and compile the make\_restart.pro script. These commands set up IDL to create a new restart file. List of commands were obtained from the GEOS-Chem Wiki under “Adding tracers to GEOS-Chem”.

Afterwards, the following code was used to create a geos5 meteorology simulation on a  $4 \times 5^\circ$  horizontal resolution grid with 47 vertical levels starting at January 1 2005 for the added APIN tracer number 94:

```
IDL> MAKE_RESTART, OUTMODELNAME='GEOS5_47L', OUTRESOLUTION=4, OUTFILENAME='new.restart.YYMMDDhh', TAU0=NYMD2TAU( 20050101L ),
DATAVALUE=1e-20, TRACERLIST=[94], UNIT='v/v', DIAGN='IJ-AVG-$'
```

Figure 2.34: IDL command to create a new partial restart file

Created a restart file with geos5 meteorology on a  $4 \times 5^\circ$  horizontal resolution grid with 47 vertical levels starting at January 1 2005 for a new APIN tracer number 94.

The  $1e-20$  value is a low initial concentration value that is used to populate the tracer before running a simulation.

Finally, the instructions in Figure 2.35 were followed to merge the data of the new restart file (the added tracer APIN) with the existing restart file (all other tracers).

```
IDL> gamap, file='restart.YYYYMMDDhh'           ; Loads original restart file & lists tracers
>> q                                           ; Quits GAMAP (saves tracers)
IDL> gamap, file='new.restart.YYYYMMDDhh'      ; Loads new restart file & lists tracers
>> q                                           ; Quits GAMAP (saves old & new tracers)
IDL> gamap, /nofile                            ; Loads tracers that are saved in memory
>> s#-#                                         ; Type tracer #s to save

You will then be prompted with a dialog box.
Type the name for the new restart file and press the SAVE button.

IDL> ctm_cleanup                               ; Clears memory
```

Figure 2.35: Merged new and old restart files in IDL

Followed the coding instructions to merge the new and old restart files to create a new restart file with the added APNIN tracer. List of commands were obtained from the GEOS-Chem wiki under “Adding tracers to GEOS-Chem”.

Once the new restart file with the added tracer was created, it was used as the new input restart file for SOA global simulations. Note that a year of spin up should always be performed to remove the effects of initialization.

All modules that were edited in Table 2.1 are archived and stored on a personal git. These modules can be accessed by request to Dr. Juliane Fry.

## Results and Discussion

The following sections include an unlumping controls analysis in which the coding changes in Section 2.5 were evaluated to determine if coding errors or biases exist between the base model and the unlumped APIN versions. The results of the  $\alpha$ -pinene-NO<sub>3</sub> zeroed pathway were compared to the unlumped  $\alpha$ -pinene control simulation using global and regional maps and time series plots for various months. Finally, global yearly budgets of monoterpenes and SOA were compared before and after the unlumping, using the unlumped  $\alpha$ -pinene control simulation as a base case for comparison.

### 3.1: Unlumping Control Analysis

In order to ensure that later changes in SOA are real and not coding error artifacts, an unlumping control analysis was performed. Before the unlumped APIN tracer term was speciated with an aerosol producing NO<sub>3</sub> yield of zero, it was first populated with the same  $\alpha$  values as that of the MTPA  $\beta$ -pinene parameterized lumped species. Essentially, the reason to keep APIN the same as MTPA is to observe if there are any rounding losses or other errors associated with unlumping  $\alpha$ -pinene out of the MTPA tracer in the model. Theoretically, the difference between the two tracers for this controls analysis should be zero.

In order to test these controls against each other, a 2006 simulation (2005 spin-up) with twelve monthly average outputs were run for both a base case model control simulation without any changes to  $\alpha$ -pinene treatment and an unlumped APIN species with  $\alpha$ -pinene assigned the same VBS parameterization as all lumped terpenes in the control MTPA (Figure 3.1). Figures were made for the month of August for this control comparison analysis, because August is the month that produces the most SOA as plant species are most actively producing VOC during this time due to the increased temperature.

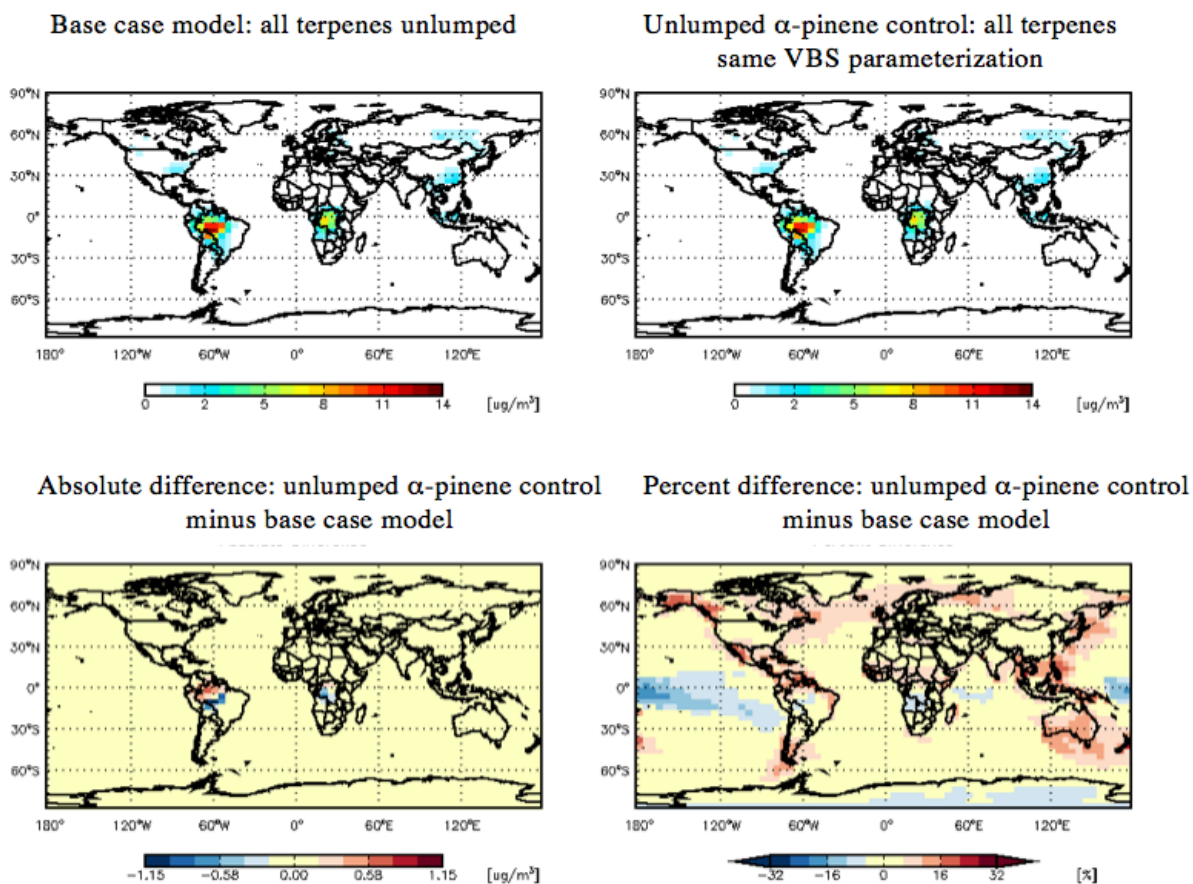


Figure 3.1: Global absolute and percent difference plots total terpene SOA mass loading (TSOA) from monoterpenes in August

The top left figure is the spatial distribution of TSOA from monoterpenes in the base case model control simulation, the top right figure is the TSOA with APIN unlumped from MTPA with the same VBS yields, the bottom left figure is the absolute differences between the two simulations (this is the  $\alpha$ -pinene unlumped control minus the base case model, so that a region in red has a larger SOA concentration for the  $\alpha$ -pinene unlumped simulation and a region in blue has a larger SOA concentration for the base case model), and the bottom right figure is the percent differences between the two simulations.

According to Figure 3.1, in terms of the absolute differences there are small underestimations and overestimations of SOA in specific source regions. The result of unlumping is prediction of greater SOA production from monoterpenes in the Amazon forested regions of Brazil and less in the Congo forests in Africa and the Northern Boreal forests in Russia. These regions seem to differ up to  $1.15 \mu\text{g}/\text{m}^3$  in magnitude. This value

seems significant; however, the absolute concentrations of SOA in these areas are on the order of 11-14  $\mu\text{g}/\text{m}^3$ , which makes the 1.15  $\mu\text{g}/\text{m}^3$  less impactful than if the difference were in the United States, which has the highest SOA producing source regions found in the Southeast producing about 2  $\mu\text{g}/\text{m}^3$ . The bottom right panel in Figure 3.1 shows percent differences up to  $\pm 32\%$ . In this view, there seem to be large differences in the Pacific Ocean. The percent differences in these areas should largely be ignored as these areas contain little to no SOA, so any large difference is a result of partitioning where the absolute differences between simulations may be very small, but percent difference is large because the denominator is also very small. In addition, the code to create a difference plot such as Figure 3.1 can be found in Appendix A in Figure A.1.

The following Figure 3.2 is of the same difference analysis performed in Figure 3.1 but for the specific volatility bins ( $C^*=0.1, 1, 10, 100$ ) found in the GEOS model. The sum of these bins in Figure 3.2 adds up to the total SOA found in Figure 3.1. A few caveats about the following figure must be made. These volatility bins are kept in the units of ppb so that the partitioning between aerosol (SOA) and gas (SOG) can be kept consistent; therefore these units are different than those in Figure 3.1. However, the analysis done for this figure concentrates on the absolute difference between the two control runs, so the units matter only relative to the variability of the simulations to each other. That is, the simulations can be kept in ppb if the comparison is the absolute difference between each other in ppb (and not necessarily comparing Figures 3.2 in ppb to 3.1 in  $\mu\text{g}/\text{m}^3$ ). In addition, because of the small absolute variability between the control runs, the percent variation is not taken into account for similar reasons discussed for Figure 3.1.

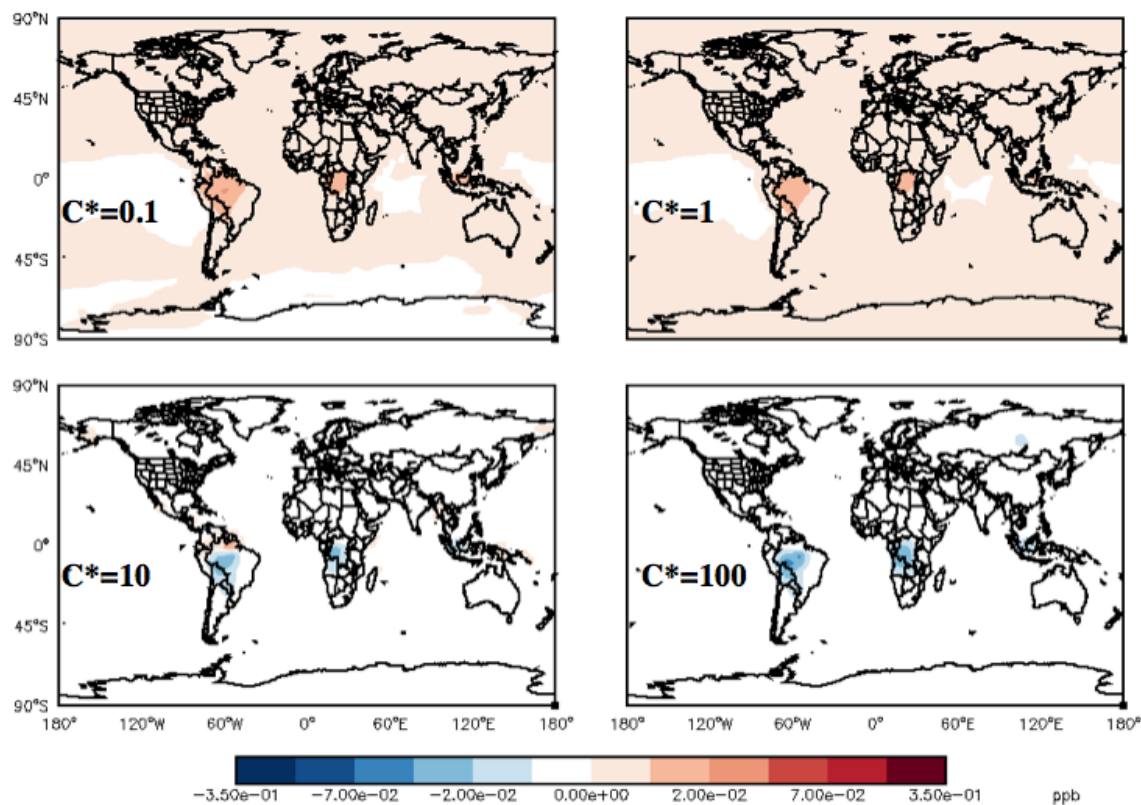


Figure 3.2: Absolute difference analysis for all  $C^*$  volatility bins in August

These absolute differences are from the  $\alpha$ -pinene un lumped control minus the base case model, so that a region in red has a larger SOA concentration for the  $\alpha$ -pinene un lumped simulation and a region in blue has a larger SOA concentration for the base case model. The volatility bins are labeled on each figure. Relative to a maximum production of SOA for each bin, the mixing ratio differences between the  $C^*$  volatility bins (0.1, 1, 10, and 100) constitute a change of less than 10%, 14%, 7%, and 14% in high producing SOA source regions, respectively.

According to Figure 3.2, no volatility bin yielded an absolute error greater than 14% between the control runs in high producing source regions. The  $C^*=0.1$  and 1 bins reveal that the APIN un lumped simulation had greater SOA produced in the Congo and Amazon forested regions than the base case model simulation. The absolute differences were much smaller than the emissions at these regions and constituted an error less than 10% and 14%, respectively. The results in the  $C^*=10$  and 100 volatility bins suggest that the base case model has greater SOA production in the Congo and Amazon than the

APIN unlumped control simulation. The differences between these high SOA emitting areas were less than 7% and 14% for the  $C^*=10$  and 100 bins, respectively.

According to the discussion of Figure 3.2, there do seem to be regions where the difference in SOA is consistently predicted. There is a regional preference in the sense that where there are differences in SOA production between the control runs, there are areas that produce a lot of VOCs from large forests such as the Amazon and Congo. However, the absolute differences between the code versions may be thought of as random or rounding error as the differences in these runs never surpass 14%. In addition, the difference as to which model run will produce a higher or lower difference in these regions for a given volatility bin is not consistent. For example, the Congo forests produce more SOA in the  $C^*=0.1$  and  $C^*=1$  bins for the APIN unlumped simulation compared to the base case control, while the same region produces less SOA in the  $C^*=10$  and  $C^*=100$  in the APIN unlumped simulation relative to the base case control. In short, we can assume there is no bias between the code versions because there is no specific directionality or preference towards either of the control simulations to conclude that the error between them is significant.

## **3.2: Global and Regional Simulation Results of a Reduced $\alpha$ -Pinene- $\text{NO}_3$ Pathway**

In this section the results of the implementation of the novel  $\alpha$ -pinene- $\text{NO}_3$  VBS scheme will be analyzed. The mechanistic scheme for the reduced APIN- $\text{NO}_3$  SOA pathway reflected that of the model structure in Figure 2.1.

For these sets of model runs, a 2006 simulation (2005 spin-up) with twelve monthly average outputs was performed for the reduced APIN- $\text{NO}_3$  SOA mechanism and compared to the unlumped control simulation from section 3.2.

Before the results of these simulations are discussed, the significance of  $\alpha$ -pinene must be reiterated. In terms of the collective understanding of monoterpenes,  $\alpha$ -pinene is thought to be the most globally abundant. Referencing Figure 1.3,  $\alpha$ -pinene may constitute up to 50% of all monoterpenes in certain areas. For the sake of comparison, the

same type of figure as Figure 1.3 was made for the monoterpene emissions in the GEOS-Chem model (v.10-01i) for both the USA and the globe (Figure 3.3 and Figure 3.4). Notice that both regionally in the USA and globally  $\alpha$ -pinene can constitute up to an average of a third of all monoterpene emissions. This value underscores a potentially large difference in the reduction of SOA from the implementation of a new APIN-NO<sub>3</sub> model scheme.

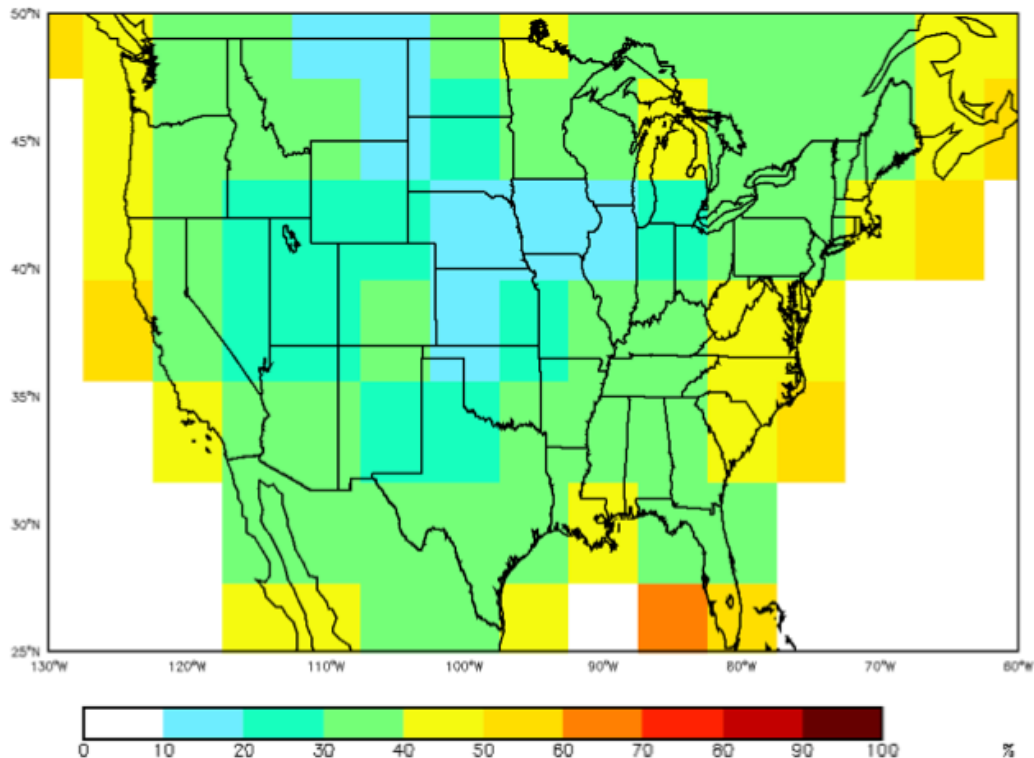


Figure 3.3: Regional distribution of  $\alpha$ -pinene during July in the USA relative to total monoterpene emissions in the GEOS-Chem model

Notice that the model output compares favorably to Figure 1.3 and that  $\alpha$ -pinene is a dominant monoterpene emitted in the United States in terms of abundance.

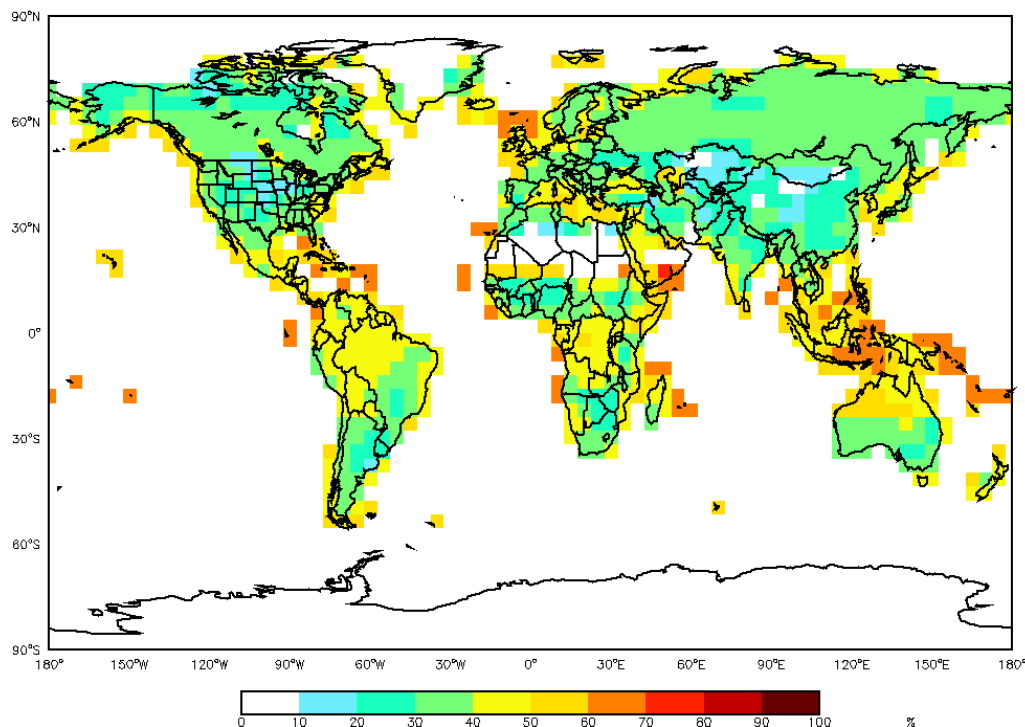


Figure 3.4: Global distribution of percent terpene emissions that are  $\alpha$ -pinene during July in the GEOS-Chem model

Globally,  $\alpha$ -pinene constitutes 42% of all monoterpene emissions in the GEOS model v.10 model. Boxes that are white either have no emissions of  $\alpha$ -pinene or no data from that region regarding  $\alpha$ -pinene.

The first method of comparing the SOA model changes is to employ difference plots similar to those in Section 3.2. The following Figures 3.5 and 3.6 are of difference plots for August and January, respectively, presenting views of the effects of implementing an APIN-NO<sub>3</sub> SOA yield of zero. Figure 3.5 reveals that both simulations generally calculate the same global distribution of SOA, but that specific source regions such as the Congo forests in Africa and the Amazon in Brazil both produce less SOA when the yield from the nitrate radical is set to zero. Figure 3.7 and Figure 3.8 are the same absolute difference plots for the month of August but with a focus on the globe and USA, respectively. In addition, Figure 3.6 for the plots in January shows a somewhat different spatial variability. The absolute differences seem only to reveal a change in the Congo forests and not necessarily for the other high VOC, SOA producing regions. This

difference is a result of the fact that in January the Northern Hemisphere is in winter with less sunlight, meaning that less VOC is produced. The Northern Hemisphere, which contains the majority of the Earth's biomass, produces the most SOA in July-August. However, the Congo forests are not in the Northern Hemisphere but are actually fairly close to the equator, which provides them with near yearlong sunlight to consistently produce VOCs and SOA. Furthermore, Figure 3.9 and Figure 3.10 are the same absolute difference plots for the month of January but with a focus on the globe and USA, respectively. Figure 3.11 is an  $\alpha$ -pinene emissions map for the United States. (Figures 3.5-11 employed a smoothing interpolation function instead of the box model grid for analysis).

In short, the largest magnitude differences are found in the summer months of June, July, and August, which can produce absolute differences of 2.37, 2.50, and 3.56  $\mu\text{g}/\text{m}^3$  in high producing SOA source regions respectively. On the other hand, the winter months yield the smallest overall differences of 1.76 and 1.37  $\mu\text{g}/\text{m}^3$  in January and February, respectively.

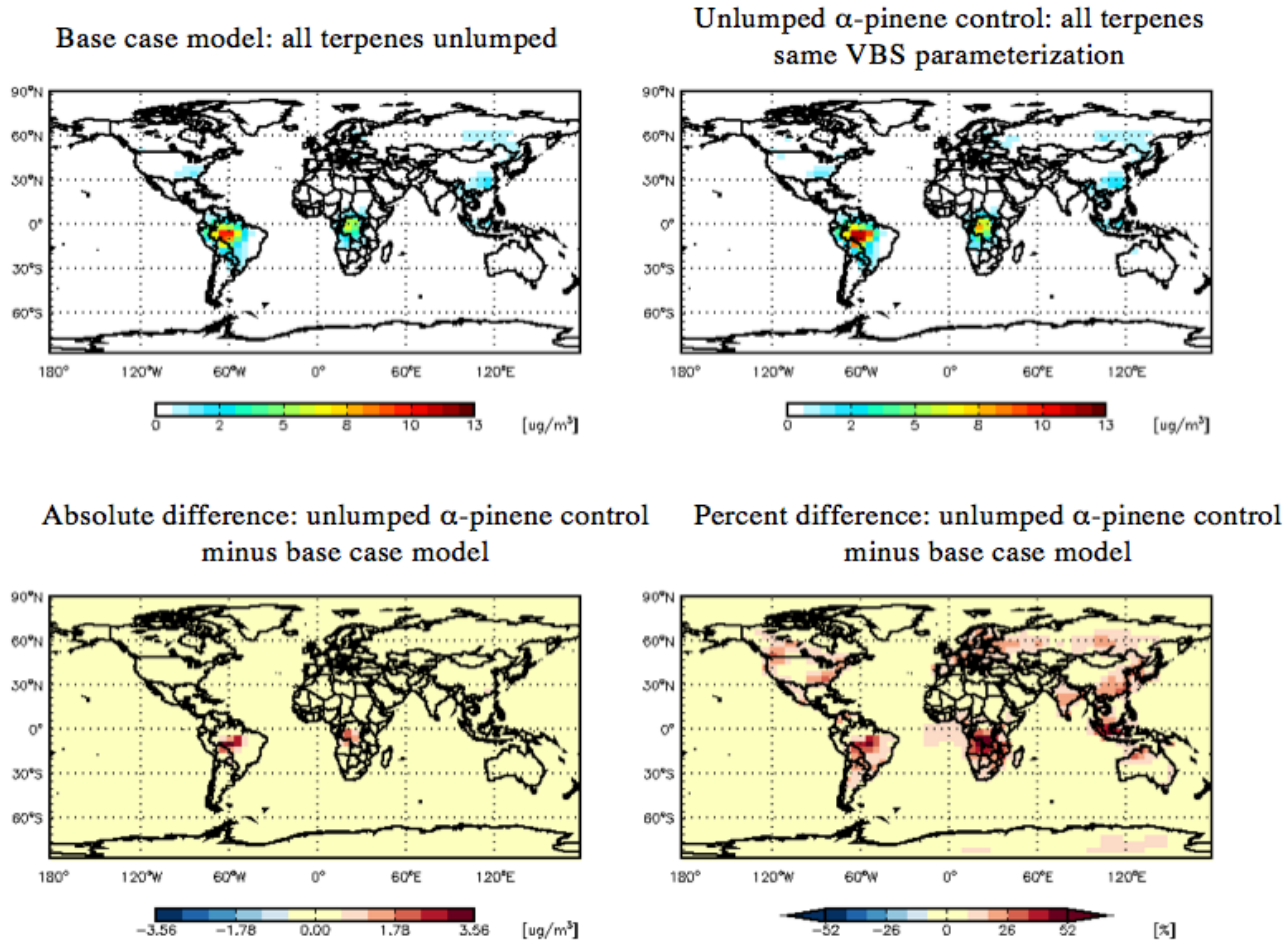


Figure 3.5: Global absolute and percent difference plots for total SOA from monoterpenes in August for the un lumped control and APIN-NO<sub>3</sub> SOA yield equal zero simulations

This difference comparison is the  $\alpha$ -pinene un lumped control minus the nitrate-zeroed model, so that a region in red has a larger SOA concentration for the  $\alpha$ -pinene un lumped simulation and a region in blue has a larger SOA concentration for the nitrate-zeroed model. The largest absolute change is found in the Congo forests, which produce up to 3.56  $\mu\text{g}/\text{m}^3$  less SOA when the nitrate pathway is reduced. Note that absolute differences in the color red represent the un lump control simulation yielding more SOA than the nitrate zeroed yield simulation.

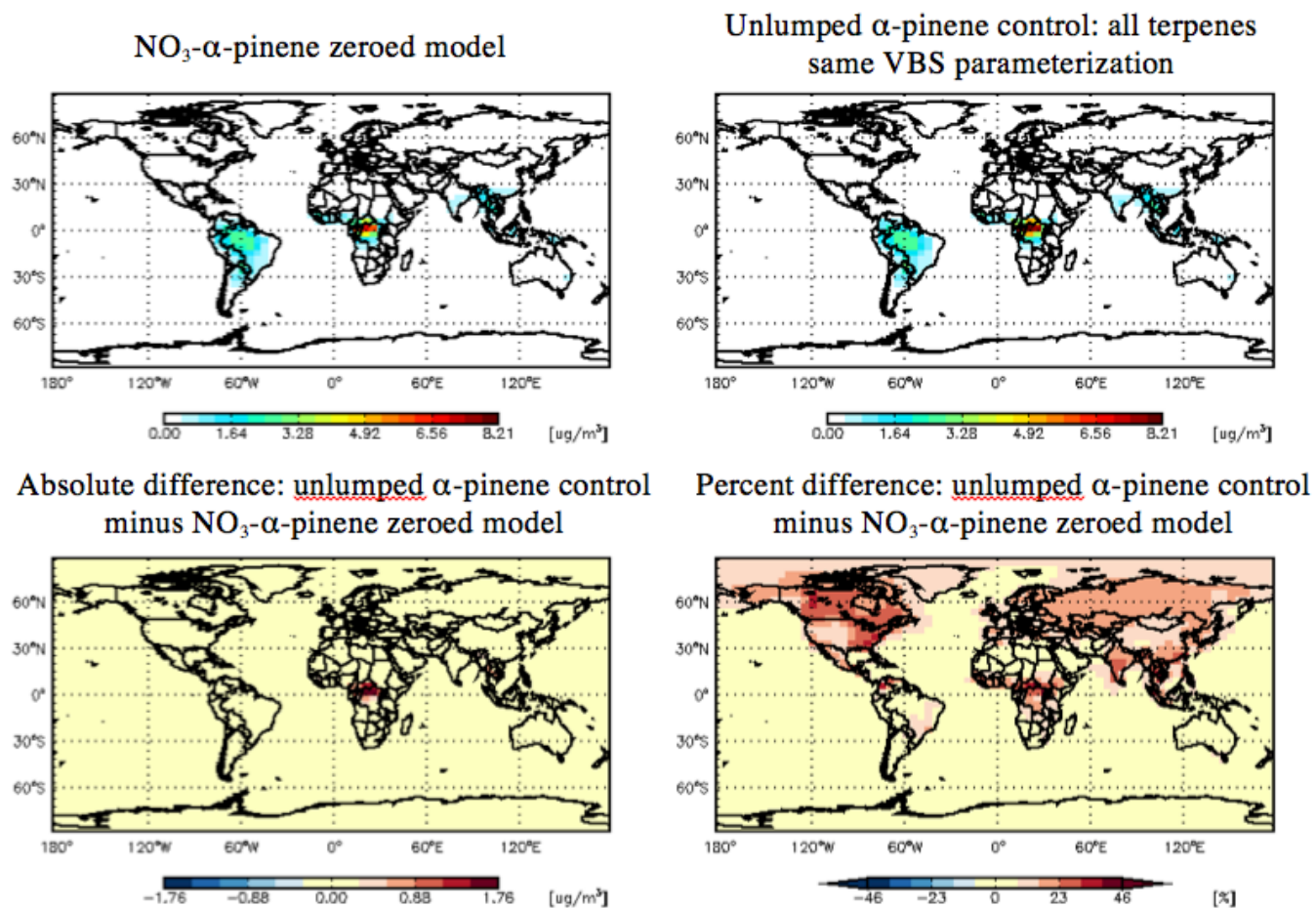


Figure 3.6: Global absolute and percent difference plots for total SOA from monoterpenes in January for the unlump control and APIN-NO<sub>3</sub> SOA yield equal zero simulations

The largest absolute change is found in the Congo forests, which produce up to 1.76  $\mu\text{g}/\text{m}^3$  less SOA when the nitrate pathway is eliminated.

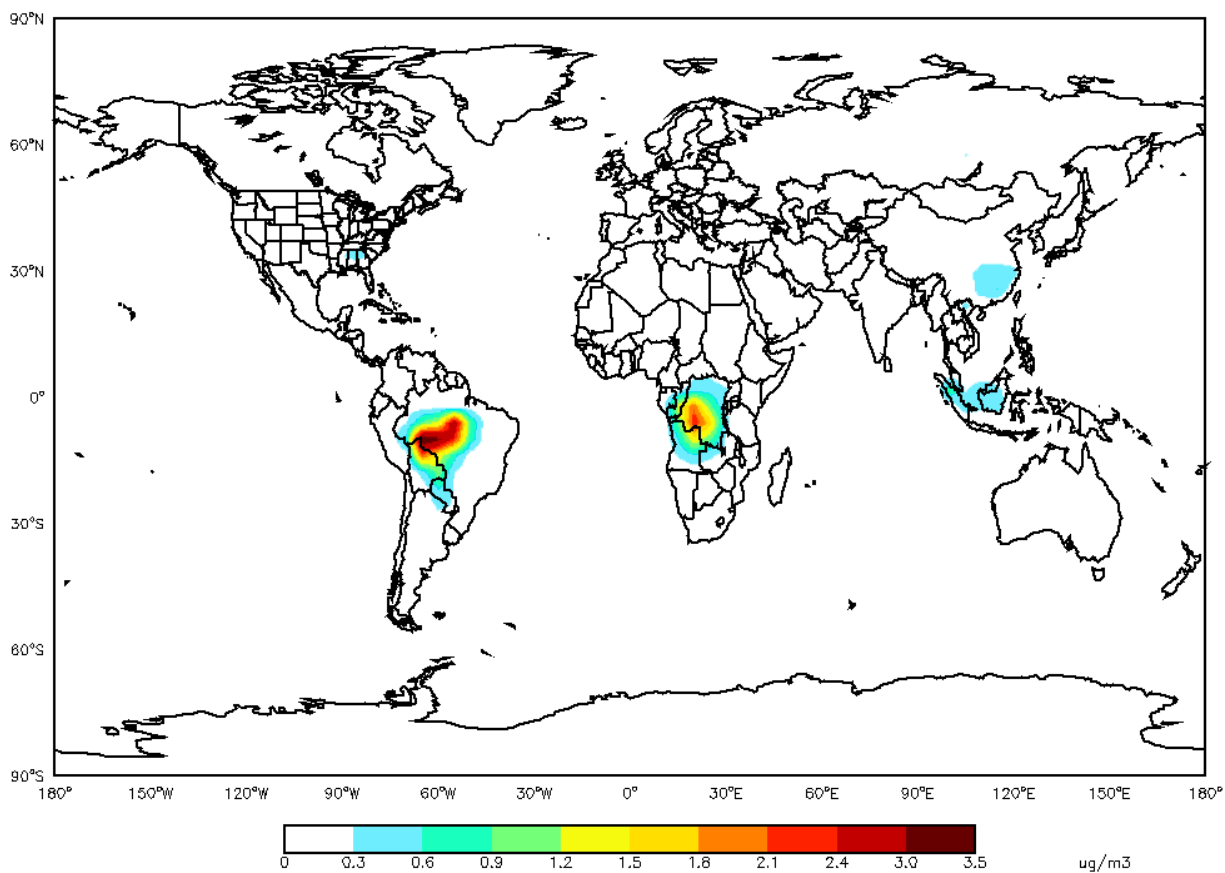


Figure 3.7: Global absolute differences for total SOA from monoterpenes in July for the un lump control and APIN-NO<sub>3</sub> SOA yield equal zero simulations  
Notice the largest differences are in high VOC/SOA producing source regions such as the Congo forests and the Amazon.

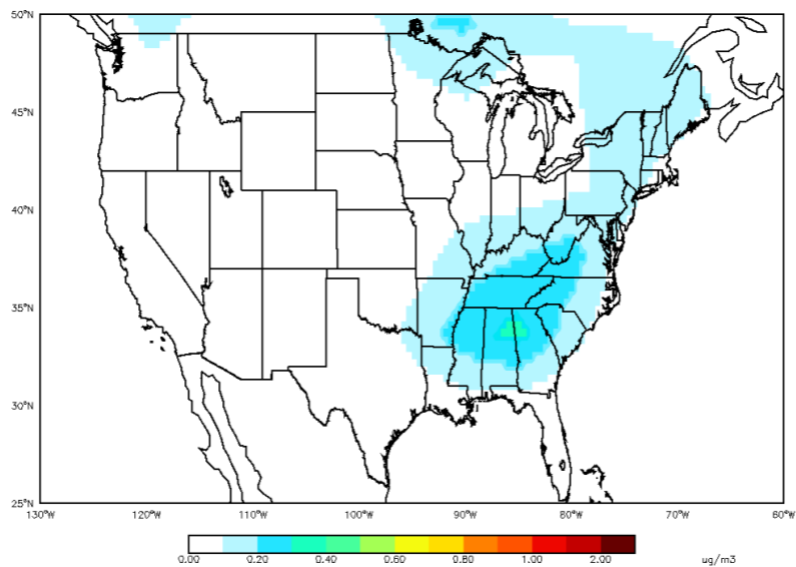


Figure 3.8: Absolute differences for total SOA from monoterpenes in August in the USA for the un lump control and APIN-NO<sub>3</sub> SOA yield zeroed simulations

Notice that the largest differences are found in the Southeastern USA, which contains many pine forests. The magnitude of these differences is much smaller compared to global values found in the Congo and Amazon.

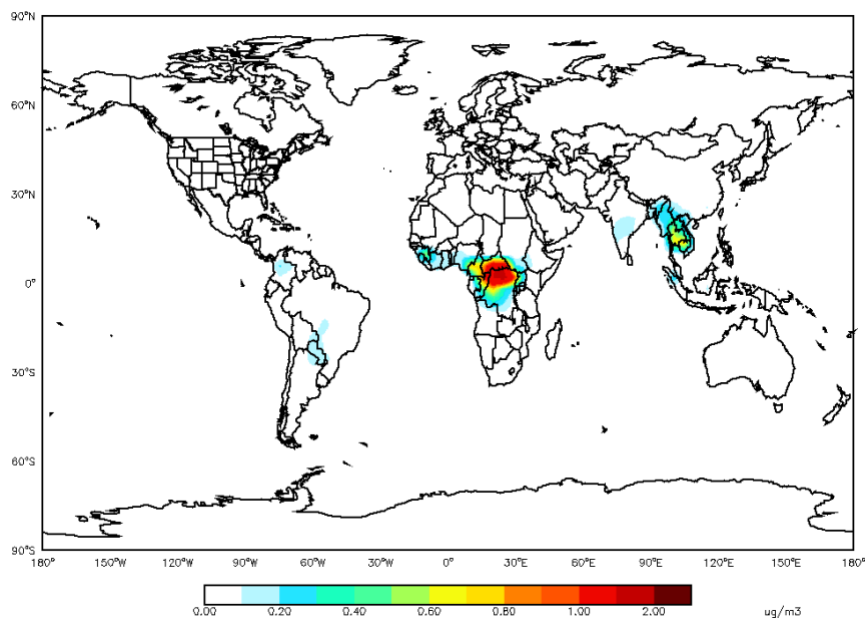


Figure 3.9: Global absolute differences for total SOA from monoterpenes in January for the un lump control and APIN-NO<sub>3</sub> SOA yield equal zero simulations

For January, the greatest differences in SOA from APIN-NO<sub>3</sub> reactions are primarily found in the Congo.

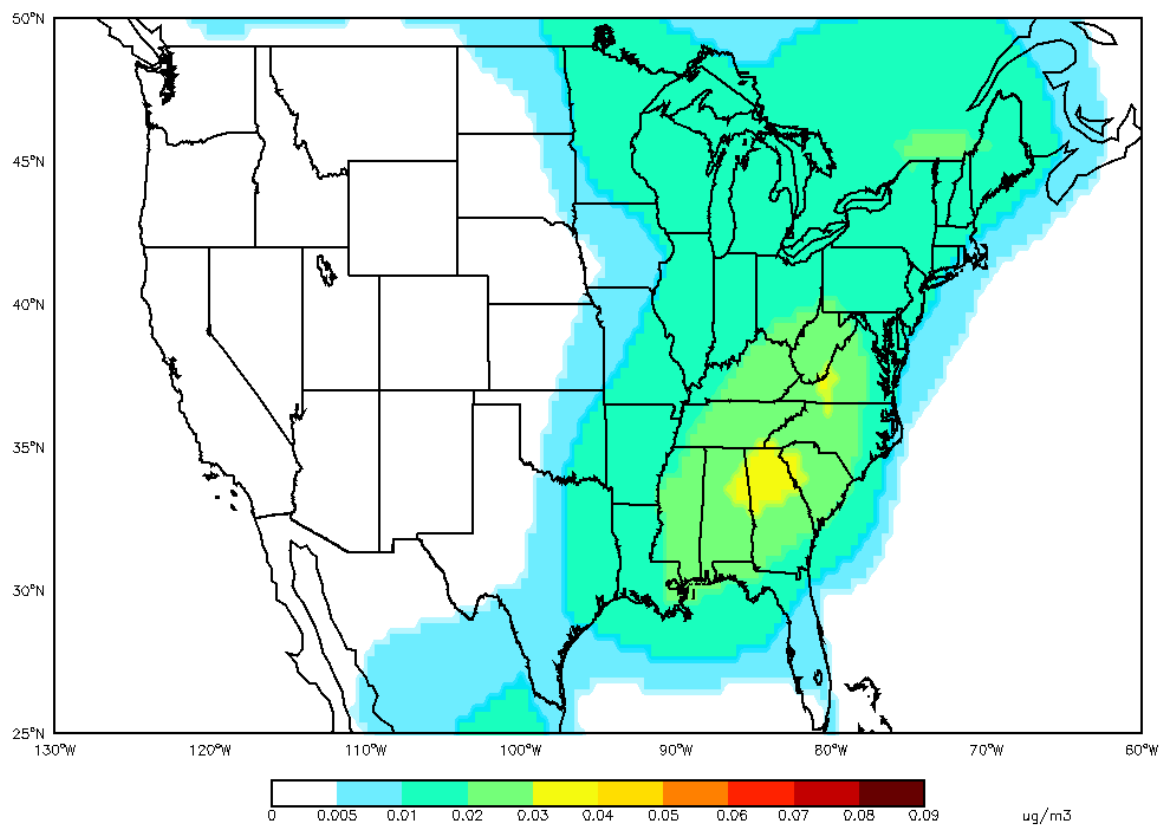


Figure 3.10: Absolute differences for total SOA from monoterpenes in January in the USA for the unlump control and APIN-NO<sub>3</sub> SOA yield equal zero simulations. Notice the magnitude of the absolute differences in SOA is much smaller during January, due to much lower terpene emissions.

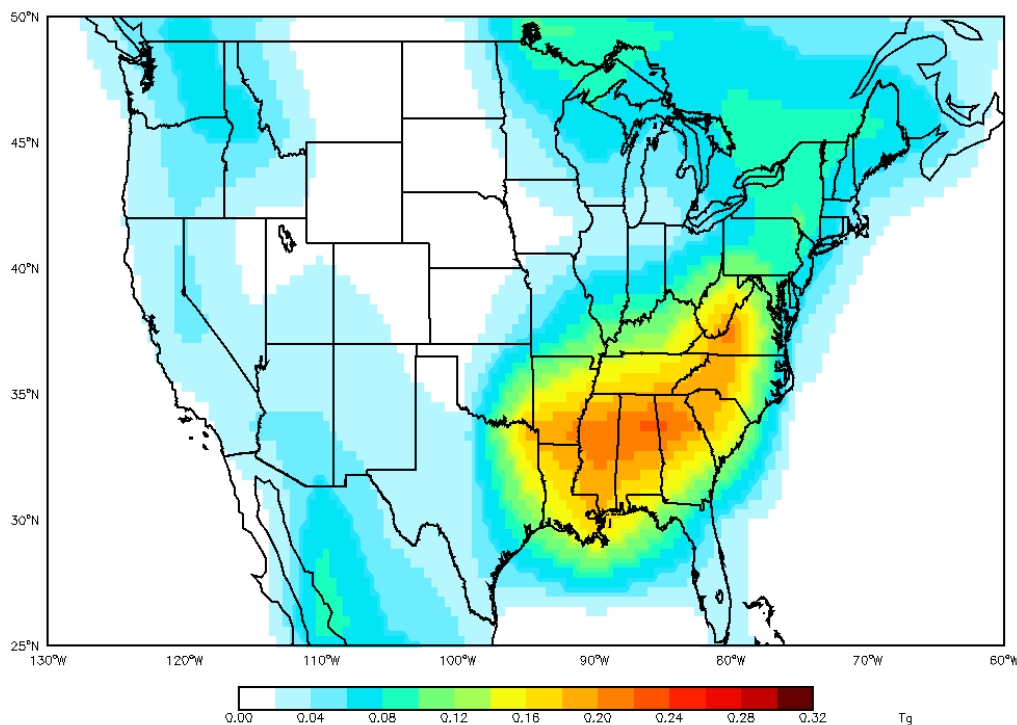


Figure 3.11:  $\alpha$ -pinene emissions in August in the GEOS model (v.10)

Emissions of  $\alpha$ -pinene are larger in the Southeast United States. The hotter, humid climate is more conducive to the production of both VOCs and SOA.

To summarize Figures 3.5-3.11, there exists both temporal and spatial variability in SOA production as the Northern and Southern Hemispheres yield relatively different amounts of SOA given the season. These figures also suggest that the greatest differences between the simulations are found in high VOC/SOA producing regions. Although nitrates may be produced from anthropogenic pollution such as vehicular exhaust, it seems that the greatest areas that produce SOA through the APIN-NO<sub>3</sub> pathway are found in large forested regions with conifers. This means that nitrate enhancement of SOA is most significant in large forests. As for the United States, the largest source of both VOCs and SOA are found in the Southeast in the GEOS model. Since the Southeast does not contain as many conifers as the Northwest, the high emissions from this region are due more to the warmer and more humid climate than to the species of indigenous trees. The coding to create the global difference and USA difference plots are found in Appendix A in Figure A.2.

In addition to difference plots, the following analysis of specific locations utilizes time series plots. Time series plots in GEOS-Chem are an easy way to compare model-to-measurement data of specific locations and to observe predicted seasonal patterns of phenomenon. For example, if there were available ambient SOA measurement data in Portland, OR (latitude: 45.523452, longitude: -122.676207), those measurements could be compared to a model time series output from GEOS-Chem. For the sake of comparison, the National Ambient Air Quality Standards (NAAQS) for the USA set by the EPA has an annual mean cutoff of  $15.0 \mu\text{g}/\text{m}^3$  for secondary  $\text{PM}_{2.5}$ . This means that if the concentration of annual  $\text{PM}_{2.5}$  surpasses  $15.0 \mu\text{g}/\text{m}^3$  then that region is considered 'polluted'. Note that this value constitutes all sources, that is, both biogenic and anthropogenic. Figure 3.12 contains data for Portland, OR for SOA from terpenes, total organic aerosol, and  $\text{PM}_{2.5}$  monitored data from the Reed College warehouse (Brooklyn Rail Yard Project). Close examination reveals that the  $\text{PM}_{2.5}$  dataset (although incomplete) is much higher in magnitude than the OA and SOA from terpenes species. These measurements were taken in an urban center. The OA and SOA from the model accounts for the average aerosol calculated for the entire  $4 \times 5^\circ$  spatial grid (Figure 3.13). Thus, the magnitude of the emissions from the model spans a much larger area and fails to accurately represent the SOA in a city, where much of the pollution would come from anthropogenic sources.

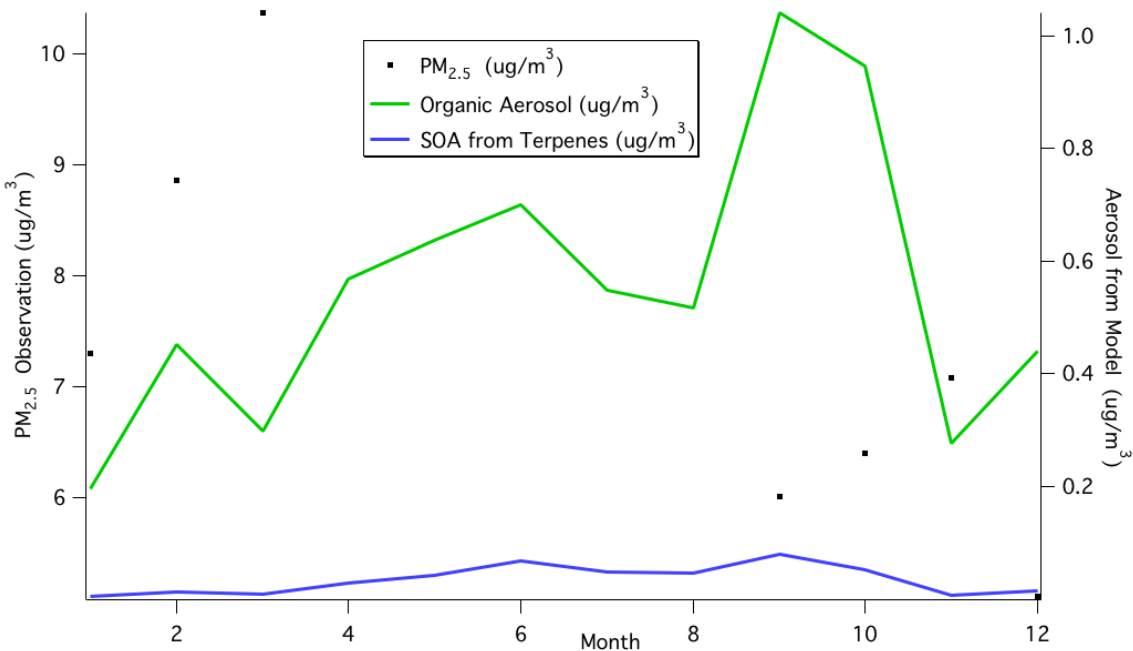


Figure 3.12: Monthly total OA, SOA from terpenes, and monitored PM<sub>2.5</sub> data from Reed College Warehouse in Portland, OR time series

The PM<sub>2.5</sub> data (black, left axis) were obtained from the Reed College warehouse monitoring site in 2014. Note that this dataset is incomplete. The total OA concentrations (green, right axis) and the SOA from terpenes (blue, right axis) are derived from the GEOS model. All time series plots made in this thesis were for the surface level.

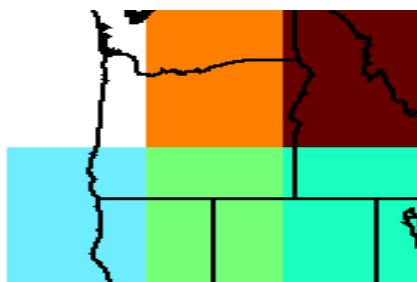


Figure 3.13: 4x5° spatial grid containing Portland, OR

The boxes are different colors in this example to show the spatial extent of a 4x5° grid box. The edges of the pixels are at the edges of the figure.

Although modeled data from Portland, OR yielded little information due to the small absolute concentrations of SOA from monoterpenes (and SOA in general), an examination of high producing source regions in both the Northern Hemisphere and Southern Hemisphere reveals more information of the spatial and temporal distribution of SOA. For the Southern Hemisphere, the high producing Congo Forests (latitude: -3.798484, longitude: 20.148926) were analyzed. Figure 3.14 reveal the monthly concentrations of total SOA and SOA from monoterpenes in the Congo Forests modeled by GEOS-Chem. The total modeled monthly SOA data suggests that the Congo forests produce much more SOA than Portland, OR, by a factor greater than 10, depending on the month. The months from June to August overwhelmingly produce the greatest magnitude of SOA, almost totaling  $30 \mu\text{g}/\text{m}^3$ . In addition, the modeled SOA specifically from monoterpenes suggests that SOA from monoterpenes alone can contribute from a third (August) to a half (January) of total SOA emissions. To be sure, this contribution is significant. For a complete analysis, Figure 3.15 was included to illustrate the absolute difference in SOA from monoterpenes between the un lumped/control simulation and the nitrate yield set to zero model run. Figure 3.15 reveals that, depending on the month, differences in SOA concentrations from monoterpenes can be up to  $2.0\text{-}2.5 \mu\text{g}/\text{m}^3$ , which correlates well to the difference plot created in Figure 3.5 for that area. The significance of the values of  $2.5 \mu\text{g}/\text{m}^3$  and the  $3.5 \mu\text{g}/\text{m}^3$  from the Amazon and their impact on the global yearly SOA budget will be discussed in Section 3.3.

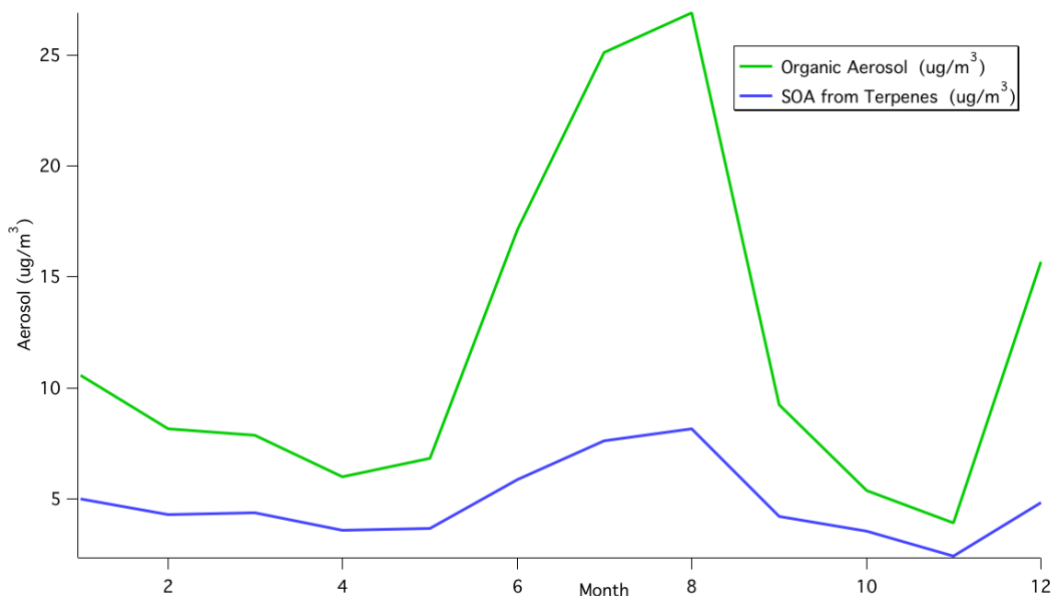


Figure 3.14: Monthly total OA and SOA from terpenes in Congo Forest time series

The total OA concentrations (green) and the SOA from terpenes (blue) are derived from the GEOS model. These monthly values are much greater than that of Portland, OR and actually exceed the annual standard set by the EPA for the USA.

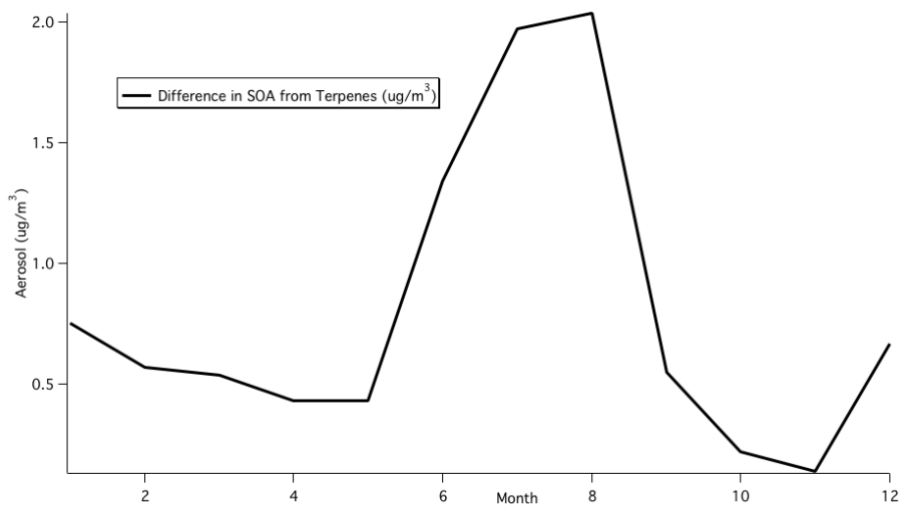


Figure 3.15: Differences in monthly SOA from monoterpenes in the Congo Forest

between the unclump control simulation and the nitrate yield set to zero run

Differences between the simulations can total up to about  $2.5 \mu\text{g}/\text{m}^3$  for the summer months.

In addition to the Congo forest, a northern Boreal forest in Russia (latitude: 56.072035, longitude: 100.371094) was analyzed to understand the spatial and regional distribution of SOA in a Northern Hemisphere forest. Typically, the Boreal forests produce the most OA in July, while the Congo and Amazon tend to produce more OA in August. Figures 3.16 and 3.17 follow the same plot types as Figures 3.14 and 3.15. Notice the incredibly high magnitude of OA in Figure 3.16. This large increase is due to a biomass-burning event that saturated the model. Perhaps this plot is not the most representative example to compare to the Congo forest in Africa as typically the Northern Boreal forest produces around  $20 \mu\text{g}/\text{m}^3$  in the summer. Although the fire event, which is incorporated in the GEOS5 meteorology, skews the data, it is important to illustrate that the GEOS model features dynamic meteorology that reflect real, historic events. However, the SOA contribution from monoterpenes alone is thus more difficult to quantify due to the skewing event. Figure 3.16 reveals that SOA from monoterpenes alone in the region can contribute up to  $7 \mu\text{g}/\text{m}^3$  in July, but the proportional contribution is harder to determine. Finally, Figure 3.17 (ignoring July) reveals that the differences in SOA concentrations from monoterpenes are typically around  $2.0 \mu\text{g}/\text{m}^3$  in the summer months for the Northern Boreal forests. Example code for the creation of these time series plots can be found in Appendix A in Figure A.3.

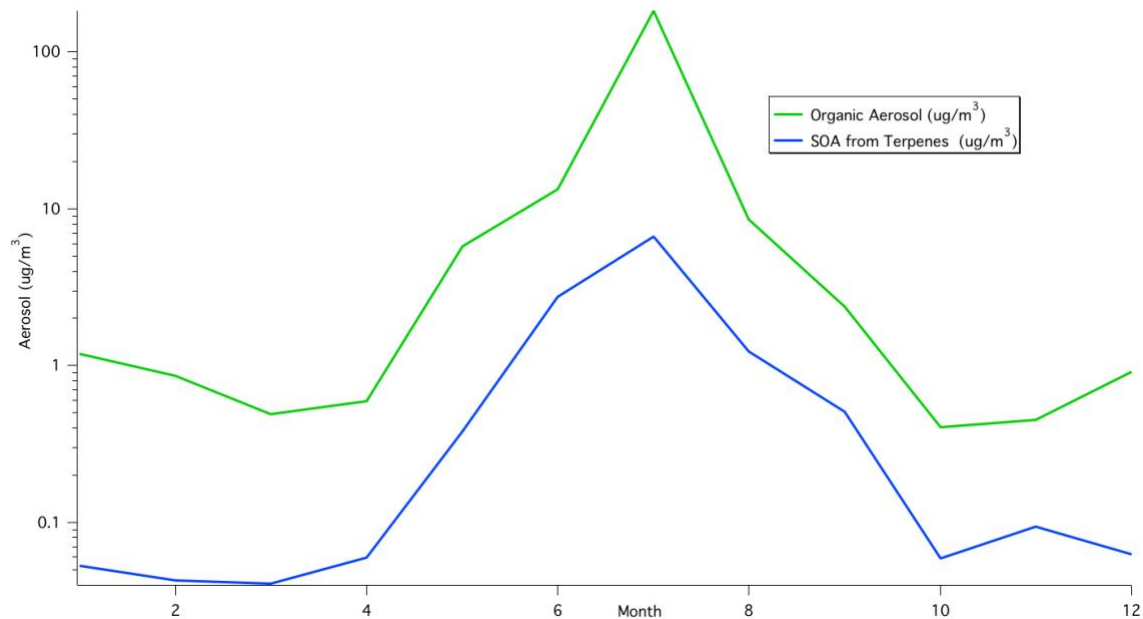


Figure 3.16: Monthly total OA and SOA from terpenes in Northern Boreal Forest in Russia time series

The total OA concentrations (green) and the SOA from terpenes (blue) are derived from the GEOS model. Note that the axis is log-based to illustrate the contribution of SOA from terpenes to total OA concentration.

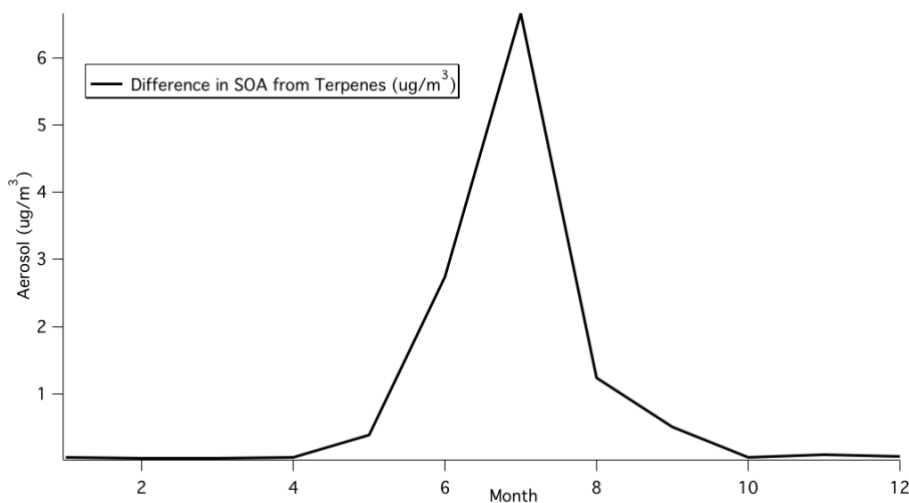


Figure 3.17: Differences in monthly SOA from terpenes in a Northern Boreal Forest between the unump control simulation and the nitrate yield set to zero run

Differences between the simulations usually total up to about  $2.0 \mu\text{g}/\text{m}^3$  for the summer months; however, because of the large biomass burning events in July, the differences totaled  $6.7 \mu\text{g}/\text{m}^3$  for that month.

### 3.3: Global Yearly Budgets

The previous sections explored the spatial and temporal distributions of SOA in the GEOS-Chem model under different model simulations. In addition to analyzing monthly differences, effects of more accurately representing  $\alpha$ -pinene SOA on the annual OA budget is also of interest. As mentioned in Section 3.2, some high producing VOC/SOA source regions can differ in SOA monthly production up to  $3.5 \mu\text{g}/\text{m}^3$  when the APIN-NO<sub>3</sub> pathway is zeroed. What does a value of that magnitude mean in terms of a global yearly difference of SOA? The yearly budgets for Pye's (et al. 2010) GEOS v.8-01-04 simulations, the unlump control, and nitrate zeroed model runs were tabulated in Table 3.1. The values for total monoterpene emissions and  $\alpha$ -pinene emissions vary between different GEOS-Chem versions (Pye ran v.8, while this work ran v.10). As a result, the comparison to Pye's work is not a completely analogous comparison because this work employed GEOS version 10, which has more monoterpenes and consequently more SOA produced in the model than Pye's version. However, when comparing the SOA produced from monoterpenes calculated in the unlump control (19 Tg) and the NO<sub>3</sub> zeroed simulations (17 Tg), this work suggests that a reduction in the APIN-NO<sub>3</sub> pathway results in a 2 Tg reduction of global OA production in this newly implemented scheme. That is, older models without this scheme may potentially overestimate the Earth's SOA budget by **2 Tg** per year.

Table 3.1: Global Yearly SOA Budgets for GEOS-Chem simulations

The total emissions of monoterpenes and of  $\alpha$ -pinene vary between every GEOS model version. However, this work suggests that by reducing the SOA yield from  $\alpha$ -Pinene-NO<sub>3</sub> reactions to be more consistent with laboratory data, there is a total reduction of 2 Tg of SOA produced in a year.

	Total Monoterpene Emissions (Tg)	$\alpha$ -Pinene Emissions (Tg)	SOA from Monoterpenes (Tg)
Pye et al. (2010)	102	34	14-15
Unlump Control	123	51	19
NO <sub>3</sub> zeroed	123	51	17

Finally, Figure A.4 in Appendix A contains a coding example to calculate the yearly budget of  $\alpha$ -pinene in the model.

## Future Work

Several other projects come to mind for future work regarding the unlumping and speciation of chemical tracers in GEOS-Chem. First and foremost, the model simulations from this work should be compared to measured data either from field work or from satellite observations. In addition, there exist other opportunities to speciate terpenes with even greater yields of SOA that are not parameterized correctly in the model such as the high yields from the sesquiterpenes and terpinolene which are both parameterized by the  $\beta$ -pinene-NO<sub>3</sub> experiments from Griffin et al. (1999a). Finally, a more computational analysis of the code versions may be interesting. That is, analyzing the effects on computation time when running multiple years of SOA chemistry and how greater degrees of speciation may affect model cost.

## Conclusions

The global chemical transport model GEOS-Chem has been used to simulate global organic aerosol from monoterpenes. A new VBS mechanistic scheme was implemented by un lumping  $\alpha$ -pinene from an existing diagnostic tracer and speciating it with its own chemistry to discern the effects of a reduced SOA producing nitrate pathway. The major finding of this work is that for high SOA producing source regions such as the Amazon, there is a  $3.5 \mu\text{g}/\text{m}^3$  decrease in predicted SOA in the summer months. Integrated over the globe, the reduction in SOA concentrations due to this updated chemistry leads to an annual difference of 2 Tg between the control and novel VBS mechanisms. The value of  $3.5 \mu\text{g}/\text{m}^3$  is significant considering regulatory thresholds and that a 2 Tg difference is nearly a 10% change in terpene organic aerosol. To be sure, these model differences clearly demonstrate the potential importance of improving SOA mechanisms in models.

Additionally, an important aspect of this work is the presentation of a deliberate and methodical way of dissecting a chemical transport model and implementing a unique chemistry for a tracer that previously had been thought common and similar to the other bicyclic monoterpenes with which it was lumped. Furthermore, there is always value in updating a model to more accurately reflect what is observed in the natural world. The large error range of models is evidence that SOA models are in many cases rough. However, the novel approach of this thesis is its identification of a technique to make one of the most well-accepted chemical transport models agree better with experimental results and its finding of a 10% change in terpene-SOA predicted. The methods implemented in this work reveal a concise and stepwise sequence to causing a large difference in GEOS-Chem. Perhaps future research may employ the information found in this work to help further constrain the SOA budget in the hopes of reaching a more accurate understanding of the air we breathe.

# Appendix A

```
Filename1 = 'Feb7sim_control.ctm.bpch'  
Filename2 = 'Feb5sim_unlump.ctm.bpch'  
  
date1= 20060701  
  
window, /free, xsize=800, ysize=600  
  
CTM_PlotDiff, 'IJ-SOA-$',Filename1, Filename2, TRACER = 43001, Level = 1, Tau0=Nymd2Tau(date1)  
  
end
```

Figure A.1: Coding a difference plot

This code is how to create a difference plot in a script for IDL. Identify the two file simulations and the date of interest for the data withdraw. “IJ-SOA-\$” is the diagnostic of interest for SOA. The tracer species ‘43001’ is SOA produced from the oxidation of monoterpenes (tracer numbers can be found in the GEOS-Chem users manual). The ‘level’ specifies from which vertical height to withdraw the data. In this case, there is only surface level data available for this diagnostic. The ‘Tau0’ function is used to define the model time in hours since 1985.

```

FileName2 = 'Feb12_no3_sim.ctm.bpch'
FileName1 = 'Feb5sim_unlump.ctm.bpch'

date1=20060701

CTM_GET_DATA, TSOAcontrol, 'IJ-SOA-$', FileName=FileName1, tracer=43001, tau0=NYMD2TAU(date1)
CTM_GET_DATA, TSOAnirate, 'IJ-SOA-$', FileName=FileName2, tracer=43001, tau0=NYMD2TAU(date1)

ptr = TSOAcontrol.data
TSOAcontrol = *(ptr)

ptr = TSOAnirate.data
TSOAnirate = *(ptr)

NetFlux = TSOAcontrol - TSOAnirate

window, /free, xsize=1000, ysize=800
T_SYMBOL = 0
SymSize = 0
c_charsize = 0

labels = ['0','0.1', '0.2','0.3', '0.4', '0.5', '0.6', '0.7', '0.8', '0.9', '1','1.5','2','3']
c_levels=[0,0.1, 0.2,0.3, 0.4, 0.5, 0.6, 0.7, 0.8, 0.9, 1,1.5,2,3]

measlon = [180]
measlat = [-90]
meas = [0]

limit=[25,-130,50,-60]

lat = CTM_GRID(CTM_TYPE('GEOS5_47L'), /YMID)
lon = CTM_GRID(CTM_TYPE('GEOS5_47L'), /XMID)

ctm_overlay, NetFlux, lon, lat, meas, measlon, measlat, c_levels=c_levels,/CBar, /CONTINENTS, charsize=charsize, cbunit='ug/m3', /COUNTRIES, /USA, annotation=labels, limit=limit; /SAMPLE

end

```

Figure A.2: Code template used to create maps for Figure 3.11-3.14

The measlon, measlat, and meas variables are dummy data needed in order to use the ctm\_overlay function. Comment out 'limit' in the final line for a global map or include it if for a map of the USA (the limit coordinates are defined a few lines above). The code /SAMPLE can be uncommented to have a map that displays box grid cells, otherwise leave uncommented for an interpolated smoothed map as found in Figures 3.11-14.

```

Title = 'Monthly Time Series Plot at a Specific Location'
FileName1 = 'Feb5sim_unlump.ctm.bpch'
FileName2 = 'Feb12_no3_sim.ctm.bpch'

date = intarr(12)
days = intarr(12) ; days in month

date = [20060101, 20060201, 20060301, 20060401, 20060501, 20060601, 20060701, 20060801, 20060901, 20061001, 20061101, 20061201]
days = [31, 28, 31, 30, 31, 30, 31, 31, 30, 31, 30, 31]

budget = fltarr(12)

FOR i = 0, 11 DO BEGIN
SUCCESS1 = CTM_GET_DATABLOCK (soa1, 'IJ-SOA-$', FileName=FileName1, LON = [100.371094], LAT = [56.072035], level= [1], tracer=43001, $
tau0=NYMDZTAU(date[i]))

SUCCESS2 = CTM_GET_DATABLOCK (soa2, 'IJ-SOA-$', FileName=FileName2, LON = [100.371094], LAT = [56.072035], level= [1], tracer=43001, $
tau0=NYMDZTAU(date[i]))

    budget[i] = MEAN((soa1-soa2))
ENDFOR

window, /free, xsize=1200, ysize=800

title='Monthly SOA in Northern Boreal Forest, Russia Simulation Differences'
xtitle='Month'
ytitle='SOA (ug/m3)'

ymin=1
ymax=0
yrange=[0, 5]

jday= [1, 32, 60, 91, 121, 152, 182, 213, 244, 274, 305, 335]

dummyv = LABEL_DATE(DATE_FORMAT=['%M'])

plot, jday, budget, yrange=yrange, thick=5, charsize=2, $
title=title, ytitle=ytitle, xtitle=xtitle, XTICKFORMAT='LABEL_DATE', XTICKUNITS = ['MONTHS'], XTICKS = 11

stop

end

```

Figure A.3: Code template used to create time series plots for Figure 3.16-3.23

For loop written to extract data from bpch files and then processed using CTM\_GET\_DATABLOCK function to create time series plots.

```

FileName1 = 'Feb12_no3_sim.ctm.bpch'
FileName2 = 'Feb5sim_unlump.ctm.bpch'

date = intarr(12)
days = intarr(12) ; days in month

date = [20060101, 20060201, 20060301, 20060401, 20060501, 20060601, 20060701, 20060801, 20060901, 20061001, 20061101, 20061201]
days = [31, 28, 31, 30, 31, 30, 31, 31, 30, 31, 30, 31]

CTM_GET_DATA, box_area, 'DXYP', FileName=FileName1, tracer=1, tau0=NYMD2TAU(date[0])

ptr = box_area.data ; units of box area are in m2
box_area = *(ptr)

totalmonocontrol= 0
totalmononitrate= 0

FOR i = 0, 11 DO BEGIN

    CTM_GET_DATA, Airmass, 'BXHGHT-φ', FileName=FileName1, tracer=24002, tau0=NYMD2TAU(date[i])
    CTM_GET_DATA, Density, 'BXHGHT-φ', FileName=FileName1, tracer=24004, tau0=NYMD2TAU(date[i])

    ptr = airmass.data ; units of airmass are kg
    airmass = *(ptr)

    ptr = density.data
    density = *(ptr) ; density has units molec air/m3

;Biogenics:
CTM_GET_DATA, monocontrol, 'BIOGSRCE', FileName=FileName1, tracer=21004, tau0=NYMD2TAU(date[i])
CTM_GET_DATA, mononitrate, 'BIOGSRCE', FileName=FileName2, tracer=21004, tau0=NYMD2TAU(date[i])

ptr = monocontrol.data
monocontrol = *(ptr)

ptr = mononitrate.data
mononitrate = *(ptr)
; adding weird conversion (100 instead of 10) because off by a factor
; of 10 in ND46 in diag3.F
monocontrolx= total((monocontrol*(1/100.)*(1/6.022d23)*136.24*1d4*box_area)*60.*60*24*days[i]/(1d12))

mononitratex=total((mononitrate*(1/100.)*(1/6.022d23)*136.24*1d4*box_area)*60.*60*24*days[i]/(1d12))

totalmonocontrol= totalmonocontrol + monocontrolx
totalmononitrate= totalmononitrate + mononitratex

ENDFOR

print, "Total Monoterpene Control Biogenic Emissions (Tg)", Total(totalmonocontrol)
print, "Total Monoterpene Nitrate=0 Biogenic Emissions (Tg)", Total(totalmononitrate)

end

```

Figure A.4: Code template used to calculate yearly global budget of  $\alpha$ -pinene

For loop written to extract data from bpch file for each month and manipulated to yield  $\alpha$ -pinene in Tg for every month. Note that there was an error found in the GEOS code (commented) and the conversion factor to convert from TgC to Tg for  $\alpha$ -pinene was 100 instead of 10 as there was an extraneous value of 10 found in the hard code.

# Bibliography

- Ayres, B., H. M. Allen, D. C. Draper, S. S. Brown, R. J. Wild, J. L. Jimenez, D. A. Day, P. Campuzano-Jost, W. Hu, J. de Gouw, A. Koss, R. C. Cohen, K. C. Duffey, P. Romer, K. Baumann, E. Edgerton, S. Takahama, J. A. Thornton, B. H. Lee, F. D. Lopez-Hilfiker, C. Mohr, A. H. Goldstein, K. Olson, and J. L. Fry. (2015). "Organic nitrate aerosol formation via NO<sub>3</sub> + BVOC in the Southeastern US." *Atmospheric Chemistry and Physics* 15, 16235–16272  
<<http://www.atmos-chem-phys-discuss.net/15/16235/2015/acpd-15-16235-2015.pdf>>
- Baltensperger, U., Dommen, J., Alfarra, R., Duplissy, J., Gaeggeler, J., Metzger, A., Cristina Facchini, M., Decesari, S., Finessi, E., Reinnig, C., Schott, M., Warnke, J., Hoffmann, T., Klatzer, B., Puxbaum, H., Geiser, M., Savi, M., Lang, D., Kalberer, M., and Geiser, T. (2008). "Combined determination of the chemical composition and of health effects of secondary organic aerosols: The POLYSOA project." *Journal of Aerosol Medicine and Pulmonary Drug Delivery* **21**(1): 145-154.
- Bey, I., Jacob, D. J., Yantosca, R. M., Logan, J. A., Field, B. D., Fiore, A. M., Li, Q. B., Liu, H. G. Y., Mickley, L. J., Schultz, M. G. (2001). "Global modeling of tropospheric chemistry with assimilated meteorology: Model description and evaluation." *J. Geophys. Res.*, **106**(D19): 23073-23095.
- Brasseur, G.P., D.A. Hauglustaine, S. Walters, P.J. Rasch, J.E. Mtiller, C. Granier, and X.X. Tie. (1998) "MOZART, A global chemical transport model for ozone and related chemical tracers", *J. Geophys. Res.*, 103, 28,265-28,289, 1998.
- Brooklyn Rail Yard Project. "Brooklyn Rail Yard Project", 2014.  
<http://www.reed.edu/brooklyn-rails/rail-line-sampling-site.html>
- Carrasco, N., Rayez, M. T., Rayez, J. C., Doussin, J. F. (2006). "Experimental and theoretical study of the reaction of OH radical with sabinene." *Physical Chemistry Chemical Physics* 8(27): 3211-3217.

- Chung, S. H. and Seinfeld, J. H. (2002). "Global distribution and climate forcing of carbonaceous aerosols." *J. Geophys. Res.*, **107**(D19).
- Collins, W.J., Stevenson, D.S., Johnson, C.E., and Derwent, R.G. (1997). "Tropospheric ozone in a global-scale three-dimensional lagrangian model and its response to NO<sub>x</sub> emission" controls, *J. Atmos. Chem.*, **26**, 223-274, 1997.
- Crutzen, P. J. & E. F. Stoermer (2000). "The 'Anthropocene'". *Global Change Newsletter* **41**: 17–18.
- Donahue, N. M., Robinson, A. L., Stanier, C. O., and Pandis, S. N. (2006). "Coupled partitioning, dilution, and chemical aging of semivolatile organics." *Environmental Science & Technology* **40**(8): 2635-2643.
- Ford, B. and C. L. Heald (2013). "Aerosol loading in the Southeastern United States: reconciling surface and satellite observations." *Atmospheric Chemistry and Physics* **13**(18): 9269-9283.
- Fry, J. L., Kiendler-Scharr, A., Rollins, A. W., Wooldridge, P. J., Brown, S. S., Fuchs, H., Dube, W., Mensah, A., dal Maso, M., Tillmann, R., Dorn, H. P., Brauers, T., and Cohen, R. C. (2009). "Organic nitrate and secondary organic aerosol yield from NO<sub>3</sub> oxidation of beta-pinene evaluated using a gas-phase kinetics/aerosol partitioning model." *Atmospheric Chemistry and Physics* **9**(4): 1431-1449.
- Fry, J. L., Kiendler-Scharr, A., Rollins, A. W., Brauers, T., Brown, S. S., Dorn, H. P., Dube, W. P., Fuchs, H., Mensah, A., Rohrer, F., Tillmann, R., Wahner, A., Wooldridge, P. J., and Cohen, R. C. (2011). "SOA from limonene: role of NO<sub>3</sub> in its generation and degradation." *Atmospheric Chemistry and Physics* **11**(8): 3879-3894.
- Fry, J. L., Draper, Danielle C., Barsanti, Kelley C., Smith, James N., Ortega, John, Winkle, Paul M., Lawler, Michael J., Brown, Steven S., Edwards, Peter M., Cohen, Ronald C., and Lee, Lance. (2014). "Secondary Organic Aerosol Formation and Organic Nitrate Yield from NO<sub>3</sub> Oxidation of Biogenic Hydrocarbons." *Environmental Science & Technology* **48**(20): 11944-11953.

- GAMAP. "Global Atmospheric Model Analysis Package Version 2.17", January 24 2014. <http://acmg.seas.harvard.edu/gamap/>
- GEOS-5. "The GEOS-5 System", March 22 2013. <http://gmao.gsfc.nasa.gov/GEOS/>
- GEOS-Chem. "GEOS-Chem Model", June 17 2015. <http://acmg.seas.harvard.edu/geos/>
- GEOS-Chem v10-01 Online User's Guide. "GEOS-Chem v10-01 Online User's Guide", June 15 2015. <http://acmg.seas.harvard.edu/geos/doc/man/>
- GEOS-Chem Wiki. "GEOS-Chem Wiki", March 7 2016. [http://wiki.seas.harvard.edu/geos-chem/index.php/Main\\_Page](http://wiki.seas.harvard.edu/geos-chem/index.php/Main_Page)
- Geron, C., Rasmussen, R., Arnts, R. R., and Guenther, A. (2000). "A review and synthesis of monoterpene speciation from forests in the United States." *Atmospheric Environment* 34(11): 1761-1781.
- Geyer, A., Alicke, B., Ackermann, R., Martinez, M., Harder, H., Brune, W., Piero di Carlo, Williams, E., Jobson, T., Hall, S., Shetter, R., and Stutz, J. (2003). "Direct observations of daytime NO<sub>3</sub>: Implications for urban boundary layer chemistry." *J. Geophy& Res.*, 108, 12, 1999.
- Griffin, R. J., Cocker, D. R., Flagan, R. C., and Seinfeld, J. H. (1999a). "Organic aerosol formation from the oxidation of biogenic hydrocarbons." *J. Geophys. Res.*, **104**(D3): 3555-3567.
- Griffin, R. J., Cocker, D. R., Seinfeld, J. H., and Dabdub, D. (1999b). "Estimate of global atmospheric organic aerosol from oxidation of biogenic hydrocarbons." *Geophysical Research Letters* **26**(17): 2721-2724.
- Guenther, A. B., Jiang, X., Heald, C. L., Sakulyanontvittaya, T., Duhl, T., Emmons, L. K., and Wang, X.. (2012). "The Model of Emissions of Gases and Aerosols from Nature version 2.1 (MEGAN2.1): an extended and updated framework for modeling biogenic emissions." *Geoscientific Model Development* **5**(6): 1471-1492.

- Hallquist, M., Wangberg, I., Ljungstrom, E., Barnes, I., and Becker, K. H. (1999). "Aerosol and product yields from NO<sub>3</sub> radical-initiated oxidation of selected monoterpenes", *Environmental Science & Technology*, 33, 553–559, 1999.
- Heald, C. L., Coe, H., Jimenez, J. L., Weber, R. J., Bahreini, R., Middlebrook, A. M., Russell, L. M., Jolleys, M., Fu, T. M., Allan, J. D., Bower, K. N., Capes, G., Crosier, J., Morgan, W. T., Robinson, N. H., Williams, P. I., Cubison, M. J., DeCarlo, P. F., and Dunlea, E. J. (2011). "Exploring the vertical profile of atmospheric organic aerosol: comparing 17 aircraft field campaigns with a global model." *Atmospheric Chemistry and Physics* 11(24): 12673-12696.
- Hoyle, C. R., Boy, M., Donahue, N. M., Fry, J. L., Glasius, M., Guenther, A., Hallar, A. G., Hartz, K. H., Petters, M. D., Petaja, T., Rosenoern, T., and Sullivan, A. P. (2011). "A review of the anthropogenic influence on biogenic secondary organic aerosol." *Atmospheric Chemistry and Physics* 11(1): 321-343.
- Huang, Y., Ho, S. S. H., Ho, K. F., Lee, S. C., Yu, J. Z., and Louie, P. K. K. (2011). "Characteristics and health impacts of VOCs and carbonyls associated with residential cooking activities in Hong Kong." *Journal of Hazardous Materials* 186(1): 344-351.
- IPCC. "Summary for Policymakers." *Climate change 2013: the physical science basis. Contribution of working group I to the fifth assessment report of the Intergovernmental Panel on Climate Change*. Eds. S. Solomon, D. Qin, M. Manning, Z. Chen, /m. Marquis, K. B. Averyt, M. Tignor, and H.L. Miller. Cambridge, UK and New York, USA: Cambridge University Press, 2013.
- Lamarque, J. F., Bond, T. C., Eyring, V., Granier, C., Heil, A., Klimont, Z., Lee, D., Liousse, C., Mieville, A., Owen, B., Schultz, M. G, Shindell, D., Smith, S. J., Stehfest, E., Van Aardenne, J., Cooper, O. R., Kainuma, M., Mahowald, N., McConnell, J. R., Naik, V., Riahi, K., and van Vuuren, D. P. (2010). "Historical (1850-2000) gridded anthropogenic and biomass burning emissions of reactive gases and aerosols: methodology and application." *Atmospheric Chemistry and Physics* 10(15): 7017-7039.

- Lawrence, M.G., P.J. Crutzen, P.J. Rasch, B.E. Eaton, and N.M. Mahowald. (1999). "A model for studies of tropospheric photochemistry: Description, global distributions, and evaluation." *J. Geophys. Res.*, 104, 26,245-26,277, 1999.
- Levy, H., W.J. Moxim, A.A. Klonecki, and P.S. Kasibhatla. (1999). "Simulated tropospheric NO<sub>x</sub>: Its evaluation, global distribution, and individual source contributions", *J. Geophys. Res.*, 104, 26,279- 26,306, 1999.
- Liao, H., Henze, Daven K., Seinfeld, John H., Wu, Shiliang, and Mickley, Loretta J. (2007). "Biogenic secondary organic aerosol over the United States: Comparison of climatological simulations with observations." *J. Geophys. Res.*, **112**(D6).
- NAAQS. "NAAQS Table", March 29, 2016.  
<https://www.epa.gov/criteria-air-pollutants/naaqs-table>
- Odum, J., Hoffmann, T., Bowman, F., Collins, D., Flagan, R., and Seinfeld, J. (1996). "Gas/particle partitioning and secondary organic aerosol yields". *Environmental Science & Technology*. 1996, 30, 2580.
- Pathak, R. K., Presto, A. A., Lane, T. E., Stanier, C. O., Donahue, N. M., and Pandis, S. N. (2007). "Ozonolysis of  $\alpha$ -pinene: parameterization of secondary organic aerosol mass fraction", *Atmospheric Chemistry and Physics*, 7, 3811–3821, doi:10.5194/acp-7-3811-2007, 2007.
- Pandis, S., Paulson, S., Seinfeld, J., and Flagan, R. (1991). "Aerosol formation in the photooxidation of isoprene and  $\beta$ -pinene." *Atmospheric Environment*, 1991, 26, 997.
- Pye, H. O. T., Chan, A. W. H., Barkley, M. P., and Seinfeld, J. H. (2010). "Global modeling of organic aerosol: the importance of reactive nitrogen (NO<sub>x</sub> and NO<sub>3</sub>)." *Atmospheric Chemistry and Physics* **10**(22): 11261-11276.
- Rowland, F. S. and Molina, M. J., Ozone depletion: 20 years after the alarm, *Chemical and Engineering News* 72, 8-13, 1994.
- Sakulyanontvittaya, T., Duhl, T., Wiedinmyer, C., Helmig, D., Matsunaga, S., Potosnak, M., Milford, J., and Guenther, A. (2008). "Monoterpene and sesquiterpene

- emission estimates for the United States." *Environmental Science & Technology* 42(5): 1623-1629.
- Seinfeld, J.H. and Pandis, S.N. *Atmospheric Chemistry and Physics: From Air Pollution to Climate Change*. New York: John Wiley & Sons, 2006, 2 ed.
- Schichtel, B. A., Malm, W. C., Bench, G., Fallon, S., McDade, C. E., Chow, J. C., and Watson, J. G. (2008). "Fossil and contemporary fine particulate carbon fractions at 12 rural and urban sites in the United States", *J. Geophys. Res.*, 113, D02311, doi:10.1029/2007JD008605, 2008.
- Spittler, M., I. Barnes, I. Bejan, K. Brockmann, T. Benter, and K. Wirtz. (2006). "Reactions of NO<sub>3</sub> radicals with limonene and  $\alpha$ -pinene: Product and SOA formation." *Atmospheric Environment* **40**, Supplement 1:116-127
- Stanier, C. O., Donahue, Neil M., and Pandis, Spyros N. (2008). "Parameterization of secondary organic aerosol mass fractions from smog chamber data." *Atmospheric Environment* **42**(10): 2276-2299.
- Turpin, B.J., and Lim, H.J. (2001). "Species contributions to PM<sub>2.5</sub> mass concentrations: revisiting common assumptions for estimating organic mass". *Aerosol Science and Technology* 35 (1), 602–610.
- Volkamer, R., Jimenez, J. L., San Martini, F., Dzepina, K., Zhang, Q., Salcedo, D., Molina, L. T., Worsnop, D. R., and Molina, M. J. (2006). "Secondary organic aerosol formation from anthropogenic air pollution: Rapid and higher than expected." *Geophysical Research Letters* **33**(17): 4.
- WRI: World Resources 1998–99: Environmental change and human health, World Resources Report, Oxford University Press for the World Resources Institute, 384 pp., 1998.
- Zhang, Q., Jimenez, J. L. Canagaratna, M. R. Allan, J. D. Coe, H. Ulbrich, I. Alfarra, M. R. Takami, A. Middlebrook, A. M. Sun, Y. L. Dzepina, K. Dunlea, E. Docherty, K. DeCarlo, P. F. Salcedo, D. Onasch, T. Jayne, J. T. Miyoshi, T. Shimono, A. Hatakeyama, S. Takegawa, N. Kondo, Y. Schneider, J. Drewnick, F. Borrmann, S. Weimer, S. Demerjian, K. Williams, P. Bower, K. Bahreini, R. Cottrell, L.

Griffin, R. J. Rautiainen, J. Sun, J. Y. Zhang, and Y. M. Worsnop, D. R. (2007). "Ubiquity and dominance of oxygenated species in organic aerosols in anthropogenically-influenced Northern Hemisphere midlatitudes." *Geophysical Research Letters* 34(13): 6.